The effects of reverse micelles on charging behavior in apolar media

Edward LeRoy Michor

A dissertation

submitted in partial fulfillment of the

requirements for the degree of Doctor of Philosophy

University of Washington

2016

Reading Committee:

Dr. John Berg, Chair
Dr. Lilo Pozzo
Dr. Qiuming Yu

Committee Members:
Dr. Alberto Aliseda, GSR
Dr. Brian Hayes

Program Authorized to Offer Degree:

Chemical Engineering

University of Washington

Abstract

The effects of reverse micelles on charging behavior in apolar media

Edward LeRoy Michor

Chair of the Supervisory Committee:
Rehnberg Professor John C. Berg
Chemical Engineering

The study of particle charging behavior in apolar media is key to the understanding and design of electrophoretic displays and inks. The charging of colloidal particles in these apolar environments relies on the presence of surfactants and their reverse micelles. Reverse micelles can undergo disproportionation reactions with one another, resulting in bulk charges in the media and an increased system conductivity. Surfactant molecules adsorbed on particle surfaces can undergo acid-base interactions with the surface functional groups, resulting in the formation of charges. The now-charged surfactant molecule is then stabilized in a reverse micelle, leaving a net charge on the particle surface.

Many factors influence the micellization and particle charging behavior of these surfactants – from environmental variables, such as temperature and humidity, to the surfactant,

particle, and solvent chemistries and structures. We show that the micellization of the surfactant Aerosol OT becomes less favorable with increasing solvent dielectric constant. Surfactant chemistries can be tuned by performing simple ion-exchange reactions with the surfactant head group. We have shown that increasing the electronegativity of the cation in the head group results in more acidic surfactants, and therefore the ability to impart higher maximum charges to particle surfaces. The critical micelle concentrations (CMCs) of a surfactant series were investigated as a function of temperature, and found to increase with increasing temperature. This same series was then used to charge colloidal particles at three temperatures, which resulted in decreasing maximum particle charge with increasing temperature. The structures of these reverse micelles were investigated using small angle neutron scattering (SANS), and it was found that the core radii of the reverse micelles decreased with increasing surfactant tail length. Tri-tailed surfactants formed reverse micelles with the smallest core radii, of ~4Å. This study suggested that in order to impart the maximum charge to colloidal particles, the reverse micelles being used must have intermediate core sizes, in order to offer a large enough polar environment to stabilize charge, but not one too large such that disproportionation reactions in the bulk cause electrostatic screening of the particle charges. Applications of this research are discussed.

TABLE OF CONTENTS

LIST OF FIGURES

LIST OF TABLES

ACKNOWLEDGEMENTS

- John C. Berg for his advice, guidance, and support
- Funding provided by Xerox and the SPC Center
- Matthew Gacek for his mentorship and welcoming nature towards a fresh grad student
- My advisory committee: Professors Qiuming Yu, Lilo Pozzo, Alberto Aliseda, and Dr. Brian Hayes
- Drs. Jeff Richards, Greg Newbloom, and Pablo de la Iglesia for countless scientific discussions, both understood and not
- Dr. Yun Liu for his assistance at NIST
- Past and present Berg Group members: Prasad Bhosale, Ben Rutz, Kyle Caldwell, and Ben Ponto
- My parents for their advice on choosing which colors to use in figures
- My friends for listening to and supporting me throughout the last five and a half years

DEDICATION

To: My friends and family, for their support and guidance throughout this degree

Chapter 1. INTRODUCTION

1.1 THEORY AND BACKGROUND

Interest in the existence of electrical charges in nonpolar media originally began in the 1940's and 1950's in the petroleum processing industry. Klinkenberg and van der Minne[1] found that small quantities of certain ionic species, presumably metal soaps produced by corrosion, would adsorb to metal surfaces. While the solution was under flow, the oppositely charged species would separate and cause the buildup of large electric fields. These fields would then discharge by sparking, resulting in what were called electrokinetic explosions. In large quantities, it was found that the same species thought to be responsible for this behavior could significantly increase the conductivity of the petroleum products. The increased conductivity prevented charge buildup leading to electrokinetic explosions. Around the same time, Nelson and Pink[2,3] showed that these charge carrying species were reverse micelles of metal soaps. Reverse micelles aggregates of surfactant monomers arranged with their polar portion at the core and their apolar moieties extending outward, as shown in Figure 1.1a. These structures are termed "reverse" or "inverse" micelles because they mimic their aqueous counterparts, Figure 1.1b, with their monomer orientation reversed.

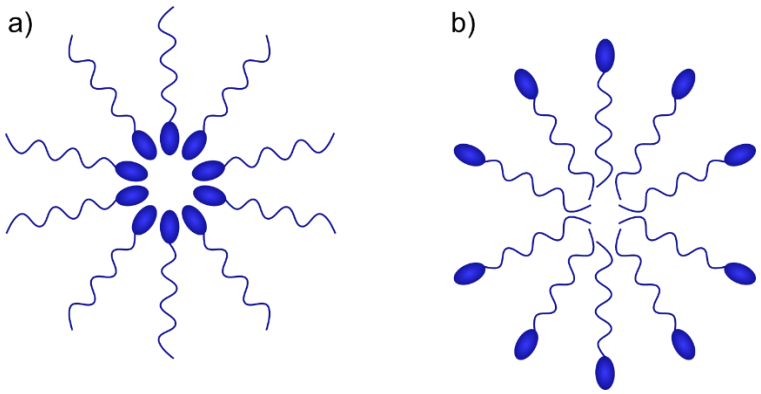

Figure 1.1. Schematic of a) a reverse micelle in apolar media and b) a regular micelle in aqueous media.

Currently, reverse micelles in apolar media have been used for a wide array of applications: metal and polymer particle syntheses,[4] membrane syntheses for ultrapurification,[5] protein extractions and purifications,[6–8] viscosity modifiers for supercritical CO_2 systems, [9–11] and the charging of colloidal particles.[12–16] Once charged, colloidal particles become stable in nonpolar dispersions and can be used in paints and inks, such as in the HP Indigo® printer,[17] as well as for use in electrophoretic displays, such as the Amazon Kindle®, where they are deposited at a desired surface using electric fields.

It had long been debated whether or not charges could exist in nonpolar environments due to the extremely low dielectric constants of those solvents.[18] A metric used to quantify the stability of an ion in a medium is the Bjerrum length, λ_B, the distance of separation where the electrostatic attraction of two ions is equivalent to the thermal energy in the system, k_BT ,and given by

$$\lambda_B = \frac{e^2}{4\pi\varepsilon\varepsilon_o k_B T}, \tag{1.1}$$

where e is the elementary charge, ε is the dielectric constant of the medium, ε_o is the permittivity of free space, k_B is the Boltzmann constant, and T is the absolute temperature. Large Bjerrum

lengths correspond to environments where ions can “feel” each other over large distances. On the other hand, small values correspond to environments where the medium screens out the charge, and oppositely-charged ions can move close to one another without risk of recombination. For reference, ions in water have a Bjerrum length of 0.7nm, while ions in an apolar environment (with a dielectric constant of 2) have a value of 28nm, shown to scale in Figure 1.2. In aqueous media, the ordered water molecules around an ion provide the necessary distance to prevent recombination of ions. In apolar environments, the solvent does not interact with ions or provide any screening. This requires the addition of a third component to the system, such as a surfactant, to form a structure, such as a reverse micelle, around the ion in order to provide the necessary separation.

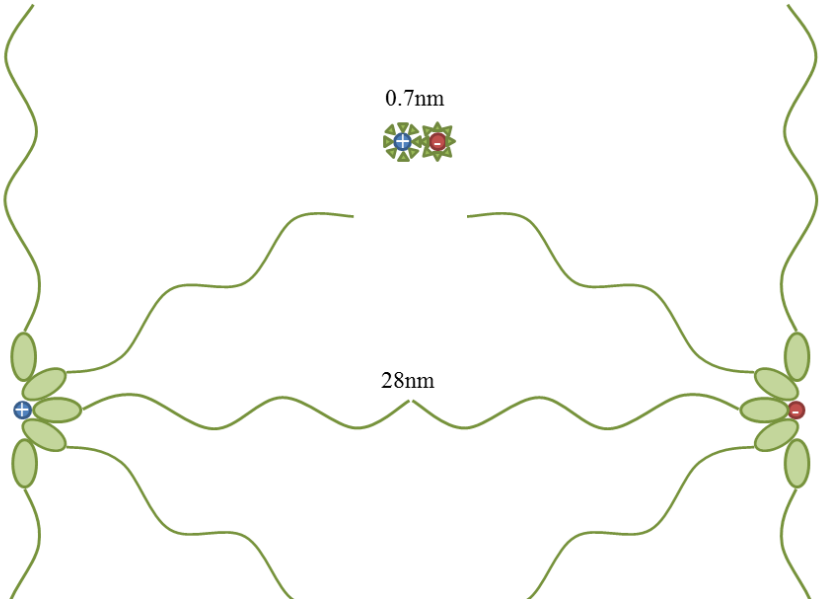

Figure 1.2. A to-scale representation of the Bjerrum lengths in aqueous (top) and apolar (bottom) media.

Understanding that reverse micelles must be present in apolar media to sustain charges, one must next look to the processes by which reverse micelles form. In aqueous media, when surfactants reach a high-enough concentration, the critical micelle concentration (CMC),

micelles spontaneously and rapidly form. Water molecules, which had been bound to the surfactant tails, are released upon micellization, causing a large rise in entropy.[19] This entropic effect is of a large enough magnitude to overcome the entropic loss due to ordering in the system, as well as the enthlapic penalty of bringing charged head-groups together. In apolar media, however, water is present in only scant quantities, and the surfactant tails are favorably dissolved in the hydrophobic solvent. This prevents the same entropic force from driving micellization in apolar environments. As the surfactant concentration increases, it is believed that pre-micellar aggregates form, resulting in the stabilization of a small amount of charges.[15] As the concentration continues to increase, the aggregates grow until reaching the CMC, at which point the reverse micelles are fully-formed. In apolar systems, the driving force for micellization is enthalpic, whereby the dipole-dipole interactions of the head-groups bring the surfactant molecules together to form aggregates and eventually reverse micelles.[16]

As mentioned previously, surfactants were originally used to enhance the electrical conductivity of petroleum products. Below the CMC, where premicellar aggregates are present, it has been found that the conductivity of solutions scales as the square root of the surfactant concentration.[13] This scaling can be explained by a dissociation reaction, whereby an ionic surfactant, AB, dissociates into its ions, A^+ and B^-, which are subsequently stabilized by premicellar aggregates. However, once the CMC is reached, the conductivity of solutions scales linearly with surfactant concentration.[13,15,20] This behavior is explained by spontaneous fluctuations leading to disproportionation, whereby two neutral micelles, M^0, collide and come apart as two, oppositely charged micelles, M^+ and M^-:

$$2M^o \rightarrow M^+ + M^- \tag{1.2}$$

By this mechanism, the conductivity, σ, goes as

$$\sigma = \frac{e^2 C_o \chi}{6\pi\eta R_H}, \tag{1.3}$$

where e is the elementary charge, C_o is the total concentration of micelles, χ is the fraction of charged micelles, η is the solution viscosity, and R_H is the hydrodynamic radius of the micelles. Figure 1.3 depicts the three regimes of concentration: entirely dissolved surfactant, pre-micellar aggregates, and fully formed reverse micelles.

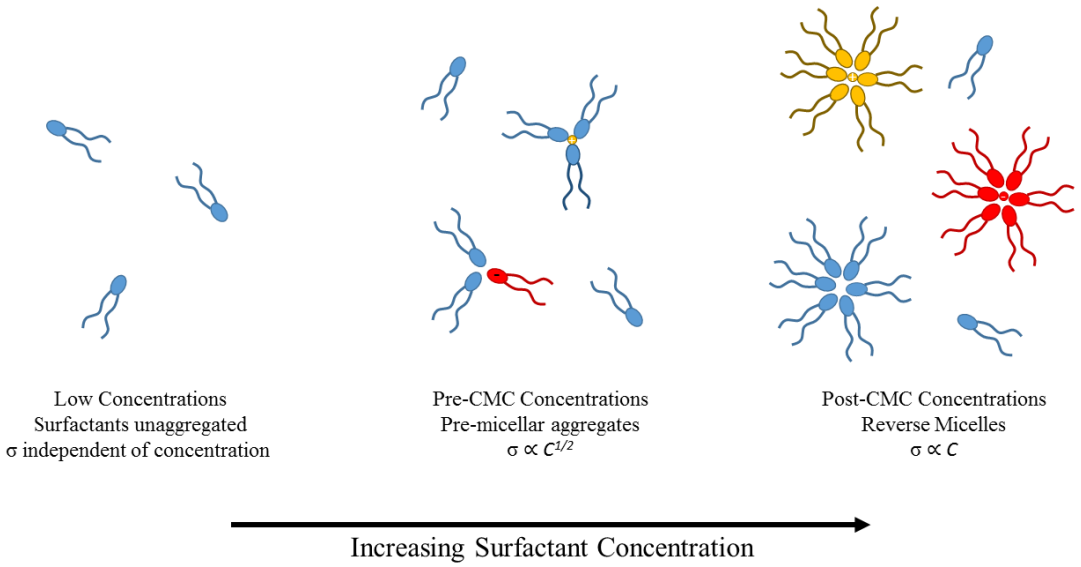

Figure 1.3. Schematic of the different regions of surfactant concentration in apolar media.

Once reverse micelles are present in solution, stabilization of charges can occur in apolar environments. When particles are added to apolar surfactant solutions, occasionally the surfactants will impart charge to the particle surfaces, often measured as an electrophoretic mobility by, for example, phase analysis light scattering (PALS).[21] Not only do the particles become charged, but the overall system conductivity increases with the addition of particles, as shown in Figure 1.4. This increase in system conductivity suggests the generation of additional charges due to surfactant-particle interactions, ruling out charged micelle adsorption to the particle surface as the mechanism for particle charging.

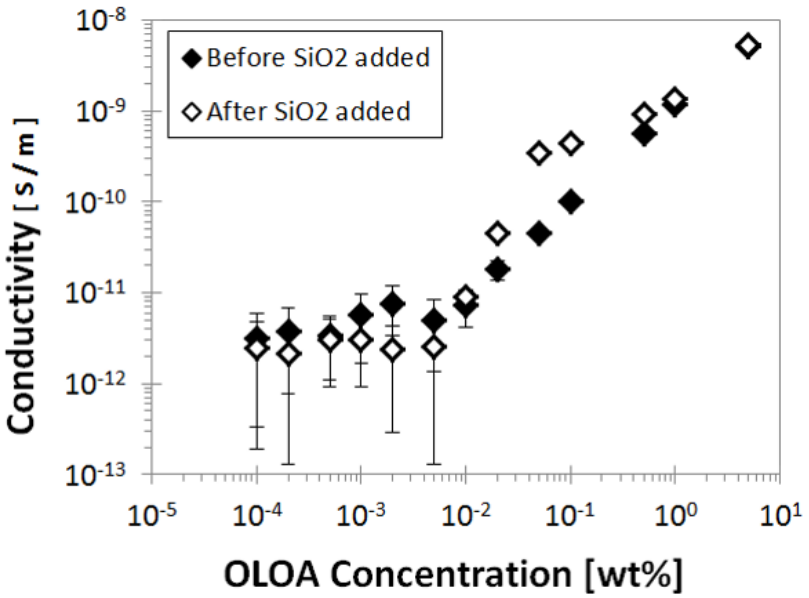

Figure 1.4. Conductivities of OLOA solutions in Isopar-L with and without silica particles. The addition of particles increases the overall system conductivity due to the increased generation of system charges. (Reproduced from [22])

The physical mechanism by which particle charging occurs is still a debated topic,[13] but it is currently believed that acid-base reactions often provide the dominant mechanism for charging in apolar environments,[23] as proposed by Fowkes[24] in 1983 when studying the charging of carbon black particles with OLOA 1200, a commercial surfactant used in oil additive packages, in dodecane. According to this mechanism, adsorbed surfactant molecules can form acid-base adducts with surface functional groups on the particle, as shown in Figure 1.5. These adducts can dissociate, resulting in charged surface functional groups and charged surfactant ions. A reverse micelle can then incorporate and stabilize a charged surfactant molecule, leaving a net charge on the particle surface. This charged functional group on the surface can then be stabilized by a hemi-micelle, as shown in Figure 1.5.

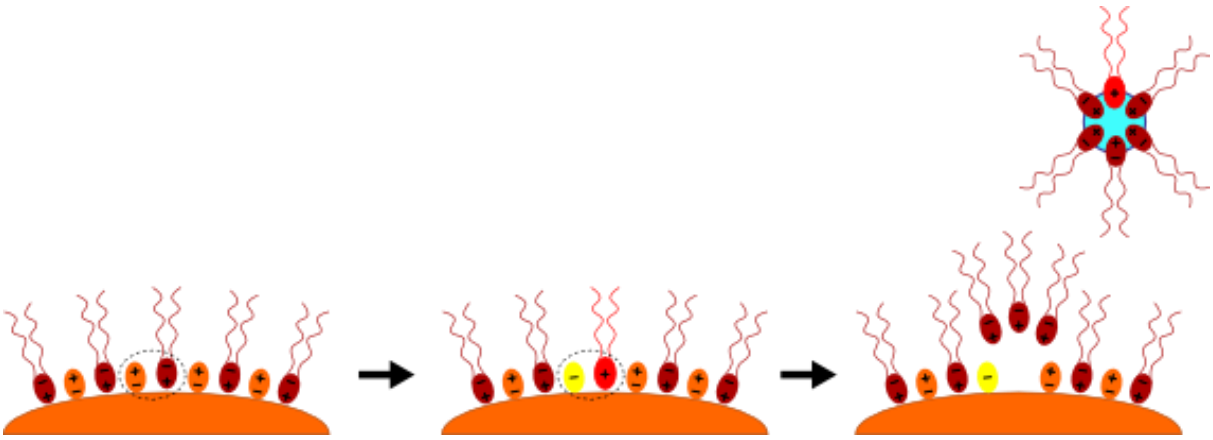

Figure 1.5. A schematic detailing the particle charging mechanism.

Previous studies from several laboratories have shown that when a surfactant is more acidic than the functional groups on the particle surface, the particles will be charged positively, and when the surfactant is more basic than the particle surface groups, the particle will charge negatively. Several techniques can be used to quantify the acidity or basicity of particles. The point of zero charge (PZC) in aqueous media is especially useful for the study of mineral oxides.[19] The PZC is defined as the solution pH at which the particle's surface charge is equal to zero. Another metric used to quantify the acid-base characteristics of a particle is its isoelectric point (IEP). The IEP is closely related to the PZC. It is defined as the pH at which the particle experiences no net charge at the shear plane, i.e. where its zeta potential is zero. The IEP can be affected by the presence of specifically adsorbing ions on the particle surface, but in their absence, the PZC and IEP are equal. Particles with PZC or IEP values above 7 are considered basic, while those with PZCs or IEPs below 7 are acidic, as depicted in Figure 1.6.

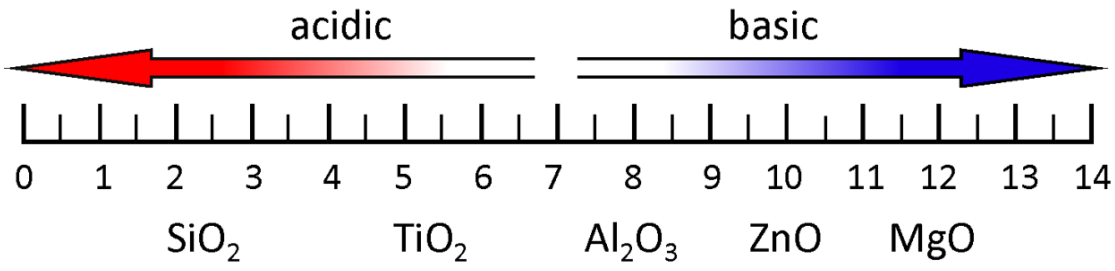

Figure 1.6. Schematic of PZC or IEP scale for mineral oxides.

These particles obtain charge in aqueous environments by the protonation or deprotonation of surface hydroxyl groups, as shown in Figure 1.7.

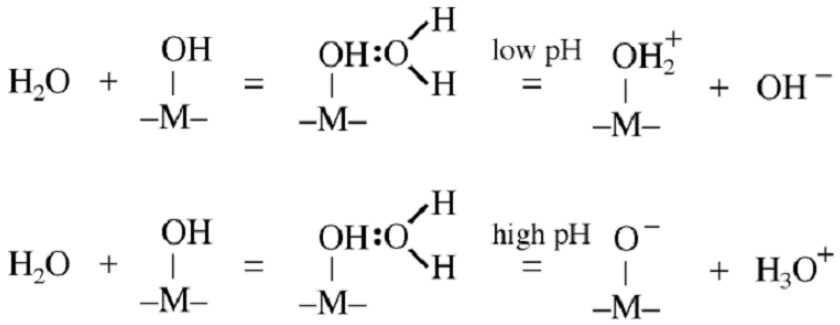

Figure 1.7. Charging mechanism of mineral oxides in aqueous environments.

Mineral oxides cover a range of PZCs or IEPs, as shown in Table 1.1. Silica and titania are both acidic particles, alumina and zinc are both amphoteric, and magnesia is basic.

Table 1.1. Experimental[12] and literature[25] values of IEP and PZC of mineral oxides

Oxide Species	Exp. IEP	Exp. PZC	Lit. PZC Range
Silica	2.1±0.3	3.0±0.3	2-3
Titania (rutile)	4.0±0.2	3.7±0.2	4-6
Alumina	7.1±0.3	7.5±1.0	8-9
Zinc Oxide	7.5±0.5	7.7±0.3	9-10
Magnesia	8.5±0.5	10.7±0.2	10-12

Not all particle types can be characterized by their properties in aqueous media, however, as certain particles decompose or are soluble in aqueous environments, but exist as stable particles in apolar media. In order to characterize the acid-base properties of these particle types, inverse gas chromatography (IGC) can be used.[19] Standard gas chromatography studies the properties of gases as they flow through a packed column of a known solid phase. IGC uses the same experimental apparatus, but instead studies the particle properties by using a series of gaseous probes, such as linear alkanes, flowing in an inert carrier gas, such as nitrogen. The dispersive component of the solid particle surface energy is calculated by measuring the retention volumes of the probes, V_N, defined as the volume of carrier gas required to elute a given probe, of, say, a series of linear alkanes. Once these values are measured, the dispersive component of the solid particles surface tension, σ_s^d, can be calculated according to

$$RT\ln(V_N) = 2a_{mol}\sqrt{\sigma_S^d \sigma_{probe}^d} + C, \qquad (1.4)^{23}$$

where R is the ideal gas constant, T is the absolute temperature, a_{mol} is the molecular area of the probe, σ_{probe}^d is the dispersive component of the probe's surface tension (energy), and C is a constant that depends on the reference state. Using linear alkanes, and plotting $RT\ln(V_N)$ as a function of $a_{mol}(\sigma_{probe}^d)^{1/2}$ one obtains a straight line with a slope of $2(\sigma_s^d)^{1/2}$, as shown schematically in Figure 1.8. Since the slope of the line is used to calculate the pertinent value, the constant, C, can be ignored.

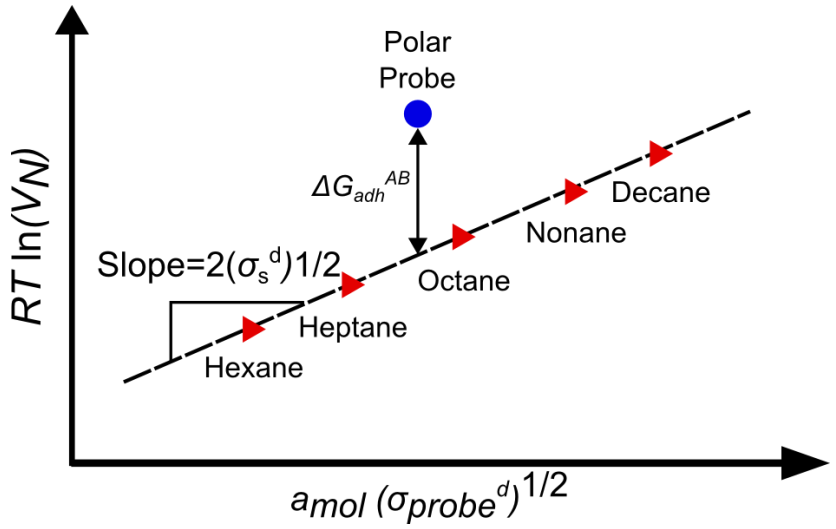

Figure 1.8. Schematic of IGC data used to determine both the dispersive component of the solid surface energy, σ_s^d, and the acid-base contribution to the change in free energy of adsorption, ΔG_{ads}^{AB} .

Once the particle's dispersive component to the surface tension is determined, acidic or basic probes can be injected to determine the relative acidity or basicity of the particle surface. If a polar probe interacts strongly with a particle surface, the V_N required to elute that probe will be higher than predicted by the alkane line. This shift makes Equation 1.4 become

$$RT\ln(V_N) = 2a_{mol}\sqrt{\sigma_S^d \sigma_{probe}^d} - \Delta G_{ads}^{AB} + C, \tag{1.5}$$

where the change in free energy of adsorption is given by $-\Delta G_{ads}^{AB}$, as shown in Figure 1.8. Using a variety of acidic and basic probes, the characteristics of the particles can be determined. This technique was used, for example, to characterize magenta and cyan pigment particles, and it was determined that magenta was extremely basic, while cyan was weakly amphoteric.[26] IGC has also been used to characterize carbon black particles, measuring them to be strongly acidic in nature,[23] reflecting the presence of oxygen-containing functional groups such as –COOH and –OH on their surfaces. Before quantifying the acid-base characteristics of a surfactant, it is necessary to examine the charging behavior of the particles by surfactants in apolar media.

As the surfactant concentration is increased and passes the CMC, the charge on the dispersed particles begins to rise. With increasing surfactant concentration, the charge rises further before going through a maximum value and decreasing. This trend, for an acidic surfactant and basic particle, is shown schematically in Figure 1.9.

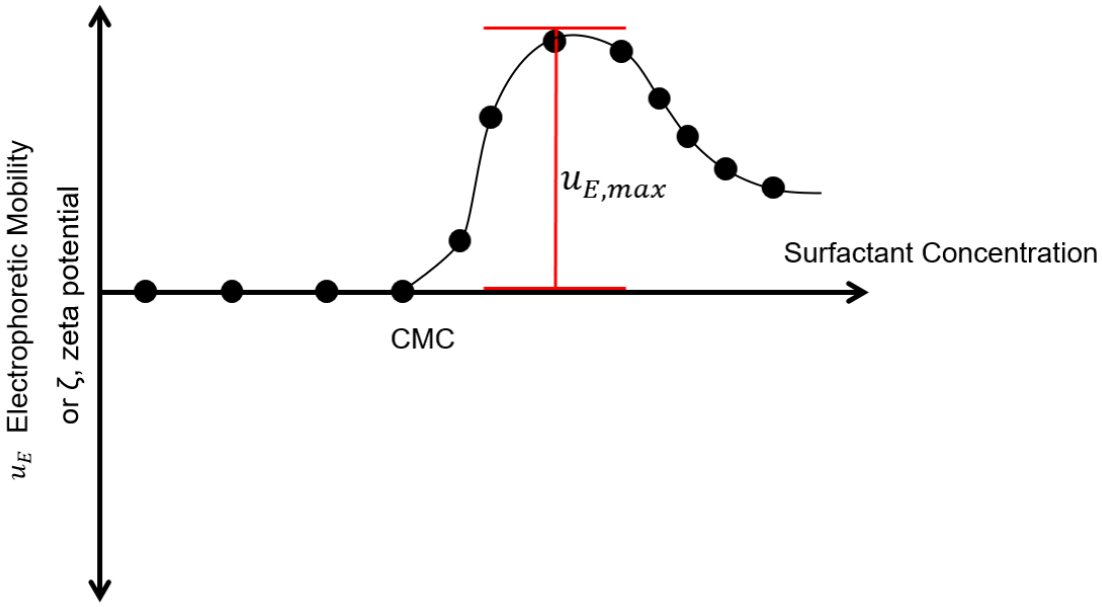

Figure 1.9. A generalized schematic of particle charge as a function of surfactant concentration.

Once reverse micelles are present, charges can be stabilized on the particle surface, and the measured magnitude of the particle mobility increases. As the surfactant concentration increases, so do the number of reverse micelles, and thus the charge which can be stabilized on the particle surface. However, as the concentration increases still further, the charged reverse micelles in the bulk solution begin to screen the charge on the particles, and thus their electrophoretic mobility decreases. The maximum achievable electrophoretic mobility or zeta potential is characteristic of a given particle-surfactant system and may be used as a metrics of the charging.

The zeta potential is defined as the electrical potential difference between the hydrodynamic slip plane which surrounds the particle in the bulk medium. In order to calculate this value using the electrophoretic mobility, u_E, two parameters, the Debye parameter, a measure of electrostatic screening in the solution,[19] and the particle radius, a, must be known. The inverse of the Debye parameter, κ, is known as the Debye length, which quantifies the distance to which electrostatic effects can be "felt" in a medium. In many aqueous systems, the polarity of the solvent screens out electrostatic interactions, which yields a small Debye length, or a large Debye parameter, for the system. In aqueous media with sufficient ion content and large particles, such that $\kappa a > 200$, the Helmholtz-Smoluchowski approximation can be used to calculate the zeta potential as[19]

$$\zeta = \frac{\eta u_E}{\varepsilon}. \tag{1.6}$$

In apolar systems, the medium does not screen out particle charges, meaning that electrostatic interactions can be felt over much larger distances. In these environments, with small Debye parameters and small particles, $\kappa a < 0.1$, which allows the use of the Hückel approximation[19]

$$\zeta = \frac{3\eta u_E}{2\varepsilon}. \tag{1.7}$$

For systems where $0.1 < \kappa a < 200$, numerical solutions must be used to calculate the zeta potential of the particles.[19] All systems presented in this dissertation can be described by this approximation.

The maximum electrophoretic mobilities of a series of mineral oxides was measured for a given surfactant species, and plotted as a function of the particle PZC, as shown in Figure 1.10.

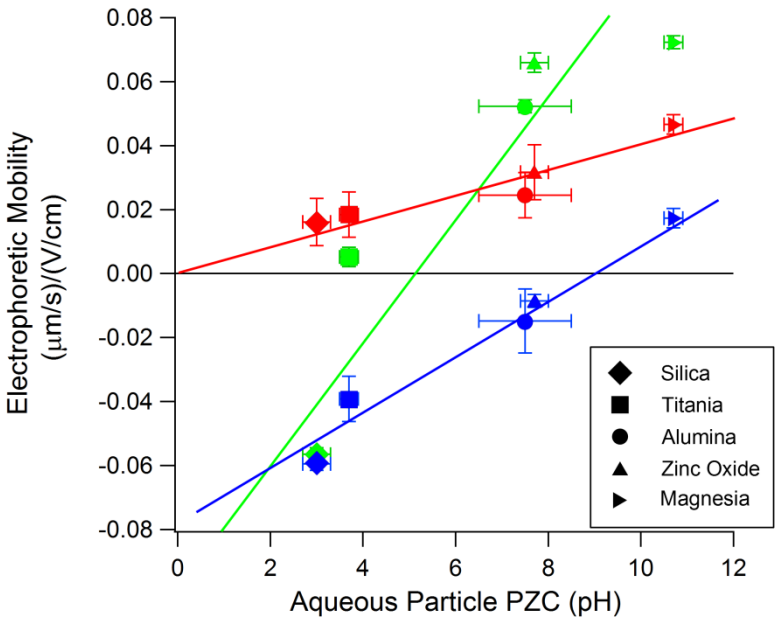

Figure 1.10. The maximum electrophoretic mobilities imparted by Aerosol OT (green markers) and Span 80 (red markers) and OLOA (blue markers) to a series of mineral oxide particles as a function of the particle PZCs. Best fit lines for each surfactants are shown to determine the effective surfactant pH values. (Arranged from [27] and [12]).

In Figure 1.10, the surfactant Aerosol OT (AOT) was used to charge five mineral oxide particles in the apolar solvent Isopar-L, a commercial mixture of C_{11} to C_{15} isoparaffins from Exxon Corporation. Particles with high PZCs charged positively, while the low PZC particle, silica, charged negatively. A best-fit line, shown in green, can be drawn through the maximum mobility points, which crosses the line of zero u_E at a PZC of 5. This charging curve shows that AOT charges mineral oxides as would an aqueous solution with a pH of 5, making it a weakly acidic surfactant. Similar experiments were performed using the surfactants Span 80, an acidic sorbitan oleate, and OLOA 11000, hereafter referred to as OLOA, a commercial surfactant from Chevron Corp. with the active species being polyisobutylene succinimide (PIBS), with the results shown in Figure 1.10. Span 80, shown with a red line, charged all five particles positive and had an extrapolated cross-over PZC of 0, making it an acidic surfactant. OLOA, shown with a blue line, charged most particles negatively, while the basic magnesia particle was charged

positively. OLOA had a cross-over PZC of 9, making it a basic surfactant. Using this metric to describe the acid-base characteristics of a surfactant, one can assign an acid-base number (ABN) to each surfactant.

The surface chemistry of mineral oxides can be adjusted by silane functionalization. A study[28] investigating the charging behavior of silica particles functionalized with the basic Aminopropyltrimethoxysilane (APS) and the acidic 3-Glycidoxytrimethoxypropylsilane (GPS) showed APS functionalized silica to have a PZC of 8.5, while the GPS treated silica had a PZC of 3.0. These particles were then dispersed in solutions of Span 80 and OLOA in Isopar-L. The charging results are shown in Figure 1.11 with the pure mineral oxide charging curves of OLOA, Span 80, and AOT given as reference.

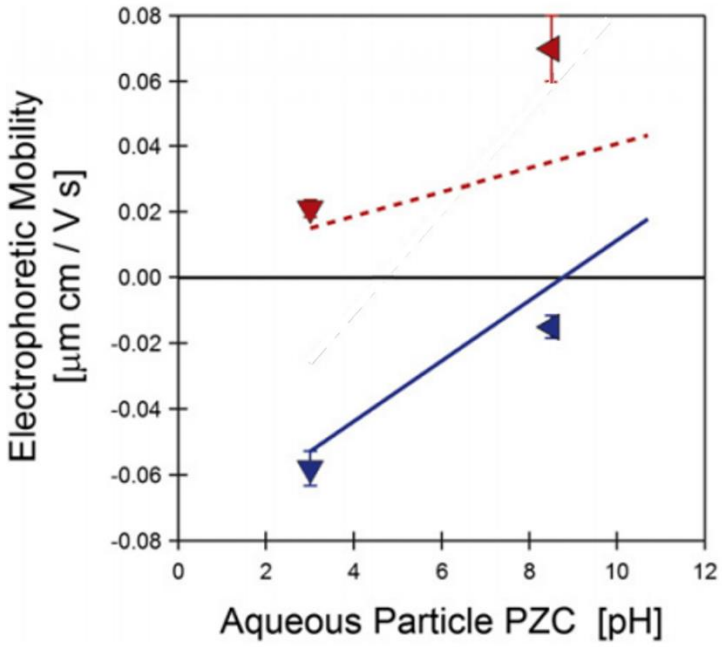

Figure 1.11. Maximum electrophoretic mobilities of APS treated silica (◀) and GPS treated silica (▼) as charged by Span 80 (red) and OLOA (blue). The pure mineral oxide charging curves of Span 80 (dotted red line), and OLOA (solid blue line). (Reproduced from [23])

The particles charged by OLOA both charged negatively and were predicted reasonably well by the pure mineral oxide charging curve of OLOA, taken from Figure 1.10. The APS and

GPS particles charged by Span 80 both charged positively, however the APS particle charged to a higher magnitude than was predicted by the Span 80 charging curve. This shows that while the relative acid-base characteristics of the surfactant-particle pair can accurately predict the polarity of the particle charge, there are other factors at play that determine the magnitude of charge imparted to the particles.

Many applications of apolar charging involve the use of pigment particles, such as magenta, cyan, and carbon black. The particle types are difficult to characterize using titration techniques and PALS in aqueous environments, and have had their acid-base behavior determined by IGC. The PZCs of four types of carbon black particle types were determined by aqueous titration and were measured to be approximately 1.0. Recall that magenta is a strongly basic particle, similar to that of a particle with a PZC between 11 and 12, cyan is amphoteric, similar to a particle with a PZC of 6. AOT, Span 80, and OLOA had been used to charge four different types of carbon black, and it was found that Span 80 imparted no significant charge to any of the four species.[23] The maximum zeta potentials imparted to each of the four carbon blacks by AOT were all negative, however the magnitude varied from -40mV to -140mV. Interestingly, the basic OLOA imparted all negative charges to the carbon blacks, with similar magnitudes, between -60mV and -120mV. If the maximum zeta potentials are plotted on the charging curves of the three surfactants, shown in Figure 1.12, this seemingly aberrant behavior can be understood.

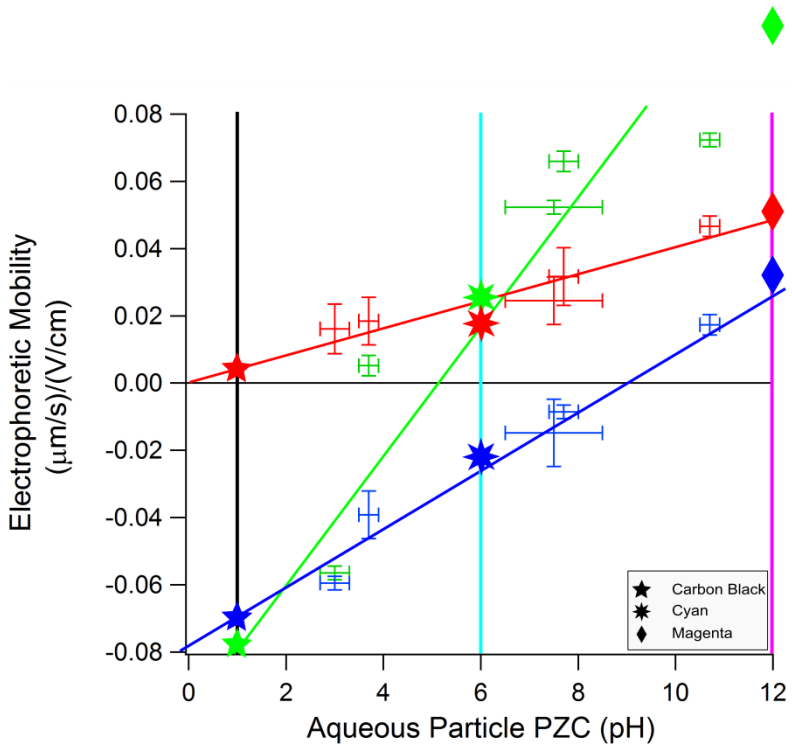

Figure 1.12. Maximum electrophoretic mobilities of carbon black[23] (★) cyan (✶) and magenta[26](♦) as charged by Span 80 (red), AOT (green), and OLOA (blue). The vertical black line represents the PZC of carbon black. The vertical cyan and magenta lines in represent the effective PZCs of their respective particle types. The pure mineral oxide charging curves of Span 80 (red line), AOT (green line) and OLOA (solid blue line) are shown with the error bars of the individual data points shown for reference. (Arranged from [22])

In Figure 1.12, the blue and green stars represent the average of zeta potentials that OLOA and AOT imparted to the carbon black particles. While one would assume that the basic OLOA should impart a higher magnitude of charge to the acidic carbon black particles than the slightly acidic AOT, it can be seen that the steeper slope of the AOT charging curve intersects the center of the green bar, while the OLOA charging curve intersects the center of the blue bar, with both curves predicting similar magnitudes of charge, with AOT being slightly more negative. The cyan particles, with an effective PZC of 6, denoted by the vertical cyan line in Figure 1.12, charged positively with Span 80 and AOT, and negatively with OLOA, well predicted by the mineral oxide charging curves and acid-base characteristics of these surfactants.

Magenta, denoted by the vertical magenta line in Figure 1.12, charged positively for all surfactants, with a significantly higher magnitude of charge from AOT than the more-acidic Span 80. Again, the steeper slope of AOT accurately predicts this behavior.

Not only are chemical functionalities of the particle and surfactant important in these systems, but the amount and location of water maybe be as well. Small amounts of water can be solubilized in the solvent itself, but these concentrations are generally below 30ppm. The addition of hygroscopic surfactants and particles increases the system water content to values as high as 1200ppm. A previous study[22] by the author and fellow researchers investigated the particle charging behavior of OLOA on silica particles dispersed in Isopar-L. Four dispersions were studied, using combinations of humidified and dried OLOA solutions and humidified and dried silica particles, in order to determine the effects of water on particle charging with OLOA. The "dry" particles were held at 250^{o}C for four hours, while the "dry" OLOA solutions were treated with molecular sieves for 48hrs. The "wet" particles and OLOA solutions were allowed to equilibrate with 80% relative humidity air for 48hrs. Water content, particle electrophoretic mobility and system conductivities were measured.

In order to decouple the effects of water on micellar charging and particle charging, solutions of OLOA were prepared in Isopar-L at three concentrations, each above the CMC, and measured using a nonpolar conductivity meter. The results are shown in Figure 1.13. Conductivity of reverse micellar solutions of OLOA as a function of the molar ratio of water to OLOA (Reproduced from [22]).

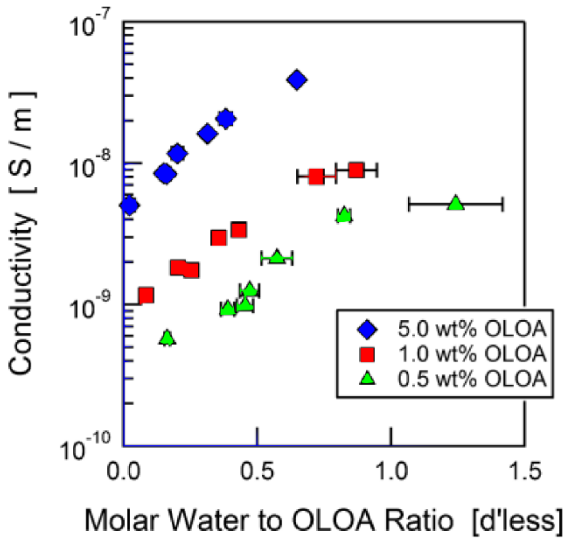

Figure 1.13. Conductivity of reverse micellar solutions of OLOA as a function of the molar ratio of water to OLOA (Reproduced from [22]).

Without the presence of particles, increasing the water content of a reverse micellar solution significantly increases its conductivity. By increasing the molar water-to-OLOA ratio from 0.1 to 1 increases the conductivity of the solution by an order of magnitude for all three OLOA concentrations studied. This increase in conductivity is due to the increasing number of charge disproportionation reactions of the reverse micelles. The concentration of charged reverse micelles of valence Z can be given by[22]

$$C_{\pm Z} = C_o \exp\left(\frac{-Z^2 \lambda_B}{2a}\right), \tag{1.8}$$

where C_o is the total concentration of reverse micelles, Z is the valence of the charged micelles, λ_B is the Bjerrum length (given by Equation 1.1), and a is the radius of the micellar core. The probability of reverse micelles charging to a valence of ±2 is 54 times less than the probability of charging to valence of ±1, making it safe to assume all charged reverse micelles carry a valence of ±1. The larger polar cores of these structures offers a more favorable environment for charge stabilization, and thus an increase in charging events.

The addition of particles to these systems would likely cause some of the water to relocate to the particle surfaces. In order to determine the location of the water, whether in reverse micelles or on particle surfaces, the water content of the systems was measured before and after centrifugation of the dispersion. After the particles were centrifuged out, the water content of the supernatant could be measured to determine the water left in the reverse micelles. The fraction of water on the particle surface could then be calculated as a function of the total system water content, as shown in Figure 1.14. It should be noted that the "dry"-"dry" dispersions were not shown in this plot due to the extremely low water contents of these systems, near 15ppm. The instrument limit of detection was 5ppm, resulting in uncertainties in these measurements of up to 100%.

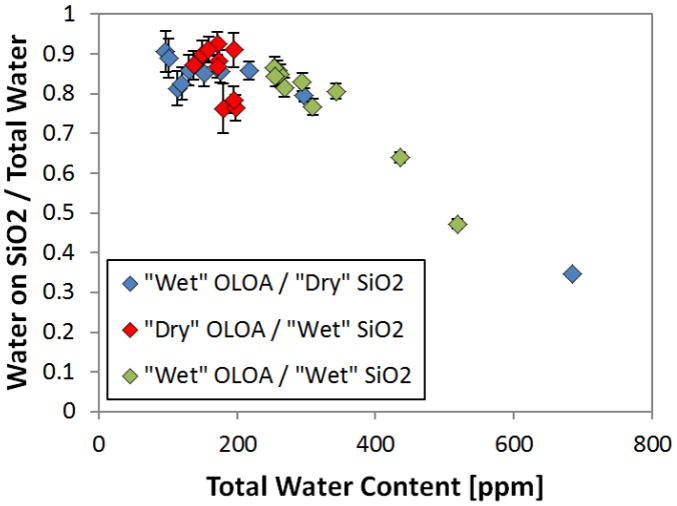

Figure 1.14. Fraction of total water on silica particle surfaces as a function of total system water content (Reproduced from [22]).

At water contents below 275ppm, 80-90% of the total system water resided on the particle surfaces. As the water content rose above 275ppm, increasing fractions of the water were located in the reverse micelles. This same trend was found regardless of whether the water was introduced to the system by the particles or the surfactant, showing that the more-

hygroscopic particles could scavenge water from the reverse micelles. This saturation limit suggested that approximately 20 monolayers of water would be stabilized on the particle surfaces before excess water began to swell the reverse micelles.

The maximum mobility of the silica particles was then measured as a function of system water content at 10 different OLOA concentrations. The results are reproduced in Figure 1.15. It is worth noting that the plotted mobilities are absolute, as OLOA charged silica particles negatively.

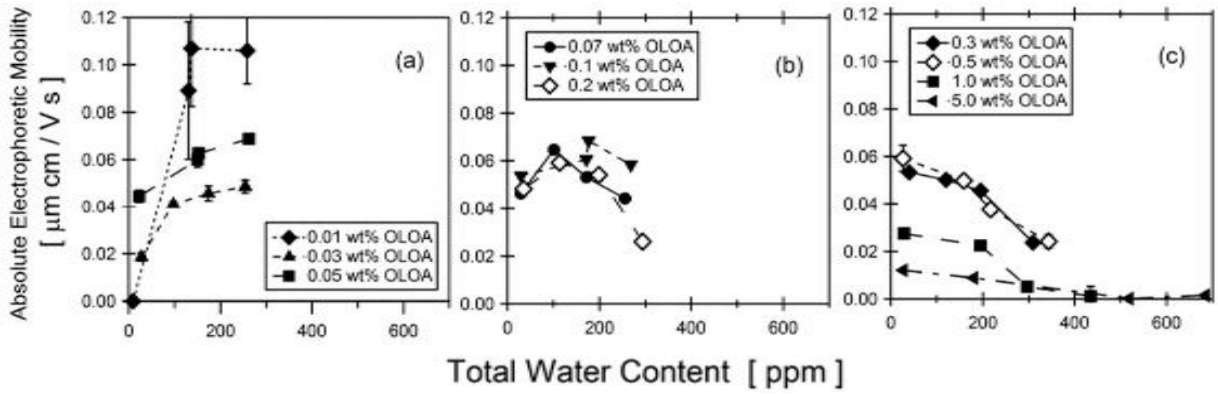

Figure 1.15. Maximum electrophoretic mobilities of silica particles as a function of system water content at OLOA concentration a) just above the CMC, b) near the concentration which resulted in the highest mobilities, and c) at concentration well above the CMC. (Reproduced from [22]).

Near the CMC, as shown in Figure 1.15a, the particle mobility was a strong function of water content, with increasing water contents resulting in increasing particle mobilities. The driest sample just above the CMC, 0.01wt%, exhibited negligible charging, but resulted the largest mobilities measured in this study with an increase in water content. It should be noted that for this system, which is just above the CMC, there was a significant amount of uncertainty in the measurements due to aggregation of the particles which resulted in settling. The increased charging is likely due to the water on the particle surface offering a more favorable environment for acid-base adducts to ionize, resulting in charges on the particle surface. Another explanation

of this behavior could be due to the increased core size of the reverse micelles. Larger polar cores offer a more favorable environment for charge stabilization, and could more readily stabilize the surfactant molecule in an ionized acid-base adduct.

At the highest surfactant concentrations, shown in Figure 1.15c, increasing water content and surfactant concentration resulted in decreasing particle mobilities. This is due to the fact that this region is dominated by electrostatic screening by charged reverse micelles in the bulk. Increasing both the number and core size of the reverse micelles increase the probability of charge disproportionation reactions, and therefore the number of screening charges in the bulk.

At intermediate OLOA concentration, shown in Figure 1.15b, the particle mobilities were almost independent of the system water content. In this region, there are a sufficient number of reverse micelles to stabilize a large number of surface charges on the particle, but not enough to result in significant electrostatic screening of the particle charge. This behavior is fortunate, as these concentrations regularly correspond to the maximum particle mobility for a given surfactant-particle pairing. This study concluded that while it is important to account for water content in charged apolar dispersions, its effect on the maximum particle mobility is negligible.

Noting that the slope of the surfactant charging curves, which appears to be related to the size of the reverse micellar cores, is important to the prediction of particle charging behavior, a study[29] investigated the particle charging behaviors of three Span surfactants, which all had the same chemically functional head group, but varied in the length and number of their tails. These surfactants varied in their hydrophilicity, which is quantified by a parameter known as the hydrophile-lipophile balance (HLB). The HLB is defined as 20 times the molecular weight of the hydrophilic portion of the molecule divided by its total molecular weight. Therefore, the more lipophilic a surfactant is, the lower its HLB value. The three Span surfactants studied were

Span 20, 80, and 85, which had HLBs of 8.6, 4.3, and 1.8 respectively. It was thought that the higher the HLB value, by virtue of the surfactant being more hydrophilic, the larger the polar core of the reverse micelle should be. The conductivity of solutions of the three surfactants were measured as a function of surfactant concentration and the results are reproduced in Figure 1.16a

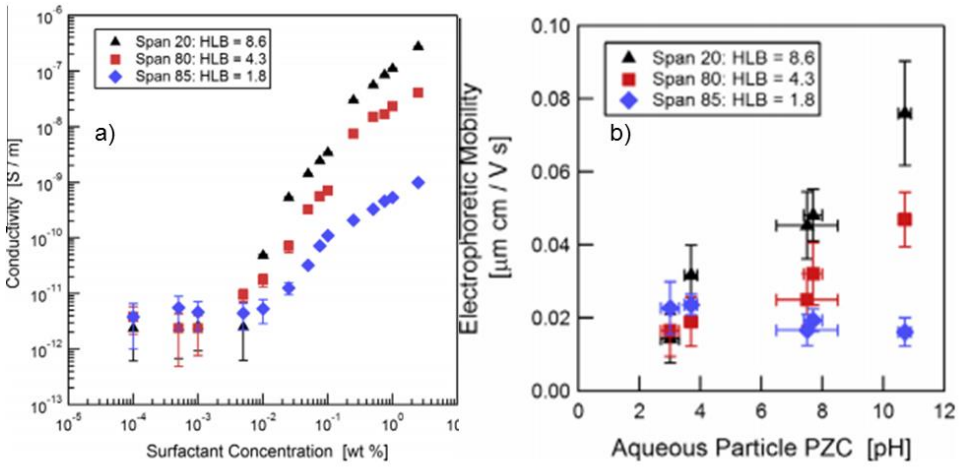

Figure 1.16. a) Conductivity as a function of concentration for the three Span surfactants. b) Maximum particle mobilities as a function of particle PZC, as charged by the three Span surfactants (Reproduced from [29]).

Span 20, with the highest HLB, had the largest conductivity of any of the three Span surfactants, and Span 85, with the lowest HLB, gave in the lowest conductivity. This is indicative of higher HLB surfactants having larger reverse micellar core sizes. As the core size of the reverse micelles increased, there is a higher probability of them undergoing disproportionation, resulting in more charges in the system and higher conductivities. Five mineral oxides – silica, titania, alumina, zin oxide, and magnesia – were then dispersed in solutions of the three Span surfactants, and the particle mobilities were measured. The maximum mobilities of each particle-surfactant pair are reproduced in Figure 1.16b. As the particle PZC increased, for all Spans, the maximum mobility of the particles also increased, suggesting an acid-base charging mechanism. Not only that, but as the HLB of the surfactant

increased, the maximum mobilities of particles also increased. This suggested that increasing the core size of the reverse micelles, as quantified by the surfactant HLB, offers a more favorable environment for charge stabilization, and therefore an ability to impart higher magnitudes of charge to the particle surfaces. One should note that while the increased core size offered a more stable environment for charges, the increased charge disproportionation also causes increased electrostatic screening. A study which investigated core size directly would need to be performed to determine its effect on particle charging. The slopes charging curves, shown in Figure 1.16b, also increase with increasing surfactant HLB. This can be related back to the charging curves presented in Figure 1.10, where AOT had a much steeper slope than Span 80 or OLOA.

The particle charging behavior of surfactants can now be understood to be a function of two parameters – the relative acid-base behaviors of the particle-surfactant pair, as given by aqueous particle PZCs and surfactant ABNs, and the slope of the surfactant charging curve, which is related to the surfactant's HLB. If the maximum particle zeta potential of a colloidal particle, as normalized by the surfactant's HLB value, is plotted against the difference between the particle PZC and the effective pH of the surfactant, a trend can be seen for all the systems studied in the author's laboratory. This can be summarized in Figure 1.17, which was reproduced from Gacek and Berg.[23]

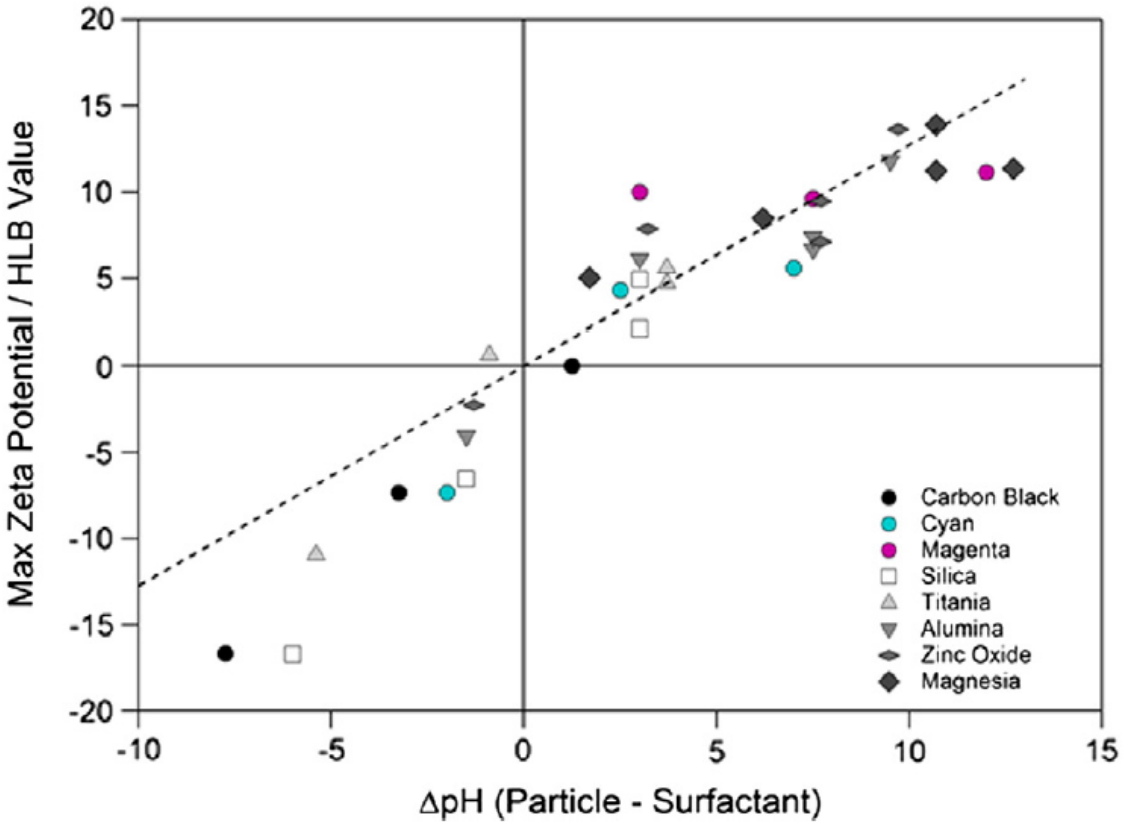

Figure 1.17. Particle charge normalized by HLB value of surfactant as a function of the difference between the effective surfactant pH and the aqueous particle PZC. (Reproduced from [23])

It is observed that for all particles more basic than the surfactant, a positive charge is imparted. Conversely, for all particles more acidic than the surfactant, a negative charge is imparted. Not only was this observed for the mineral oxide and pigment particles shown above, but for polymer particles, carbon blacks, and organic pigments as well.[14] While there are many more particle types left to study, to date all follow this acid-base mechanism of charging in apolar environments.

Still several questions remained unanswered. AOT is a surfactant which can form both regular and reverse micelles, yet no investigations had been made to determine the conditions in which it forms these structures. A study, presented in Chapter 2, was conducted which varied

the dielectric constant of the solvent and investigated the critical micelle concentrations of AOT across a spectrum of solvent compositions.

The several surfactants which form reverse micelles in apolar environments have all been extensively studied as particle charging agents, and found to charge particles by acid-base mechanisms. By exchanging the cation in the head group of AOT for di- and trivalent species, a new class of surfactants could be synthesized, which vary in cation electronegativity. These surfactants form reverse micelles, as verified by small angle x-ray scattering (SAXS), and were used to charge three mineral oxide particle types. This study is detailed in Chapter 3.

While micellization in apolar media is understood to be an enthalpic, rather than an entropic, phenomenon, no studies have investigated the temperature effects on this process. Electrophoretic printing relies on particles maintaining charge at elevated temperatures, from 60-150^{o}C. A two-fold study was performed using the Span series of surfactants, all six of which have the same, sorbitan head group, but vary in the length, number, and saturation of the tails. The CMCs of these surfactants were measured at five temperatures, and used to determine the thermodynamic properties of micellization – the free energy, enthalpy, and entropy of micellization. These same surfactants were used to charge basic magnesia particles at three temperatures to determine the effects of surfactant structure and temperature on particle charging. The results of this study, presented in Chapter 4, suggested that surfactant structure influenced the maximum mobility that could be imparted to particles, thus warranting a study of the reverse micellar structures. A small angle neutron scattering (SANS) study, detailed in Chapter 5, was then performed to determine the effect of surfactant structure on reverse micellar structure, in order to investigate its influence on particle charge.

The author had also conducted two studies which were not published. The first study, presented in Appendix A, investigated the effects of water content on the conductivity of reverse micellar solutions. An extension to the prevailing theory modelling conductivity of these solutions was presented and used to predict the behaviors of three systems. It was found that this extended theory predicted conductivities that were 30-100 times lower than experimental values, while the prevailing theory predicted conductivities 5-12 times lower than experimental values.

The second study, detailed in Appendix B, investigated electroviscous effects in apolar, colloidal dispersions. Viscosity measurements were used in combination with PALS data to determine that the charged particles caused increases in viscosity above what would be predicted for uncharged particles. It was found that equations which model electroviscous behavior in aqueous systems do not accurately predict this phenomenon in apolar media.

1.2 MATERIALS AND METHODS

1.2.1 *Materials*

Throughout the course of these studies, many of the same species have been used. To prevent repetition, these chemicals will be discussed only in this section.

1.2.1.1 Isopar-L

Isopar-L, supplied from Exxon-Mobil (Houston, TX) is the most commonly used solvent in these studies. A mixture of C_8 to C_{15} isoparaffins, with an aromatic content less than 30ppm, Isopar is an extremely apolar solvent with a dielectric of 2.0. At room temperature, this mixture has a viscosity of 1.6cP, which decreases to 1.1cP at 60^{o}C.[16]

1.2.1.2 Aerosol OT

Aerosol OT (AOT), also known as sodium dioctyl sulfosuccinate, is one of the most studied surfactants given its ability to form both normal and reverse micelles.[21] It is supplied as a waxy solid. In aqueous media, AOT forms ellipsoidal micelles with axes of 2.2nm and 1.2nm respectively.[30] In apolar environments, AOT forms spherical reverse micelles with radii of approximately 1.7nm.[31] Its chemical structure is shown below in Figure 1.18.

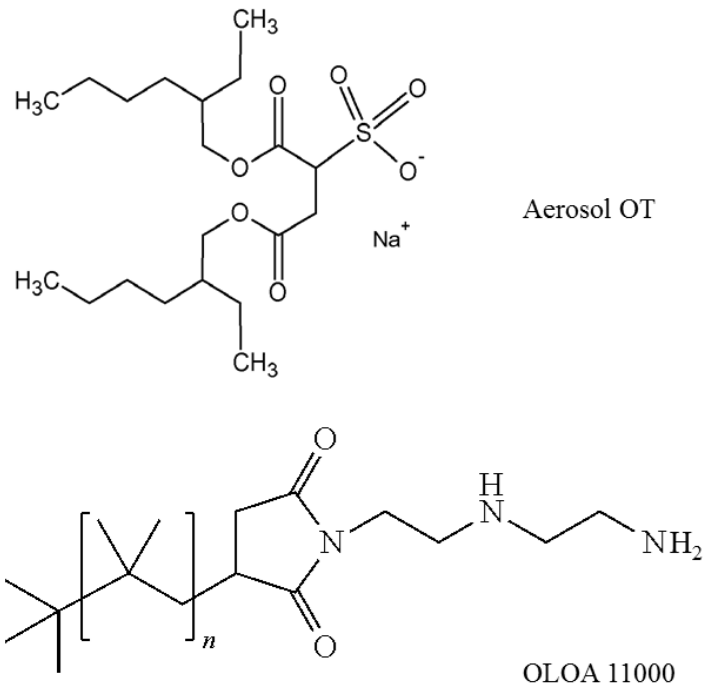

Figure 1.18. The chemical structures of Aerosol OT (top) and OLOA 11000 (bottom).

1.2.1.3 OLOA 11000

OLOA 11000 is a basic, polyisobutylene succinimide (PIBS) surfactant obtained from Chevron Oronite (San Ramon, CA). OLOA is supplied as a viscous, yellow fluid that is 72% active component dissolved in silicon oil. Due to the synthesis routes used to produce OLOA, the product contains "manifold"[18] components, including di-PIBS compounds and tails of varying length. However, the "active" structure is shown in Figure 1.18, with a reported molecular weight of 1200 g/mol and an *n*-value of approximately 30. It was found that OLOA reverse micelles had an average radius of 5.3nm.[32]

1.2.1.4 Span Surfactants

The Span series of surfactants was obtained from Sigma-Aldrich (St Louis, MO) and Uniqema (New Castle, DE). All species in this series consist of the same acidic, sorbitan head group while varying in number and length of tails. The chemical structures of the series are shown below in Figure 1.19.

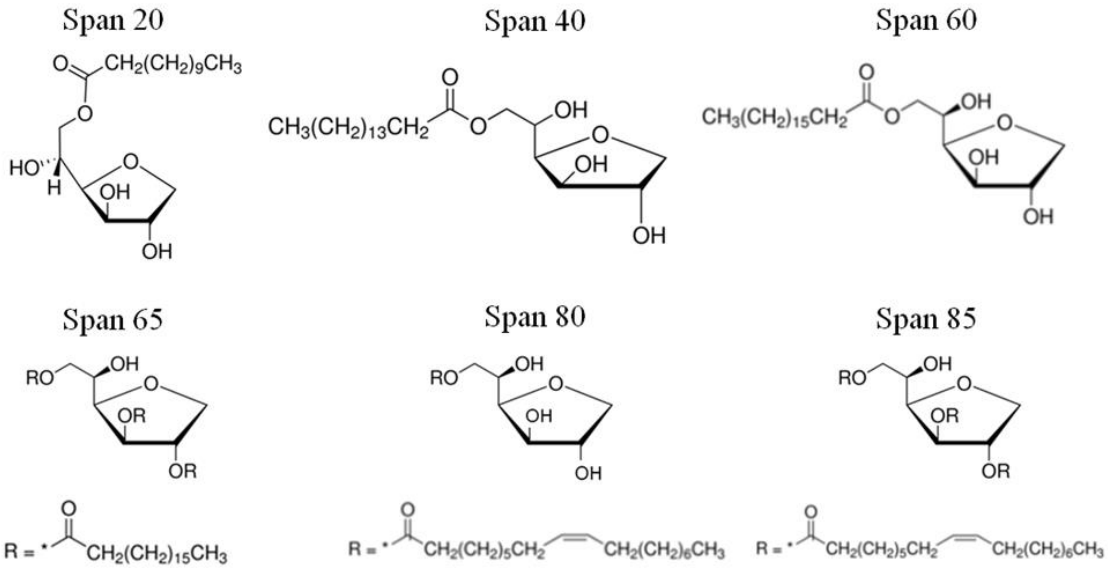

Figure 1.19. The chemical structures of the Span surfactants.

Span 20, 40, and 60 have linear, saturated C_{11}, C_{15}, and C_{17} tails. Span 65 is a three-tailed analog of Span 60. Span 80 has a C_{17} tail with a double bond in the tail. Span 85 is the three-tailed analog of Span 80. Span 20, 80, and 85 are all supplied as viscous liquids and are extremely soluble in apolar media, upward of 10wt% at room temperature. Span 40, 60, and 65 are all supplied as waxy solids and are only sparingly soluble at room temperature. These species are soluble up to 1wt% at 50°C.[16]

1.2.2 *Methods*

1.2.2.1 Conductivity measurements for the determination of the CMC

Conductivities of the samples are measured using a Dispersion Technologies (Bedford Hills, NY) DT-700 Nonaqueous Conductivity Probe. Samples are allowed to equilibrate in a constant temperature bath at five temperatures before being measured.

The conductivity of each sample is measured 20 times and the average plotted as a function of surfactant concentration. Error bars are calculated using the standard deviation of the 20 measurements. Before a CMC is reached, a region of negligible charging is observed, where the conductivity is near the lower limit of detectability by the instrument used and independent of surfactant concentration. Other researchers[15,33] have observed a region before the CMC, where premicellar aggregates contribute to the conductivity of the solution. While this region likely exists in the systems used in these studies, the lower limit of detection of the DT700 prevents its accurate measurement. There is evidence that ion and ion-pair formation can affect the conductivity of non-polar systems.[34,35] However, this theory is most applicable to nonaqueous systems of intermediate dielectric constants, such as alcohols, as well as to very high surfactant concentrations. Due to the very low dielectric constant of Isopar, as well as the low

surfactant concentrations used in these studies, increases in conductivity best follow the linearly-increasing behavior predicted by intermicellar disproportionation reactions.[15,18,21] The CMC is determined by finding the intercept of two, best-fit lines through these regions as shown schematically in Figure 1.20.

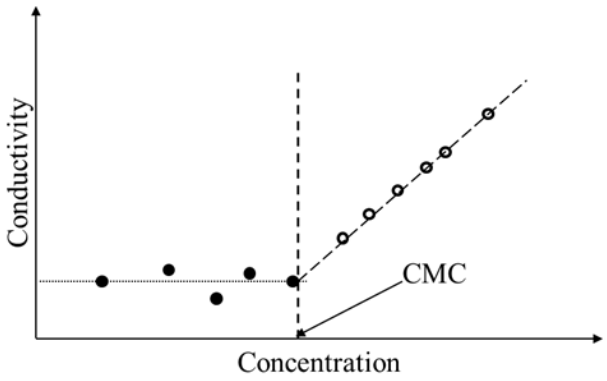

Figure 1.20. Schematic of CMC determination method.

1.2.2.2 Measuring water content by Karl-Fischer titration

Karl Fischer (KF) titration is a method by which a reagent- consisting of an alcohol, a base (RN), SO_2, and I_2 – is mixed with the sample of interest to determine its water content. This is accomplished by a series of two reactions, as shown below.

$$CH_3OH + SO_2 + RN \leftrightarrow [RNH]SO_3CH_3 \quad (1.9)$$

$$[RNH]SO_3CH_3 + I_2 + H_2O + 2RN \leftrightarrow [RNH]SO_4CH_3 + 2[RNH]I \quad (1.10)$$

In the first reaction, the sulfur dioxide, base, and alcohol react to form an intermediate. In the second reaction, the intermediate reacts with iodine and water *in equimolar amounts*. By tracking the amount of I_2 that has been converted to I^-, one can track the amount of water that has been consumed. This is accomplished using bipotentiometric titration, a method by which the extent of reaction is measured by changes in sample conductivity. In the second reaction,

$SO_3CH_3^{2-}$ is oxidized to $SO_4CH_3^{2-}$ and releases two electrons. In the same reaction, I_2 consumes the two electrons to reduce to two iodide ions. The generation and consumption of the electrons changes the electrical potential in the system, which is tracked by the electrodes. Once all of the water is consumed, the reaction ceases and the electrodes measure a large voltage drop.

There are two types of KF titration, volumetric and coulombic. Volumetric titration is best for samples containing 0.1-100% water, while coulombic titration is best for samples containing 0.001-0.1wt% water.[36] Given the extremely low water contents involved in apolar media, coulombic KF titrations using a Mettler Toledo (Columbus, OH) Karl Fischer Titrator. Since the previously described reactions occur in an aqueous environment, the reagents used for apolar studies contain small amounts of chloroform and xylene to aid in improving the solubility of the two phases.

1.2.2.3 Dynamic Light Scattering (DLS) for the determination of reverse micelle hydrodynamic radii

Multiple techniques can be used to gather size data from colloidal systems. However, due to its simplicity and ease of use, dynamic light scattering (DLS) is one of the most common. The hydrodynamic radius of a multitude of colloidal objects – micelles, polymer coils, particles – can be found anywhere within the range of 1nm up to a few microns.[37] This technique relies on the Brownian motion experienced by these objects, which in turn can be converted to a diffusion coefficient, and thus the hydrodynamic radius, R_H, as calculated by the Stokes-Einstein equation,

$$R_H = \frac{k_B T}{6\pi\eta D}, \tag{1.11}$$

where k_B is the Boltzmann constant, T is the absolute temperature, η is the solution viscosity, and D is the translational diffusion coefficient. By knowing the viscosity, temperature, and solvent

refractive index of a system, and measuring the diffusion coefficient, one can calculate the equivalent sphere hydrodynamic size of the objects.

As light passes through a sample, it is scattered by the colloidal objects dispersed within. The scattered light is detected usually by two detectors, one at 90^o and one a 173^o, for backscattering. The intensity of the scattered light varies with time, of the order of microseconds, due to the Brownian diffusion of the scattering colloids. The intensity, *I(t)*, as a function of delay time, τ, can be converted to an autocorrelation function, *C(*τ*)*, as

$$C(\tau) = \frac{\int_0^T I(t)I(t+\tau)\mathrm{d}t}{\langle I(t)I(t)\rangle} = 1 + \beta exp(-2\Gamma\tau), \tag{1.12}$$

where T is the total measuring time, β is a constant relating to the laser alignment in the instrument, and Γ is the decay constant. When the delay time is small, the correlation is high, since the colloids have not had time to diffuse far from the original position. As the delay time increases, the correlation decays exponentially due to the movement of the particles. It should be noted that Equation 1.12 holds only for monodisperse colloids. For polydisperse systems, the exponential decay is a series function. The decay constant is given by,

$$\Gamma = Dq^2, \tag{1.13}$$

where D is the diffusion coefficient and q is the magnitude of the scattering vector, given by

$$q = \frac{4\pi n}{\lambda}\sin{}^{\theta}/_{2}, \tag{1.14}$$

where n is the solvent refractive index, λ is the wavelength of scattering light, and θ is the detection angle. Once the diffusion coefficient is known, it can be plugged back into the Equation 1.11 to calculate the hydrodynamic radius.

This technique is of limited use for the measurement of reverse micelles in apolar media, however, due to the low refractive index difference between the hydrocarbon tails of the

surfactants and the hydrocarbon media. This, coupled with the small size of the reverse micelles, results in very weak scattering signals, which renders the extraction of data difficult. However, the technique has proven to be useful for the detection of reverse micelles and approximate sizing information.[38]

1.2.2.4 Phase Analysis Light Scattering (PALS) for determination of particle mobility and zeta potential

When charged particles are placed in an electric field, they undergo electrophoretic movement. The velocity at which these particles move depends on the degree of charge on the particles, or the zeta potential, and the strength of the electric field. Since the zeta potential, the electric potential at the slip plane of the particle, is not directly accessible, techniques have been developed to measure the electrophoretic mobility of particles. The electrophoretic mobility is the velocity of the particle as normalized by the applied electric field. Once the mobility has been measured, the zeta potential can be calculated using the appropriate theory. One of the most common techniques used is phase analysis light scattering (PALS).

PALS uses a split laser source to measure these mobilities. The first beam is scattered by the sample, which is placed in an electric field, before being collected at a detector. The second, reference, beam travels past the sample, often through a modulator, before being collected at the same detector. The scattered beam will be frequency shifted in accordance with the Doppler effect. The reference beam will also be frequency shifted, but by a known amount due to the modulator. When the two beams are combined at the detector, an autocorrelation function, similar to those used by DLS, can be used to extract the colloidal velocities, and therefore electrophoretic mobilities, which caused the frequency shift.

Once the electrophoretic mobility is measured, it can be used to calculate the zeta potential. One of two limiting cases may be identified. When particle radius, *a*, is large with respect to the Debye length, κ^{-1}, the "thickness" of the electric double layer around a particle, such that $\kappa a \geq 200$, the Helmholtz-Smoluchowski approximation is used. This applies to aqueous dispersions of micron-sized particles with salt concentrations higher than several millimolar. However, when the particles are small with respect to the electric double layer, $\kappa a \leq 0.1$, such as in dispersions of nanoparticles in apolar media, the Hückel approximation, given by

$$\zeta = \frac{3\eta U_E}{2\varepsilon}, \tag{1.15}$$

where ζ is the zeta potential, η is the solution viscosity, U_E is the measured electrophoretic mobility, and ε is the dielectric of the solvent. The Helmholtz-Smoluchowski approximation differs by a factor of 3/2. For cases where $0.1 \leq \kappa a \leq 200$, a more general method must be used to extract the zeta potential.[19] Given that all studies in this work had been conducted in apolar environments with sub-micron particles, the Hückel approximation is valid. Electrophoretic mobilities and zeta potentials are measured using a Brookhaven (Holtsville, NY) ZetaPALS instrument.

1.2.2.5 Small angle x-ray scattering (SAXS) and small angle neutron scatterings (SANS) for structural information of reverse micelles

All small angle scattering (SAS) techniques have the same general set-up. Radiation is emitted from a source, passes through a sample, and the scattered radiation is collected in a two dimensional array for analysis, as show in Figure 1.21.

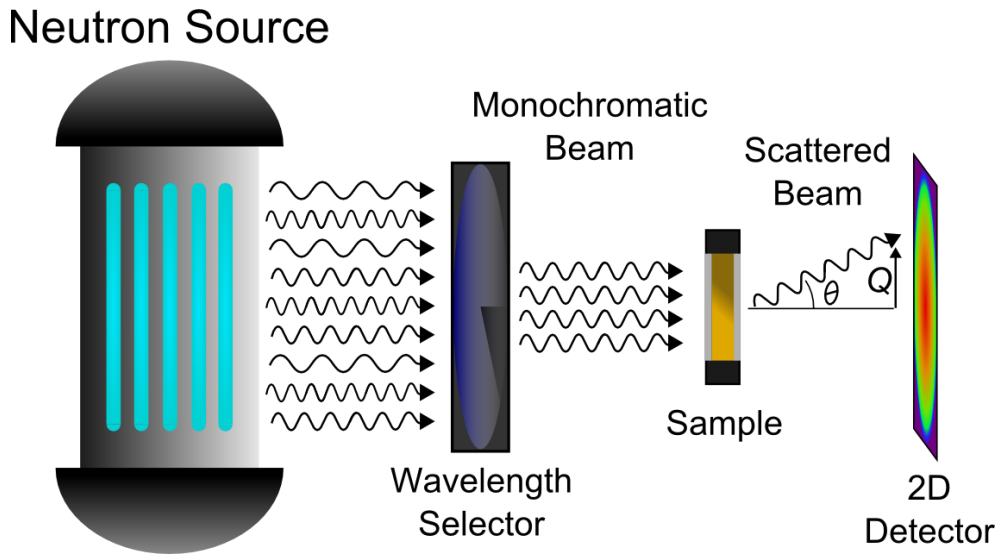

Figure 1.21. A simplified small angle scattering system. A radiation source is monochromated, scatters off a sample, and is collected at a detector.

The way the radiation scatters depends on the type of radiation being used, and can be characterized by a scattering length. In light scattering, the photons scatter due to refractive index differences. In x-ray scattering, the photons are scattered by the electron clouds of the atoms. Neutrons, conversely, are scattered by the atomic neucli.[39] In SAXS experiments, since the x-rays are scattered by the electron cloud, larger elements scatter more strongly. In SANS, however, there is no trend with atomic size. Interestingly, isotopes of the same element scatter very differently. Where hydrogen actually has a negative scattering length, meaning the scattered beam is out of phase with the incident beam, deuterium has a larger in magnitude, positive value. Some visual examples of differences in scattering length can be seen in Figure 1.22, reproduced from The SANS Toolbox.[40]

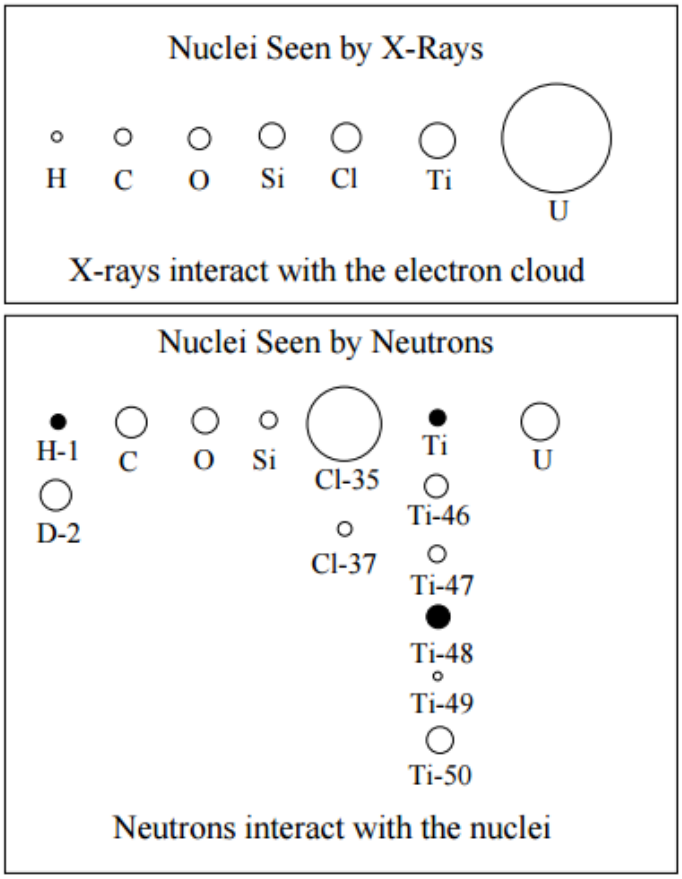

Figure 1.22. Comparison of scattering lengths of several elements. Dark circles represent negative values.

In SAXS and SANS, radiation can also be scattered coherently or incoherently. Coherent scattering refers to radiation that varies in intensity as a function of the scattering vector, q, as given for low scattering angles by

$$q = \frac{4\pi n}{\lambda}\sin\left(\theta/_2\right) = \frac{2\pi n}{\lambda}\theta, \tag{1.16}$$

where θ is the detection angle and λ is the wavelength of the radiation. Incoherent scattering, however, is independent of the scattering vector and does not give any information about the sample. In SANS, hydrogen has a large incoherent scattering length. Incoherent scattering is a constant background and can interfere with the analysis of data at higher-q values.

To obtain structural information from scattering data, the coherent, absolute scattering intensity, $\frac{d\Sigma(q)}{d\Omega}$ must be correlated to the scattering vector. For an incompressible system, the absolute scattering intensity of a dispersion of particles can be written as

$$\frac{d\Sigma(q)}{d\Omega} = \left(\frac{N}{V}\right) V_p^2 \Delta\rho^2 P(q) S(q), \tag{1.17}$$

where *N/V* is the number density of particles, V_p is the individual particle volume, $\Delta\rho$ is the difference in scattering length densities of the solvent and particles, *P(q)* is the single particle form factor, and *S(q)* is the inter-particle structure factor. The scattering length density, ρ, is the material's scattering length, *b*, divided by its molecular volume. The scattering length is a measure of a species' propensity to scattering neutrons, with positive values corresponding to coherent scattering, and negative values corresponding to incoherent scattering. The scattering length of a material can be calculated as

$$b = 2\pi \frac{1-n}{\lambda^2 \rho_m}, \tag{1.18}$$

where *n* is the material's refractive index, ρ_m is the material density, and λ is the neutron wavelength. The form factor is given for the shape of the individual particles. The structure factor is given by how the particles interact with one another in the solvent, whether by electrostatics, hard-sphere interactions, or in very dilute conditions, not at all. Form factors and structure factors have been developed for a wide variety of shapes and interaction potentials.

In the case of reverse micelles in an apolar environment, the surfactant tail groups and the solvent are chemically similar, both hydrocarbons. For SAXS, this means that the electron densities of the tails and solvent are very similar, and thus the outer shell of the reverse micelles is indistinguishable from the solvent. If the surfactant head groups are electron dense enough, there may be enough contrast with the solvent that SAXS can be used to determine core size. In SANS, however, it is to be noted that hydrogen and deuterium have very difference scattering

lengths. If a deuterated solvent is used, the shell of the reverse micelle and the solvent will have a significant contrast, and the scattering data can be used to determine the shell structure of the reverse micelle. This technique is known as contrast variation, by which certain components are selectively deuterated or hydrogenated in order to obtain the desired contrast.

Chapter 2. THE MICELLIZATION BEHAVIOR OF AEROSOL OT IN ALCOHOL/WATER SYSTEMS

Michor, E.L. and Berg, J.C. *Langmuir* **2014**, *30*(42), pp 12520−12524

2.1 ABSTRACT

This chapter examines the effects of solvent composition on the micellization behavior of the surfactant Aerosol OT. The critical micelle concentrations of AOT in the pure solvents methanol, ethanol, propanol, and isopropanol were measured using conductiometric techniques. These solvents were then mixed with water to create solvent spectra from pure alcohol to pure water in twelve increments. Critical micelle concentrations were measured at each solvent composition. Dynamic light scattering was used to verify the presence or absence of micelles in the solvent mixtures. It was found that inverse micelles exist over a range of solvent compositions where ε_{eff} <48 with CMC's increasing with increasing solvent polarity. Micellization was found not to occur when 48< ε_{eff} <80. Regular micelles formed in pure water, with the measured CMC agreeing with the literature value of 2.25mM.

2.2 INTRODUCTION

The use of surfactants as charge control agents in nonpolar media has long been studied. Aerosol OT (dioctyl sodium sulfosuccinate) is of considerable interest because it is soluble in both nonpolar solvents and water.[21] This gives AOT the potential to form both regular and reverse micelles. Small Angle Neutron Scattering (SANS) studies have shown that in water, AOT micelles form ellipsoids with a semi-major axis of 2.2nm and semi-minor axes of 1.2nm.[30] These structures are affected by salt concentration, with the aggregation number increasing with

salt content. In apolar systems such as decane, AOT forms spherical reverse micelles of approximately 1.7nm in radius.[31] However, little is known about micellization in media of intermediate composition.

A previous study by Hollamby, et al.[41] investigated the effects of solvent properties on the micellization behavior of AOT using small angle neutron scattering. In that study, the solvent was varied from water to 1,4 dioxane (ε=2.2) in increments of 25wt%, then from 1,4 dioxane to cyclohexane (ε=2.0) in 25wt% increments. It was found that AOT forms regular micelles in high dielectric media, but as the dielectric constant of the solvent decreases below 60, AOT stops forming micelles. As the dielectric constant drops below 20, reverse micelles begin to form. However, a precise range of dielectrics was not found in this study due to the fact that only four systems were measured above a dielectric constant of 20. In order to investigate micellization in the dielectric region between aqueous and apolar, compounds with intermediate dielectric constants, also known as leaky dielectrics, are needed. Low-molecular weight alcohols (methanol, ethanol, 1, and 2-propanol) are compounds that fit this classification. Not only do these alcohols possess intermediate dielectric constants, but they are also fully miscible with water. This property allows a systematic variation between water and the pure alcohol, and therefore small variations in dielectric constant of the mixed solvents.

This study investigated the critical micelle concentration (CMC) of AOT in these mixed-solvent systems as a function of composition, and therefore of dielectric constant. Dynamic light scattering (DLS) was used to corroborate the presence or absence of micelles in the systems. Due to the low refractive index difference and small size of AOT micelles, as well as the knowledge that AOT micelles are not always spherical, DLS was not intended as a measurement of true size or structure of the AOT micelles.

2.3 EXPERIMENTAL

2.3.1 *Chemicals*

Solid, anhydrous sodium dioctylsulfosuccinate (AOT) was purchased from Fischer Scientific and used as received. Isopropanol (IPA) was purchased from Macron Chemicals. 1-propanol (PrOH) was purchased from Fischer Scientific. Ethanol (EtOH) was purchased at 200 proof from Decon Labs. Methanol ≥99.9% (MeOH) was purchased from Sigma Aldrich. All alcohols were dried for 12 hours using molecular sieves. Deionized water was generated in-house and used without any further purification. For each alcohol used, a solvent mixture was made at ten increments, ranging from pure water to pure alcohol (i.e. 0 ...100mol% alcohol). The dielectric constants for all solvents and solvent mixtures are given in Table 2.. For each solvent composition, a series of 15 AOT concentrations was made ranging from approximately $2x10^{-2}$ to 22mM AOT. We did not exceed 22mM AOT in the samples due to the solubility limit of AOT (~24mM)[42] in water.

2.3.2 *CMC Determination by Conductivity*

A Mettler-Toledo (Columbus, OH) SevenCompact Conductivity meter was used to determine the conductivities of the AOT solutions. Two conductivity probes were used in this study, the Mettler-Toledo InLab 738 and 741, which had ranges of $10\text{-}10^{6}$ and 10^{-3}-500μS/cm respectively. The appropriate probe was used for the conductivity range of each solvent mixture. None of the systems studied fell outside these ranges. For each solvent composition, a plot of conductivity vs AOT concentration was generated. Two linear regions were established and trendlines were created for each region. The CMC was determined by calculating the intersection of the two trendlines. This technique for CMC determination is outlined

elsewhere.[19] As an example. Figure 2.1 plots the conductivity of AOT in isopropanol as a function of concentration.

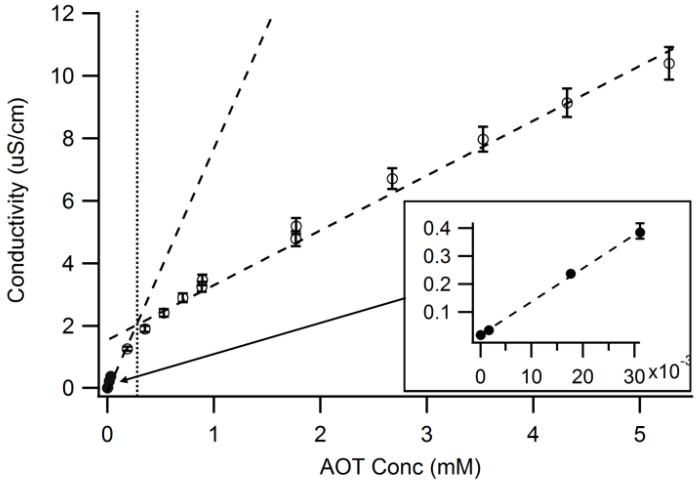

Figure 2.1. Conductivity of AOT in IPA. Pre-micellar data points are given by (●), while post-micellar data points are given by (○). Best fit lines (---) are shown with the vertical line corresponding to the CMC. The inset shows the premicellar region at a higher magnification.

Other systems indicating a CMC behaved similarly to isopropanol. If the conductivity curve yielded a single straight line, with no break in slope, it was inferred that no micellization occurred in the system.

2.3.3 *Micelle Presence by Dynamic Light Scattering*

Validation of the presence or absence of micelles was determined by a Malvern (Malvern, UK) Nano Zetasizer HT dynamic light scattering (DLS) instrument. The technique was used only as supportive evidence of the presence of structures larger than AOT monomers. Samples were filtered using Whatman 450nm nylon filters. The correlation function was converted to intensity distributions by the Zetasizer Nano Software. In most cases, significant noise existed in the correlation function at time scales longer than 10^4 μs. This resulted in the

software suggesting the presence of 1-100μm structures. Since the samples were filtered through a 450nm sieve, it was determined that any intensity peaks corresponding to larger values could be ignored. Since an AOT molecule is approximately 1.2nm in length[42], micelles were determined to be present if the peak was present at that value or larger.

In order to determine that DLS was an appropriate technique to determine the presence of micelles in a solvent, two systems with known AOT micelle sizes were measured. AOT in water is known to form ellipsoidal micelles with axes of 2.2nm and 1.25nm respectively.[30] A system of 20.2mM AOT in water was prepared and measured by DLS. It was found that there was a peak at 2.01nm, 9% smaller than the literature value of the major axis determined by SANS. AOT in decane is known to form spherical inverse micelles with a radius of 1.74nm.[31] A system of 14.8mM AOT was prepared in decane and measured by DLS. It was found that there was a peak at 1.85nm, 6% larger than the literature value determined by SANS. Figure 2.2 plots the scattered intensity, as a percent of total scattering, as a function of the hydrodynamic radii of the scatterers for both of the former systems, and indicate the presence of structures of the expected size.

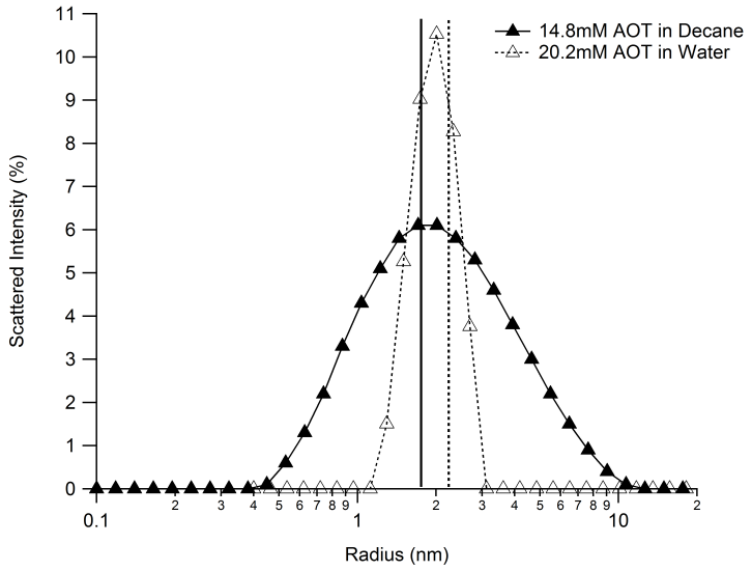

Figure 2.2. DLS determined hydrodynamic radii for 14.8mM AOT in decane (-▲-) and 20.2mM AOT in water (-Δ-). The vertical solid line indicates the literature radius for AOT in decane and the vertical dashed line represents the literature value for AOT in water.

In order to determine the presence or absence of micelles or other multimolecular structures in the systems of interest, it also needed to be determined whether DLS could detect their presence as a system crosses its CMC. Solutions of AOT in water were prepared at concentrations ranging from 0.22mM to 15.73mM. DLS measurements taken at seven concentration increments within this range are plotted in Figure 2.3.

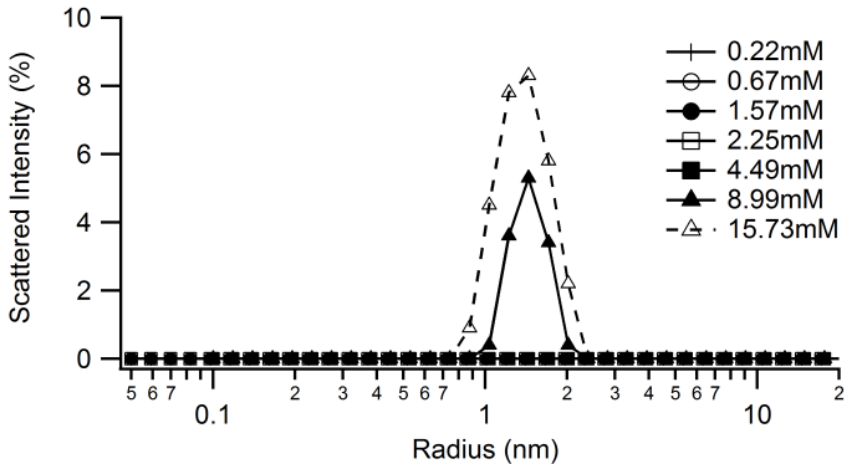

Figure 2.3. Scattered intensity as a function of scatterer radius for a series of AOT solutions in water. No peaks are present from 0.22mM AOT to 4.49mM AOT. At 8.99mM AOT (-▲-), 1.44nm micelles are detected.

At the lowest concentrations of AOT, no peaks were detected up to 100nm. As the concentration increases up to and past the CMC of 2.25mM[41], still no peaks were detected. At 8.99mM, a micelle peak appears at 1.44nm and increases in scattered intensity at 15.73mM AOT. This series shows that DLS does not pick up any scattering at or below the CMC which could interfere with micellar scattering peaks. However, it is necessary that the concentration of micelles be high enough to allow DLS to detect their presence.

It was determined that DLS could detect the formation of micelles in a system as well as detect the presence of normal and inverse micelles within 10% of literature radii values. However, it must be stressed that this study did not intend to use DLS to measure size or structure characteristics of the AOT micelles, but only to determine whether or not micelles were present in a given solvent mixture.

2.3.4 *Results and Discussion*

The conductivity data used to calculate the CMCs for the pure alcohol series are shown in Figure 2.4.

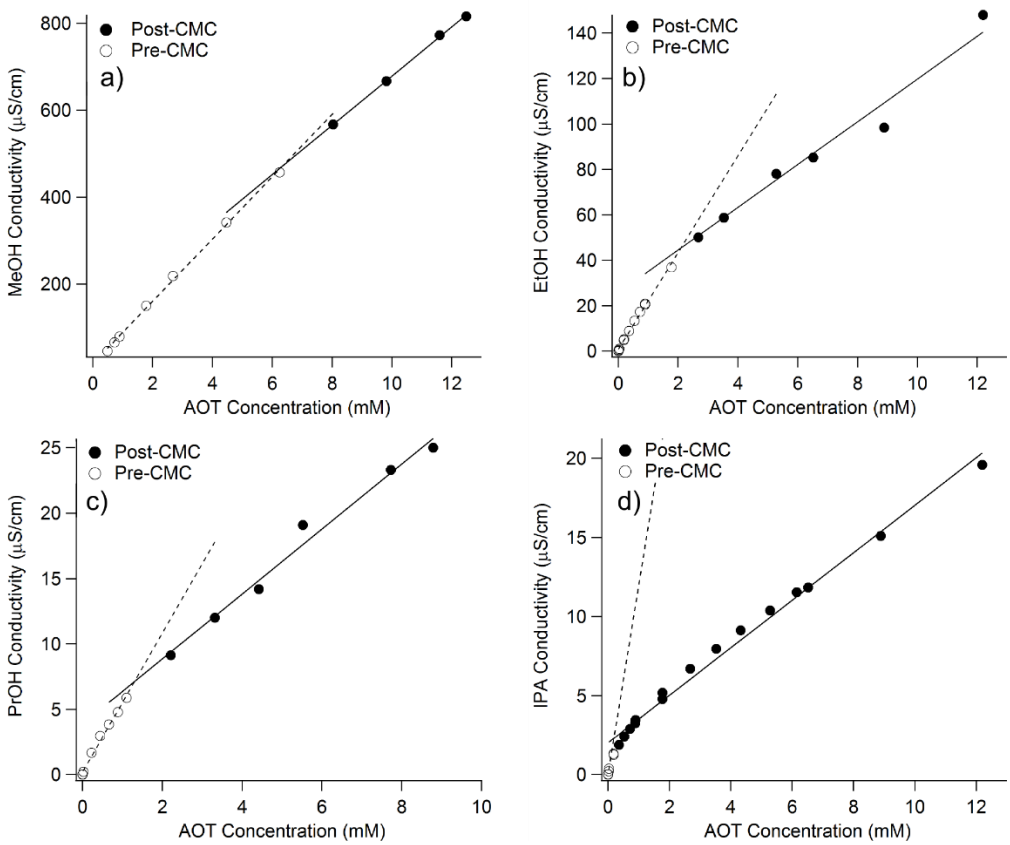

Figure 2.4. The conductivity data for AOT in a) MeOH, b) EtOH, c) PrOH, d) and IPA as a function of the molar concentration of AOT. Post-CMC data is given by filled markers and pre-CMC data is given in hollow markers. Linear fits for both pre- and post-CMC data are shown with dashed and solid lines respectively.

These graphs are representative of each alcohol/water solvent system. As the dielectric constant of the solvent mixture increases, the difference in pre- and post-CMC conductivity slopes decreases, making it increasingly difficult to determine a CMC, if one is indeed present. This decreasing slope change can be observed in Figure 2.4, where for IPA, the slope changes from 12 to 1.5µS/cm/mM, while in MeOH, the slope changes from 72 to 65µS/cm/mM.

Figure 2.5 shows the CMC's of AOT as a function of the solvent composition for all aqueous alcohol systems investigated.

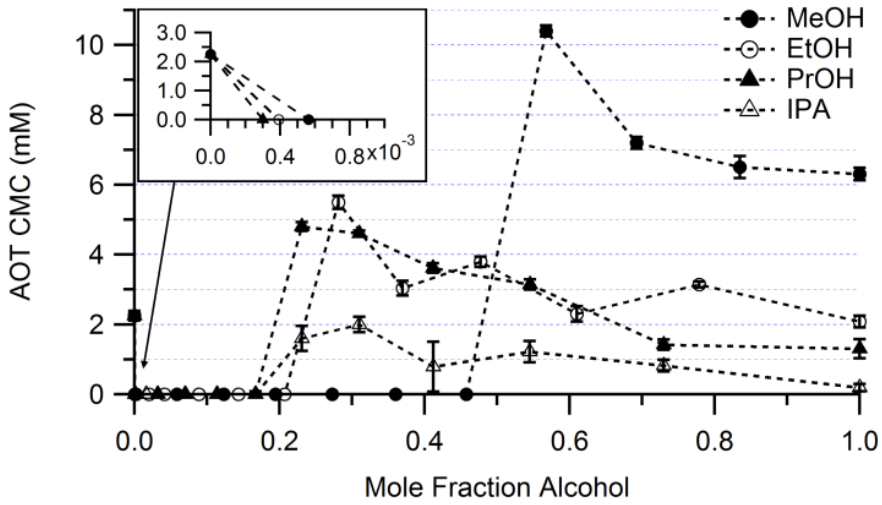

Figure 2.5. The CMC's of AOT for MeOH (-●-), EtOH (-○-), PrOH (-▲-), and IPA (-Δ-) as a function of the mole fraction of alcohol in the solvent mixture. The dashed lines are intended to guide the eye. CMC's of zero (0) simply denote the absence of micelles in a system. The inset shows the lowest alcohol content systems at higher magnification.

The commonly used Lichtenecker's equation for calculating the dielectric constant of a mixture[43] can convert the mole fraction of the solvents to effective dielectric constants for each solvent mixture and the CMC's can be plotted as shown in Figure 2.6.

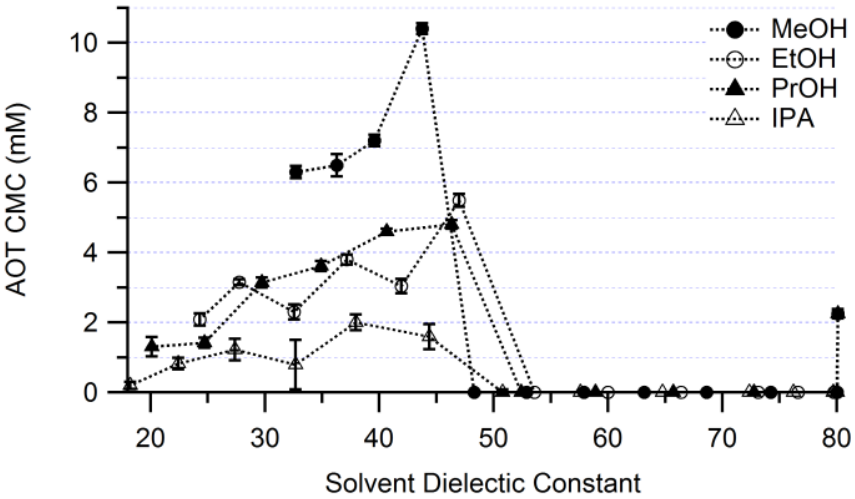

Figure 2.6. The CMC's of AOT for MeOH (-●-), EtOH (-○-), PrOH (-▲-), and IPA (-Δ-) as a function of the effective dielectric constant of each solvent mixture. The dashed lines are intended to guide the eye. CMC's of zero (0) simply denote the absence of micelles in a system.

In pure water a CMC of 2.25 mM was calculated, which agrees with literature values. As soon as a small amount of alcohol (0.03 mol%) was added, no micellization was observed to occur. It should be noted that in Figure 2.5 and Figure 2.6 that a CMC of zero designates that no micellization occurs in that system. No micellization occurred until approximately 23mol% for PrOH and IPA, 28mol% for EtOH, and 57mol% for MeOH. At this point inverse micelles form at CMC's higher than that of the pure alcohols. As the solvents became richer in alcohol, the CMC of AOT decreased until the solvent was pure alcohol. As the alcohol became less polar, the CMC of AOT decreased from 6.3mM in MeOH, 2.1mM in EtOH, 1.3mM in PrOH, to 0.2mM in IPA. This decrease can be explained by the primarily enthalpic nature of reverse micelle formation, explained in further detail later.

While the same trends can be seen in Figure 2.5, it becomes apparent in Figure 2.6 that a region of dielectric constant exists in which AOT cannot micellize, specifically between a dielectric of 48 and 80. Below ε_{eff} =48, reverse micelles form with a CMC that decreases as the solvent dielectric constant decreases.

While inverse micelles exist over a range of dielectrics in this system, Figure 2.5 shows that regular micelles exist only in pure water. The addition of $5.6x10^{-2}$ mole percent of alcohol results in the inability of AOT to form micelles, as detectable by DLS or conductivity measurements. With the addition of small amounts of alcohol into the system, it is possible that the alcohol molecules can preferentially orient themselves around the AOT tail groups. At the CMC of AOT in water, the addition of $5.6x10^{-2}$ mol% methanol, the lowest concentration of methanol used in this study, results in about 26 methanol molecules per AOT molecule. The preferential orientation of the alcohol molecule would create a local environment around the AOT tail groups that is more favorable than that of water. Since water is not locked up in the

ordered structures surrounding the tails, the entropic driving force for micellization is diminished. Table 2. summarizes the CMC's and dielectric constants for each solvent composition studied. CMC's of zero (0) designate that no micellization occurred.

Table 2.1. Summary of CMC's and Effective Dielectric Constants for Alcohol/Water Systems

Methanol												
Mol Fraction	0	$5.6x10^{-4}$	$5.9x10^{-2}$	$1.2x10^{-1}$	$1.9x10^{-1}$	$2.7x10^{-1}$	$3.6x10^{-1}$	$4.6x10^{-1}$	$5.7x10^{-1}$	$6.9x10^{-1}$	$8.4x10^{-1}$	1
ε_{eff}	80.1	80	74.2	68.6	63.2	57.9	52.9	48.3	43.8	39.6	36.3	32.7
CMC (mM)	2.2±0.1	0	0	0	0	0	0	0	10.4±0.2	7.2±0.2	6.5±0.3	6.3±0.2
Ethanol												
Mol Fraction	0	$3.9x10^{-4}$	$4.2x10^{-2}$	$8.9x10^{-2}$	$1.4x10^{-1}$	$2.1x10^{-1}$	$2.8x10^{-1}$	$3.7x10^{-1}$	$4.8x10^{-1}$	$6.1x10^{-1}$	$7.8x10^{-1}$	1
ε_{eff}	80.1	80	73.2	66.4	60	53.6	47	41.9	37.2	32.5	27.8	24.3
CMC (mM)	2.2±0.1	0	0	0	0	0	5.5±0.2	3.0±0.2	3.8±0.1	2.3±0.2	3.1±0.1	2.1±0.2
Propanol												
Mol Fraction	0	$3.0x10^{-4}$	$3.2x10^{-2}$	$7.0x10^{-2}$	$1.1x10^{-1}$	$1.7x10^{-1}$	$2.3x10^{-1}$	$3.1x10^{-1}$	$4.1x10^{-1}$	$5.4x10^{-1}$	$7.3x10^{-1}$	1
ε_{eff}	80.1	80	72.8	65.7	58.9	52.4	46.3	40.6	34.9	29.7	24.7	20.1
CMC (mM)	2.2±0.1	0	0	0	0	0	4.8±0.1	4.6±0.1	3.6±0.1	3.1±0.1	1.4±0.1	1.3±0.3
Isopropanol												
Mol Fraction	0	$3.0x10^{-4}$	$3.2x10^{-2}$	$7.0x10^{-2}$	$1.1x10^{-1}$	$1.7x10^{-1}$	$2.3x10^{-1}$	$3.1x10^{-1}$	$4.1x10^{-1}$	$5.4x10^{-1}$	$7.3x10^{-1}$	1
ε_{eff}	80.1	76.2	72.4	64.8	57.6	50.8	44.4	37.9	32.7	27.4	22.4	18.2
CMC (mM)	2.2±0.1	0	0	0	0	2.0±0.1	1.6±0.1	2.0±0.2	0.8±0.7	1.2±0.3	0.8±0.2	0.2±0.1

DLS was employed to ensure that micelles were present in the pure alcohols and that no micelles were present in the intermediate dielectric range. Solvents were mixed at 6-12 mol% alcohol/water and 17.7mM AOT. The DLS results are shown in Figure 2.7.

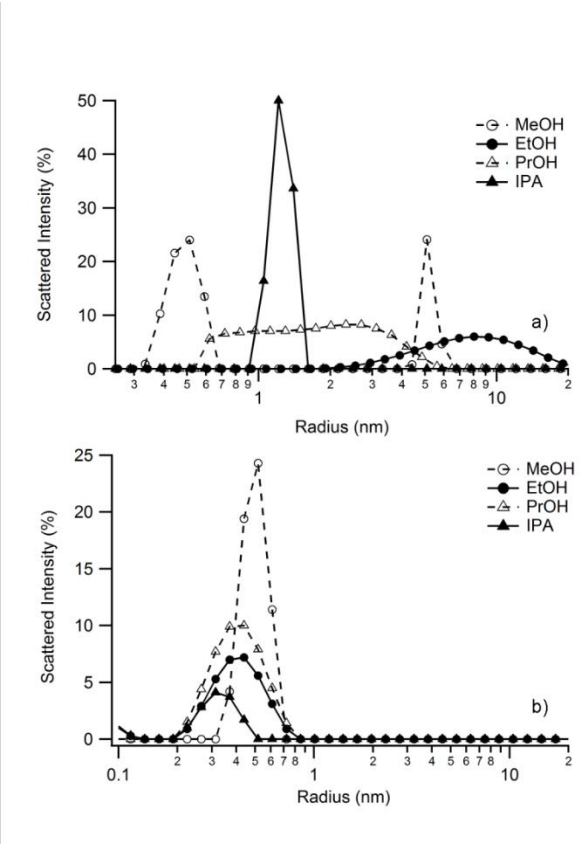

Figure 2.7. a) Scattered intensity for solution of 17.7mM AOT in pure alcohols. Micelles in IPA (-▲-) were found with radii of 1.3nm, in PrOH (-Δ-) with a range of sizes with a peak at 2.7nm, in EtOH (-●-) at 6.8nm, and MeOH (-○-) at 5.1nm. A submicellar peak was found in MeOH at 0.5nm. b) Scattered intensity for 17.7mM solutions of AOT in 6-12mol% alcohol/water solutions. No peaks existed for scatterers with radii between 1.2 and 20nm.

From Figure 2.7, it was determined that AOT forms micelles in all four pure alcohols, and that it does not form micelles in intermediate water-rich alcohol/water mixtures. The submicellar peaks present in this intermediate range could be small complexes of two or more AOT molecules or even single AOT molecules, but as the radii of these scatterers are less than the length of an AOT molecule it cannot be said that they are true micelles. It is also of note that the Malvern Zetasizer has a lower detection limit of 0.3nm. A follow-up study using SANS is intended to elucidate how solvent composition influences these micellar structures.

In the pure alcohols, the CMC decreases as polarity of the alcohol decreases, with AOT in MeOH having the highest CMC and in IPA, the lowest. This is to be expected, as the formation of a reverse micelle is primarily an enthalpic process. In apolar solvents, the dipole-dipole (AOT head group) interactions are more pronounced than they are in solvents of higher polarity. Therefore, as the polarity of the solvent decreases, the head group – head group interactions increase, and the formation of a reverse micelle becomes more favorable.

As the solvent mixture becomes increasingly polar with the addition of water to an alcohol, not only does the head group interaction strength become less prevalent, but the chance of the AOT molecule dissociating also increases. If an AOT molecule is charged before micellization, there will be repulsive forces further decreasing the favorability of micellization.

One can calculate the probability, p, of a neutral AOT molecule dissociating in an in infinite medium of dielectric constant, ε, as,

$$p = \mathrm{C} \cdot exp\left(\frac{-Z^2e^2}{4\pi\varepsilon\varepsilon_o kT}\left(\frac{1}{r_+} + \frac{1}{r_-}\right)\right), \tag{2.1}$$

where Z is the valence of the charge, e is the fundamental charge, ε_o is the dielectric permittivity of a vacuum, k is Boltzmann's constant, T is the absolute temperature, r_+ and r_- are the radii of the sodium cation and AOT anion respectively, and C is a constant. The constant C is a prefactor which accounts for the bond energy of a sodium ion bonded to the sulfosuccinate anion. While this could be included in the exponential, the bond energy is constant regardless of environment, and therefore can be factored out as a constant. Assuming a monovalent sodium cation, Na^+, of radius 1.1nm, a singly charged AOT anion of radius 5.5nm, and a system at 298K, Equation 2.1 can be used to plot the probability of sodium dissociation (p/C) as a function of solvent dielectric constant as shown in Figure 2.8.

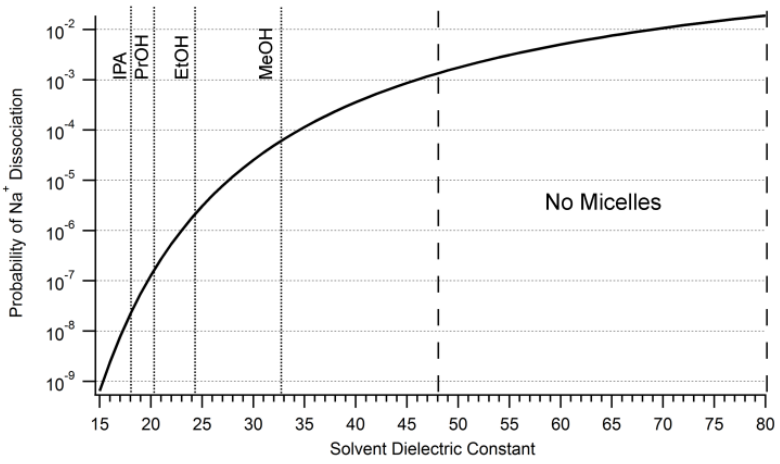

Figure 2.8. Probability of a sodium ion dissociating in an infinite solvent as a function of solvent dielectric constant. The vertical dotted lines (⋮) represent the dielectric constants of each of the four alcohols. The area between the vertical dashed lines (---) represents the dielectric range in which no micelles were observed.

An AOT molecule in IPA has only a 2.2×10^{-8} chance of dissociating, while in MeOH this chance rises to 6.6×10^{-5}. The greater probability of charged AOT molecules corresponds to a lower affinity for AOT to form an inverse micelle. This trend is also true for each alcohol as water is added and the solvent polarity increases. The increased polarity, and thus increased probability of charged AOT molecules, corresponds to an increased CMC for AOT in these systems. According to Walden's rule, the product of the molar conductivity and the viscosity should be constant for the same ions in different solvents. Plotting the conductivities of 1.8mM solutions of AOT in all solvent mixtures multiplied by the solvent's viscosity[44–47] vs the probability of a sodium ion dissociating in the given solvent gives Figure 2.9.

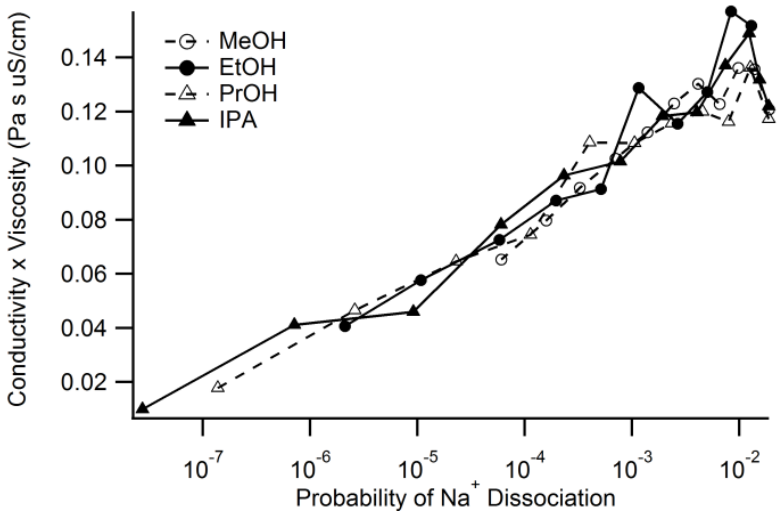

Figure 2.9. Viscosity normalized conductivity of 1.8mM AOT solutions in MeOH/water (-●-), EtOH/water (-○-), PrOH/water (-▲-), and IPA/water (-Δ-) mixtures as a function of the probability of a Na^+ ion dissociating as calculated in Figure 2.8.

It can be seen that as the probability of a sodium ion dissociating increases, the viscosity normalized conductivity increases. The AOT concentrations in every solvent mixture are the same, but the concentration of dissociated AOT increases as the alcohol-rich solvent becomes more water-rich.

2.4 CONCLUSIONS

The micellization behavior of Aerosol OT in alcohol/water mixtures has been studied through conductiometric methods and DLS. Four alcohols - methanol, ethanol, propanol, and isopropanol – were mixed with water to create spectra ranging from pure water to pure alcohol. Critical micelle concentrations were measured at increments across each alcohol/water spectrum. DLS was then used to verify the presence or absence of micelles at multiple solvent compositions. The polarity of the solvent has been found to affect the CMC as well as whether or not AOT can form micelles. Inverse micelles existed in pure alcohols and in solvent mixtures of dielectric constants up to 48. AOT exhibited increasing CMC's in each of the four alcohols

with increasing polarity of the solvent mixture. CMC also increased with increasing polarity of the pure alcohol, with $CMC_{MeOH} > CMC_{EtOH} > CMC_{PrOH} > CMC_{IPA}$. Solvent mixtures with dielectrics between 48 and 80 exhibited no CMC, and the absence of micelles was confirmed by DLS. Regular micelles existed only in pure water.

Chapter 3. THE PARTICLE CHARGING BEHAVIOR OF ION-EXCHANGED SURFACTANTS IN APOLAR MEDIA

Michor, E.L. and Berg, J.C. *Colloids and Interfaces A.* **2017**, *512*, pp 1-6.

3.1 ABSTRACT

This chapter investigates the effects of surfactant counterion electronegativity on the micellization and particle charging behavior of a series of ion-exchanged surfactants in apolar media. The sodium cation in Aerosol OT (AOT) was exchanged for four divalent cations and one trivalent cation, resulting in five AOT analogs. The critical micelle concentrations (CMCs) of each of these AOT analogs was measured by conductometric techniques. For each surfactant, dispersions were made with three different mineral oxides, spanning a range of points of zero charge (PZC), and their electrophoretic mobilities were measured. It was found that all five surfactants behaved as acids, charging all particles positively, with zeta potentials up to 201mV. It was also found, generally, that as the electronegativity of the surfactant head-group increased, the imparted particle mobilities also increased. The trivalent AOT analog imparted higher mobilities than an electronegatively comparable divalent analog.

3.2 INTRODUCTION

Three major surfactant types have been of interest to the field of charging in nonpolar media: two non-ionic, viz. the Span series and polyisobutylene succinimides (PIBS), and one ionic, Aerosol OT. The Span series consists of an acidic sorbitan head-group, and varies in the length, number, and saturation of the tail groups. PIBS surfactants, such as the commercial OLOA 11000, impart charge to colloids through the basic, polyamine head-group. The ionic

surfactant, Aerosol OT (NaAOT) is one of the most extensively studied. NaAOT has a head group consisting of a sodium ion bound to an SO_3^- group. This surfactant is of interest due to its hygroscopic nature, the ability to swell to large emulsion droplets, and its ability to form either normal or reverse micelles.[21] While NaAOT forms spherical reverse micelles in most apolar media[31], exchanging the sodium ion for another metal results in changes of the reverse micellar structure. Exchanging the sodium for divalent cations such as Mg^{2+} and Ca^{2+} still yields spherical reverse micelles, while Ni^{2+} and Zn^{2+} produce rod-like structures.[48] Upon swelling with water, the rod-like structures undergo a rearrangement to spherical droplets. The use of tri- and pentavalent cations- Al^{3+}, Fe^{3+}, and V^{5+}- yields reverse micelles that are ellipsoidal structures.[49]

These AOT analogs have been studied as viscosity modifiers in supercritical CO_2 systems[9,10,50], as templates for the synthesis of metal, polymer, and doped nanoparticles[4,51,52], as well as multi-phase reaction systems.[53,54] While NaAOT has been extensively studied as a particle charge control agent in apolar systems[12,14,27], the ion-exchanged analogs have only been briefly investigated. One study investigated Mn^{2+} and Co^{2+} analogs,[55] but was unable to determine a consistent particle charging mechanism for both analogs, suggesting that surfactant molecules could adsorb either head or tail down on the particle surface. A more recent study exchanged the Na^+ ion for four of the monovalent, alkali metals.[56] The authors did not find any trend in particle charging behavior with the size of the exchanged ion, instead finding that sodium was able to impart the largest charge to the polymer particles.

Given that NaAOT behaves as a slightly acidic surfactant, charging oxide particles similar to their charging in an aqueous medium with a pH of approximately 5, replacing the sodium ion with more electronegative, polyvalent cations, would be expected to yield AOT

analogs of an increasingly acidic nature. Specifically, increasing the electronegativity of the head group, a surfactant should act as a stronger electron acceptor, and thus a stronger Lewis acid. The goal of this study was to test the extent to which ion-exchanged surfactants will charge mineral oxides, and to correlate their charging with effective acidity, as quantified by the electronegativity of the cation in the head-group. A secondary goal of this study was to determine the relative sizes of these reverse micelles to assist in the interpretation of the charging results.

3.3 MATERIALS AND METHODS

3.3.1 *Synthesis of AOT Analogs*

Solid sodium dioctyl sodium sulfosuccinate (NaAOT) was purchased from Fischer Scientific and used as received. The AOT analogs were synthesized using four divalent cations- Ba^{2+}, Mg^{2+}, Zn^{2+}, and Ni^{2+}- following increasing electronegativity from 0.9, to 1.2, to 1.6 and 1.9.[57] Two analogs were prepared with the trivalent cations, Al^{3+}, with an electronegativity of 1.5, and Fe^{3+}. A saturated, ethanolic solution of NaAOT was slowly added to a saturated, aqueous solution of the metal nitrate salt and stirred continuously for one hour. The resulting mixture became cloudy with the insoluble analog surfactant. A liquid-liquid extraction into hexane was then performed to remove the AOT analog. This solution was then washed with deionized water five times to remove excess metal salt and unreacted AOT. The hexane solution was finally dried at 35°C for 72 hours, yielding a finished, waxy product. The iron analog, $Fe(AOT)_3$ was a viscous, rusty colored liquid after drying. The dried surfactants are shown in Figure 3.1.

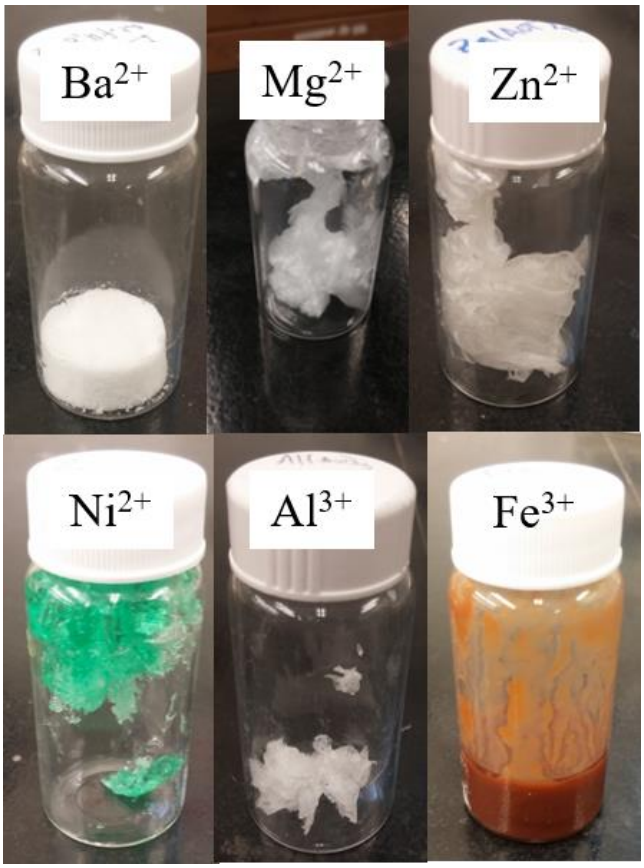

Figure 3.1. Pictures of the six synthesized surfactants. Top row: $Ba(AOT)_2$, $Mg(AOT)_2$, $Zn(AOT)_2$. Bottom row: $Ni(AOT)_2$, $Al(AOT)_3$, and $Fe(AOT)_3$.

The AOT analogs were then dissolved in Isopar-L (Univar, Redmond, WA), a mixture of C_{11} to C_{14} isoparaffins. The Isopar was treated with molecular sieves for at least 24 hours prior to use in order to minimize the water content in the systems. It was found that, even after one week of stirring, the iron analog, $Fe(AOT)_3$ was insoluble in Isopar. For each of the five remaining surfactants, a series of 15 concentrations was made ranging from 10^{-5} to 1wt% surfactant. The viscosity of these solutions was found to be independent of surfactant concentration under the range used in this study.

3.3.2 *Characterization of AOT Analogs*

Energy dispersive x-ray spectrometry (EDS) was performed on the synthesized surfactants in order to determine the coordination number of AOT^- tails to the metal cations. An FEI (Hillsboro, OR) Sirion-XL30 scanning electron microscope was used conjunction with an Oxford (Oxfordshire, UK) EDS instrument, and operated at 20kV and a working distance of 5mm. The elemental analysis measured the atomic percentages of the metal cation, as well as the single sulphur molecule in each AOT^- tail. Normalizing the percentages to those of the metal cations, one can determine the number of sulphur molecules per metal cation and therefore the tail coordination number of the synthesized surfactants. Figure 3.2 summarizes the results.

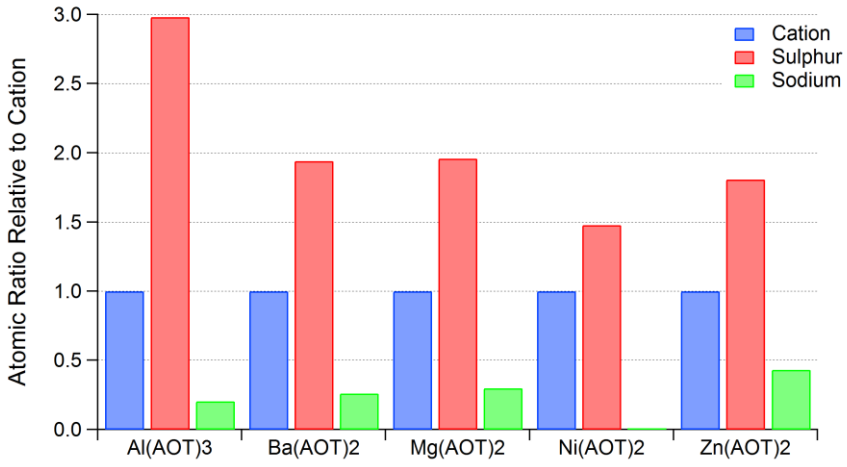

Figure 3.2. EDS results for the five synthesized surfactants. The red bars indicate the molar ratio of sulphur to the cation in the surfactant head group, thus indicating the coordination number of AOT^- tails per cation. Sodium is shown in green.

The red bars represent the molar ratio of sulphur in the AOT^- tails to metal cation in the head group. As expected, the aluminum surfactant had a 3:1 ratio of $S:Al^{3+}$. Both the barium and magnesium surfactants also had ratios of 1.95:1 for $S:M^{2+}$. The nickel surfactant had a ratio of 1.5:1 $S:Ni^{2+}$, indicating a possibly incomplete ion-exchange reaction, however no unreacted Na^+ was found in this sample. It is possible that some unreacted $Ni(NO_3)_2$ remained in the final

surfactant, while the NaAOT was washed out. The zinc surfactant also had a lower-than-expected S:Zn^{2+} of 1.8:1. In this sample, however, unreacted Na^{+} was detected. This suggests the possibility of unreacted NaAOT being present alongside the $Zn(AOT)_2$.

Critical micelle concentrations (CMCs), in Isopar-L, of the AOT analogs were measured using conductometric techniques, determined with a Dispersion Technologies DT700 Nonaqueous Conductivity Meter (Bedford Hills, NY), as outlined in a previous study.[16] The CMC was determined as the concentration at which the conductivity of the solution begins to scale linearly with surfactant concentration. In the pre-micellar region, the measured conductivities are low, but finite values which are independent of surfactant concentration. Other groups have measured pre-micellar conductivities which scale with the square root of the surfactant concentration[58–60] and it is likely that this region also exists in the present study, however the lower limit of detection of the DT700 prevents the accurate measurement of such behavior in these systems.

Structural information of the inverse micelles was obtained using small angle x-ray scattering (SAXS). A SAXS instrument (Anton-Paar, Austria) with a wavelength of 1.54 Å was used. Data were acquired using Fujifilm (Greenwood, SC) image plates and a Perkin-Elmer Cyclone (Covina, CA) image plate reader. The two-dimensional data were reduced to a one-dimensional, intensity (I) versus scattering vector (q) plot using SAXSquant^{TM} (Anton-Paar, Austria) software. It should be noted that this technique was used only to obtain qualitative trends with respect to reverse micellar core sizes. Due to the low-q limit of this instrument, quantitative values were not able to be obtained for several of the species.

3.3.3 *Electrophoretic Mobility Measurements*

Surfactant samples were prepared as previously described, with concentrations ranging from 10^{-5} to 1wt%. Three mineral oxide particles- 250nm silica (Fiber Optics Center Inc., New Bedford, MA), 300nm alumina (Baikowski, Charlotte, NC), and 300nm magnesia (US Nano, Houston, TX)- were used, with PZC's of 3, 7.5, and 10.7 respectively.[27] The particles were baked at 100°C for one hour before being added to the surfactant samples at loadings of 0.5mg per 25mL. These dispersions were allowed to sit for 12 hours before being sonicated and measured. Electrophoretic mobilities were determined using a Brookhaven Instruments (Holtsville, NY) ZetaPALS. Each sample was measured five times, and error bars were calculated using the average and standard deviation of the five measurements.

3.4 Results and Discussion

3.4.1 *Characterization of AOT Analogs*

Figure 3.3 summarizes the CMCs of each of the AOT analogs. Figure 3.3a) is an example of the conductivity curve as a function of surfactant concentration, shown for the aluminum analog. For each concentration, the conductivity was measured 50 times, and error bars were calculated as the standard deviation of these measurements. Error bars cannot be seen on this plot, as they are of the order of 10^{-12} S/m, i.e., smaller than the data markers. Prior to the axis break at 10^{-3}mM, semi-log coordinates were used, and all conductivities were in the range of $3\pm2\cdot10^{-12}$S/m, which is above the limit of detection of the instrument. At approximately 0.008mM, conductivity begins increasing linearly with concentration, indicating the formation and disproportionation of reverse micelles. Similar results were obtained for the other surfactants investigated.

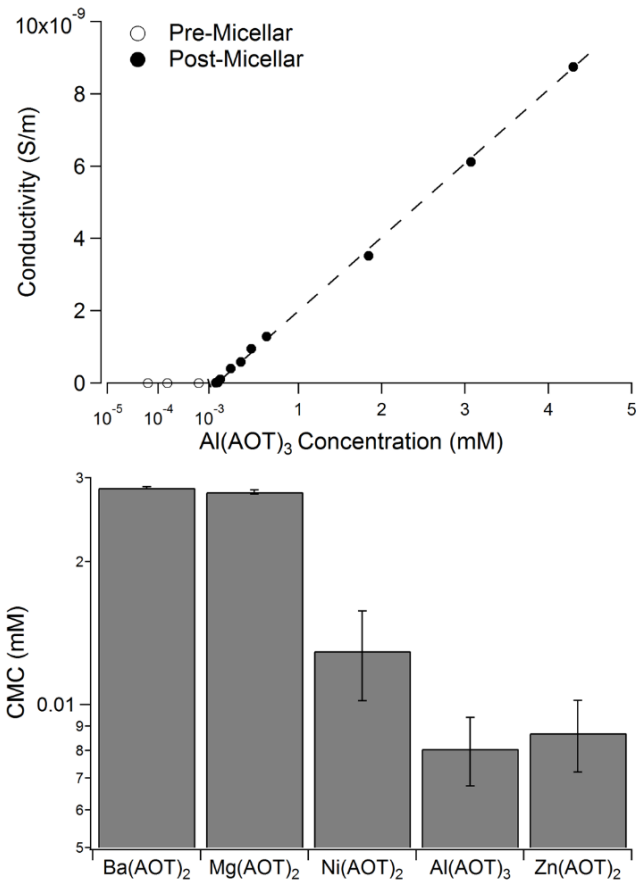

Figure 3.3. a) Conductivity vs $Al(AOT)_3$ concentration plot used to calculate the CMC. Open circles (○) indicate pre-micellar conductivities, while closed circles (●) indicate post-micellar conductivities. The dashed line represents the linearly increasing region. b) Summary of CMC's for all five AOT analogs.

As shown in Figure 3.3b) CMCs of the surfactants ranged from approximately 0.008 to 0.03mM. No systematic trend in CMC with respect to cation electronegativity was observed. It may be noted that the trivalent analog, $Al(AOT)_3$, displayed a lower CMC than any of the divalent compounds.

Small angle x-ray scattering (SAXS) was performed on all five AOT analogs with a concentration of 1wt%, at which the surfactants were fully dissolved and the samples did not display any turbidity. The x-ray contrast (scattering length density) in these experiments was primarily between the metal cations in the head group and the hydrocarbon solvent. This made it

such that any fitting of these profiles resulted in the radius of the reverse micellar cores. The intensity vs scattering vector (*I* vs *q)* profiles for all five surfactants are shown below in Figure 3.4.

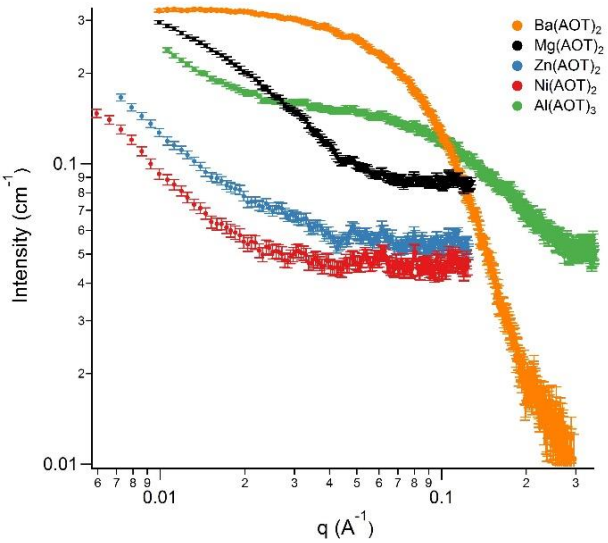

Figure 3.4. SAXS profiles of all five AOT analogs at concentrations of 1wt%.

These scattering profiles were fit to a sphere form factor, for which a levelling out of the intensity at lower *q* values is expected. It can be seen in Figure 3.4 that only $Ba(AOT)_2$ exhibits this behavior. When fit using SasView software (www.sasview.org), core radii of 2.2nm and 1.4nm were calculated for the barium and aluminum analogs respectively. A rise in the scattering intensity of the aluminum analog can be observed at low-*q* values. While this may be indicative of larger structures, such as undissolved surfactant, it is unlikely that this is the case. All samples measured in this study were entirely transparent, with no measurable turbidity. Dynamic light scattering was performed on these samples, but was unable to detect any structures, large or small, due to the small size of the reverse micelles and poor refractive index contrast. Previously, groups have observed that bulk electrostatic interactions, such as between charged reverse micelles, can lead to such low-*q* increases in scattering intensity.[61] The other

three surfactants did not exhibit this levelling behavior necessary to fit the profiles. This is due to the fact that the low-*q* limit of the instrument was reached before the profiles could level out. What it appears can be said about these three surfactants, is that they form larger reverse micelles than either the barium or aluminum analogs. Again, it is important to note that the authors only intend to use these scattering profiles to note the qualitative size differences between the various reverse micellar species.

3.4.2 *Particle Charging Behavior*

Figure 3.5 details the particle charging behavior of $Ba(AOT)_2$, $Mg(AOT)_2$, $Zn(AOT)_2$, and $Al(AOT)_3$, as a function of the surfactant concentration. Figure 3.6a) summarizes the particle charging capabilities of the $Ni(AOT)_2$. At concentrations below the CMC, no measurable mobilities are observed since no reverse micelles are present to stabilize the charges. As the concentration increases past the CMC the particle mobility increases to a maximum value, before decreasing again due to electrostatic screening by charged reverse micelles in the bulk solvent. Figure 3.6b) summarizes the maximum particle mobilities for each surfactant-particle pairing.

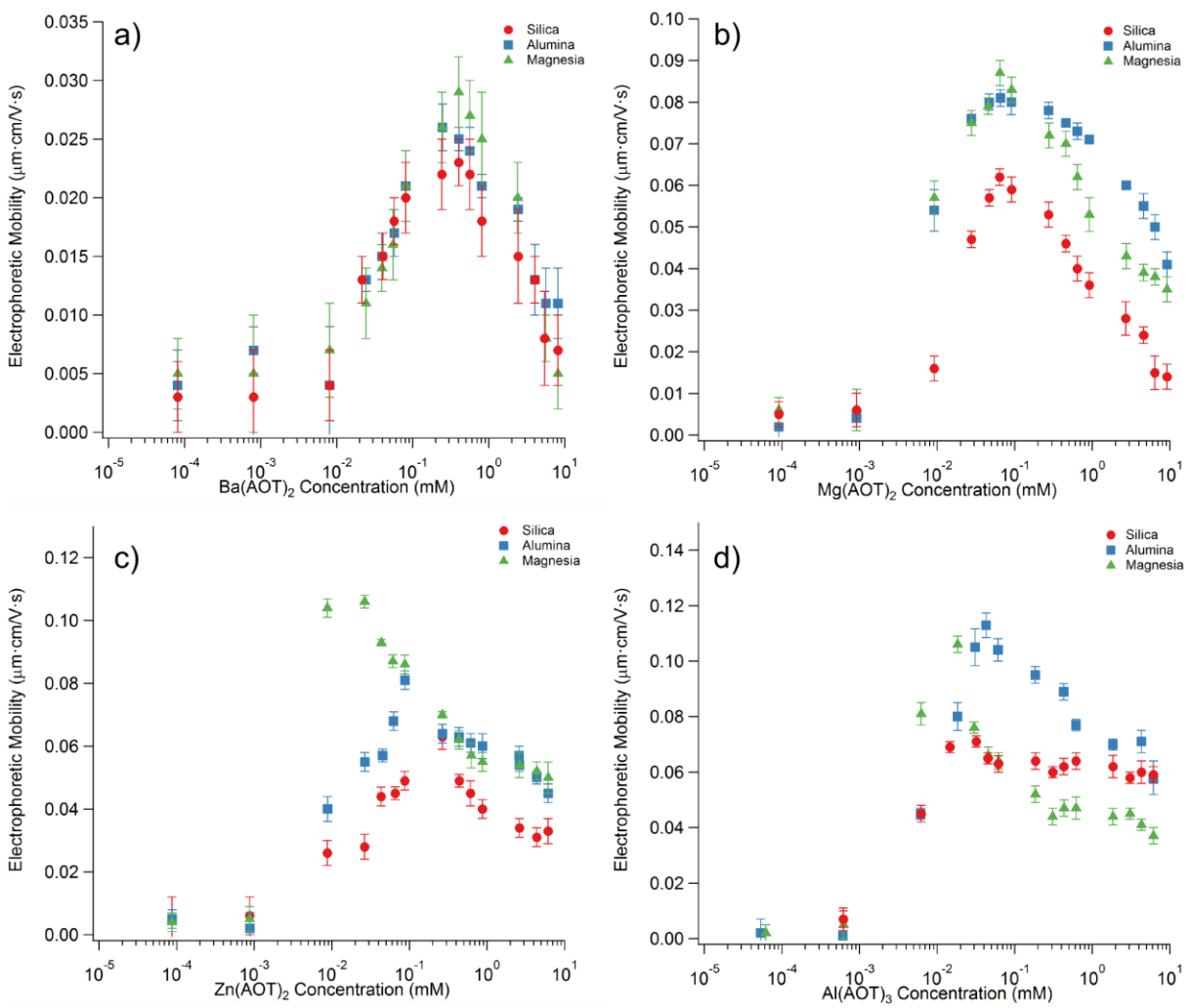

Figure 3.5. The particle charging behavior of a) $Ba(AOT)_2$, b) $Mg(AOT)_2$, c) $Zn(AOT)_2$, and d) $Al(AOT)_3$ with three different mineral oxides. No charging is observed before the CMC is reached. Particle mobility increases to a maximum value before decreasing due to micellar screening.

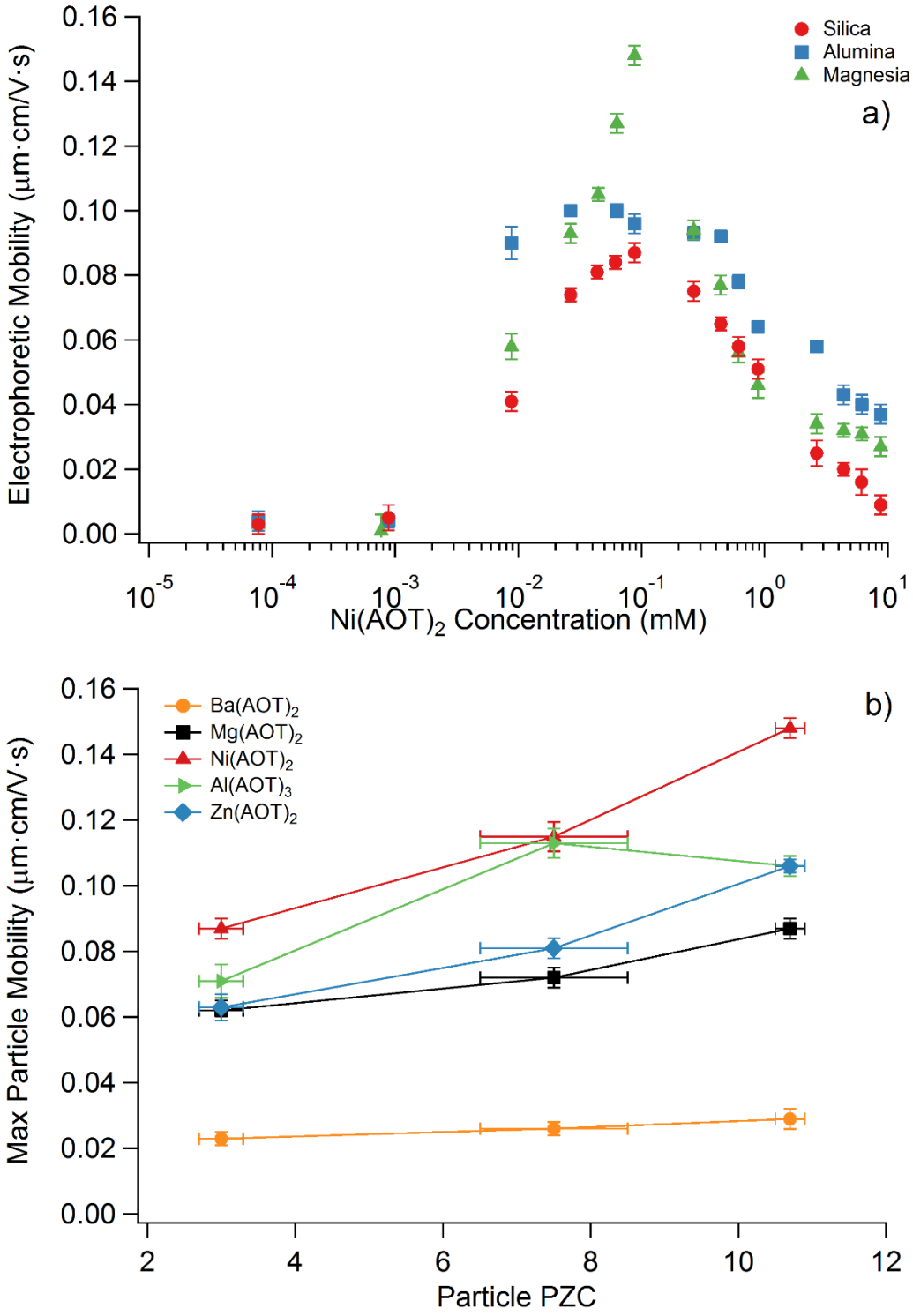

Figure 3.6. a) The particle charging behavior of $Ni(AOT)_2$ with three different mineral oxides. No charging is observed before the CMC is reached. Particle mobility increases to a maximum value before decreasing due to micellar screening. b) The maximum particle mobilities plotted as a function of the particle PZC for each of the five surfactants.

For all surfactants but one, the trivalent, aluminum surfactant, as the PZC of the particle increased, the maximum mobility that the surfactant imparted also increased. $Al(AOT)_3$ imparted the largest mobility to the alumina particles, which had a moderate PZC. It is worth noting that all imparted mobilities in this study were positive, and, in many cases, extremely large. The zeta potentials of these particles can be calculated using the Hückel equation, [19]

$$\zeta = \frac{3\eta U_E}{2\varepsilon\varepsilon_o}, \tag{3.1}$$

where ζ is the zeta potential, η is the solution viscosity, U_E is the electrophoretic mobility, ε is the dielectric constant of the solution, and ε_o is the dielectric permittivity of free space. The viscosities of these systems were measured and found to be independent of surfactant concentration up to 1wt%, therefore the pure solvent viscosity was used in these calculations. The equation is valid in these systems due to the large electric double-layers and small particle size (κa<0.01, where κ is the Debye parameter and a is the particle radius).[19] Zeta potentials imparted by the barium analog ranged from 31±3 to 39±4mV, a range commonly seen in apolar systems. The nickel analog, however, produced zeta potentials up to 201±4mV! Table 3.1. Summary of maximum zeta potentials (in mV) for each surfactant particle pairing summarizes the maximum zeta potentials obtained for each surfactant-particle pairing.

Table 3.1. Summary of maximum zeta potentials (in mV) for each surfactant particle pairing

	Maximum Zeta Potential (mV)				
	$Ba(AOT)_2$	**$Mg(AOT)_2$**	**$Zn(AOT)_2$**	**$Ni(AOT)_2$**	**$Al(AOT)_3$**
Silica	31±3	84±4	85±5	118±4	96±7
Alumina	35±3	98±4	110±4	156±6	153±6
Magnesia	39±4	118±4	144±3	201±4	144±4

The observed behavior in these systems can be explained by the acid-base nature of charging events in apolar media. For systems in which the effective pH of the surfactant is less than the PZC of the particle, the particle will charge positively.[29] The magnitude of this charge is a function of several parameters: the relative acidity-basicity of the surfactant and the particles, the probability of a charge-transfer event, the ability of a micelle to sequester a charge, and the affinity of the micelles to undergo disproportionation. In this study, the goal was to determine if the acidity of the surfactant could be controlled by adjusting the electronegativity of the cation in the head-group. If the maximum particle mobilities are plotted as a function of the surfactant electronegativity, as in Figure 3.7, a trend can be observed.

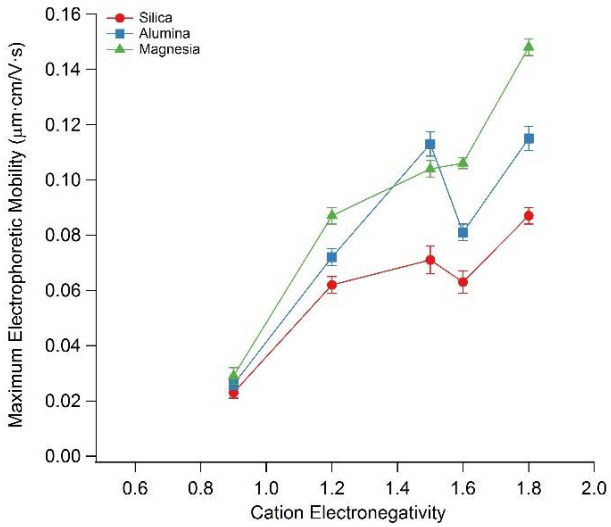

Figure 3.7. Maximum particle mobilities for silica, alumina, and magnesia as a function of the electronegativity of the cation in the surfactant.

What becomes apparent is that, generally, as the electronegativity of the surfactant counterion increases, the maximum particle mobility also increases. This behavior was expected, given that a more electronegative cation acts as a stronger electron acceptor, and thus a stronger Lewis acid. It should be noted that one surfactant did not follow this trend. The

$Zn(AOT)_2$ surfactant, with an electronegativity of 1.6, imparted lower mobilities to the alumina and magnesia particles than the less electronegative $Al(AOT)_3$, with an electronegativity of 1.5.

As mentioned previously, the maximum mobility imparted to a particle depends not only on the relative acidity-basicity of the surfactant-particle pairing, but also on the propensity for the reverse micelles to undergo disproportionation. If more reverse micelles disproportionate, more charge exists in the bulk, thus screening out charges on the particle surface. At 6.1mM, the $Al(AOT)_3$ and $Zn(AOT)_2$ surfactants had conductivities of $2.83 \cdot 10^{-8}$ and $3.51 \cdot 10^{-7}$ S/m respectively. This suggests that reverse micelles of the zinc analog have a significantly higher propensity to undergo charging events in the bulk. This is further corroborated by the SAXS results in Figure 3.4. $Al(AOT)_3$ reverse micelles were found to have core radii of 1.4nm, while the $Zn(AOT)_2$ reverse micelle cores were significantly larger. The zinc analog's scattering profile, while unable to be fit, was shifted approximately an order of magnitude to lower q values, suggesting a comparable increase in core radius. Larger core sizes have been found to undergo increased disproportionation in the bulk, measured by increased system conductivities.[16,29]

Previous studies have found that NaAOT, not tested here, charges silica, alumina, and magnesia to mobilities of -0.06, 0.05, and 0.07 μm cm/V s, respectively.[27] Given that Na has an electronegativity of 0.93, comparable to that of Ba, one would expect similar charging behavior if the maximum mobility relied only on cation electronegativity alone. It is evident that other factors must be involved. One must note that the maximum measured mobility of a particle does not necessarily describe the extent to which it is charged. Screening by reverse micelles in the bulk will decrease the measured particle mobility, resulting in artificially lowered values. The maximum particle mobility is still a worthwhile metric to describe the particle charging behavior

in apolar systems, not just due to its practical applicability, but because it does correlate with predictions.

Figure 3.6b) and Figure 3.7 show that the $Al(AOT)_3$ surfactant deviated from its expected behavior by imparting the highest magnitude of mobility to the alumina particles, which have a lower PZC than the magnesia particles. It could be possible that this surfactant-particle pairing undergoes a charge transfer event which involves the Al^{3+} cation becoming part of the particle structure. This cation may be able to replace the hydrogen of a surface hydroxyl group, thus leaving an overall +2 charge on the particle surface.

3.4.3 *Proposed Charging Mechanisms*

The surfactants that were used in this study differ from the standard apolar surfactants used in previous particle charging studies. Span 80 and OLOA 11000, the standard acidic and basic surfactants currently used, have the chemical functionality to form a classical acid-base adduct on the surface which can then dissociate to donate or accept a proton (H^+). The acidic Span surfactants have hydroxyl groups in the head group, while the basic OLOA has a polyamine head group. NaAOT can form an adduct which can dissociate to either donate its Na^+ ion or to accept a proton from the surface. After the surfactants donate or accept a charge, the now-charged surfactant can be stabilized within a reverse micelle in the bulk. It should be noted that reverse micelles can only stabilize a single, monovalent charge due to the small radii of their polar cores. As discussed in Guo et al.[15], the probability of reverse micelles undergoing charging events scales as $\exp(-Z^2\lambda_B/2a)$, where Z is the valence of the charge in the core, λ_B is the Bjerrum length (~28nm for nonpolar systems), and a is the radius of the polar core. This suggests that reverse micelles are 54 times less probable to become charged to a valence ±2, and 8100 times less probable to become charged to a valence of ±3.

The di- and tri-valent AOT analogs do not have the chemical functionality to donate or accept a proton from a particle surface, which would appear to prevent these surfactants from engaging in the full range of acid-base charging mechanisms as described above. However, this study showed that these surfactants still charge particles as would a highly-acidic, aqueous solution. It is possible that the acidic, associated head group forms an acid-base adduct with a surface functional group on the particle. The dissociation event could involve the uptake of one of the negative, AOT^- tails by a reverse micelle in the bulk. In the case of the magnesium-AOT analog, this would leave a monovalent $Mg(AOT)^+$ species on the particle, thus imparting an monovalent, positive charge to the surface. This process is shown schematically in Figure 3.8. While it is possible that the presence of trace water on the particle surfaces could influence particle charging events and the mechanisms by which they occur, both the particles and solutions were dried prior to being tested. The low water contents, below 250ppm, and intermediate surfactant concentrations at which the maximum zeta potentials occurred are indicative of a region where water has minimal influence on the charging behavior.[22]

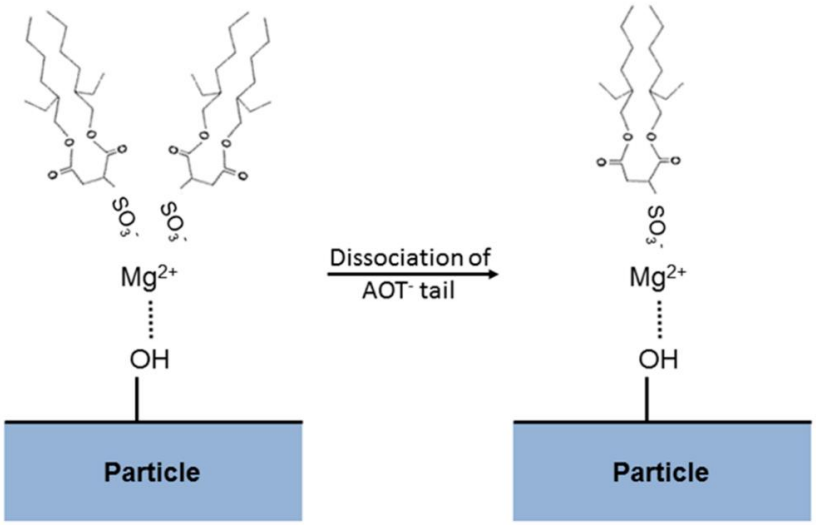

Figure 3.8. Schematic of the proposed acid-base particle charging mechanism. An $Mg(AOT)_2$ molecule would form an adduct with a surface hydroxyl group on the particle. A dissociated AOT^- group could then be stabilized in a nearby reverse micelle. The remaining $Mg(AOT)^+$ species would impart a positive charge on the particle surface.

3.5 CONCLUSIONS

Aerosol OT undergoes ion-exchange reactions with divalent and trivalent cations, resulting in surfactants with a range of counterion electronegativities. These surfactants were synthesized and dissolved in the apolar solvent, Isopar-L, and able to form reverse micelles of varying core radii.

These AOT analogs behaved in an acidic manner, charging mineral oxide particles to produce positive electrophoretic mobilities for every particle-surfactant pairing. Generally, as the PZC of the particle increased, the magnitude of the particle mobility increased as well. The $Al(AOT)_3$ surfactant imparted the largest electrophoretic mobility to the alumina particles, which had a moderate PZC of 7.5. It was also found, generally, that as the electronegativity of the surfactant counterion increased, the magnitude of the imparted particle mobilities increased as well. The $Al(AOT)_3$ surfactant, with an electronegativity of 1.5, imparted larger mobilities than the $Zn(AOT)_2$ surfactant, with an electronegativity of 1.6.

Micellar core sizes were investigated using small angle x-ray scattering (SAXS) and it was found that the trivalent $Al(AOT)_3$ formed the smallest reverse micelles, while the divalent-exchanged analogs increased in core radii with an increase in cation electronegativity. The three largest reverse micelles were unable to be fit to a sphere form-factor due to the low-q limit of the instrument used in this study. Thus it is speculated that the high mobility of the aluminum surfactant was due to the fact that the reverse micelles of this compound had a significantly smaller core size, resulting in less bulk disproportionation and therefore less electrostatic screening of the particle charges.

This study is significant for researchers who wish to tune the magnitude of particle charges. By simply exchanging the cation in the surfactant head-group, one can vary the

magnitude of the particle zeta potentials between 39 and 201mV. It appears that exchanging sodium for a trivalent cation creates reverse micelles with smaller core sizes than those of divalent cation exchanged surfactants. This makes it such that trivalent surfactants of similar electronegativies are likely to impart higher electrophoretic mobilities than their divalent counterparts.

Chapter 4. THE TEMPERATURE EFFECTS ON MICELLE FORMATION AND PARTICLE CHARGING WITH SPAN SURFACTANTS IN APOLAR MEDIA

Michor, E.L. and Berg, J.C. *Langmuir* **2015**, *31*(35), pp 9602-9607

4.1 ABSTRACT

This chapter examines the effects of temperature on the micellization and particle charging behavior of the Span surfactant series in an apolar environment. The critical micelle concentrations of each of six surfactants at five temperatures were measured by conductometric techniques. The thermodynamic properties of micellization were calculated using Gibbs-Helmholtz analysis. Magnesia particles were then dispersed in solutions of these surfactants, and their electrophoretic mobilities measured at three temperatures. Preliminary small angle neutron scattering (SANS) experiments were conducted to measure the size of aggregates (referred to as reverse micelles) of three of the surfactants. It was found that for all but one of the surfactants, the critical micelle concentration (CMC) increased by as much as an order of magnitude across a 40^{o}C range of temperature. One of the surfactants exhibited a decrease in CMC upon increasing temperature, likely due to a de-crystallization of the tails upon reverse micelle formation. The maximum particle mobilities decreased upon increasing temperature due to the increased electrostatic screening by charged reverse micelles at higher temperatures.

4.2 INTRODUCTION

The study of surfactants as charge control agents in apolar media has long been of interest.[18,21] Originally used as a means to stabilize particles and increase conductivities in motor oils and inks, surfactant aggregates referred to as reverse micelles are used in current technologies such as the Amazon Kindle Paperwhite® reader and the Indigo® electrophoretic ink. Of the surfactants that form reverse micelles, a series of six sorbitan oleates, known as the Span series, pictured in Figure 4.1, is of particular interest in many applications. These species share the same sorbitan head group, while varying the tail length, tail saturation, and number of tails. Current studies have used reverse micelles of Span 60 and Span 85 as means of protein extraction.[7,8,62] Other studies have used Span 80 reverse micelles to synthesize mesoporous titania membranes for ultrafiltration purposes.[5] Many recent studies have looked at the ability of Span surfactants to charge particles in apolar solvents, measuring the magnitudes and signs of the particle electrophoretic mobilities.[13–15,29,63] Given the wide array of applications of these compounds, many different operating conditions are used. Protein extractions are often done at or near room temperature, while ink-jet printers require the particles be charged at around 100ºC. Current technology used by the HP Indigo® printer relies on the electrophoresis of submicron particles to an adjustable printing plate through an oil medium, to create a high resolution image at temperatures ranging between 60-150ºC.[17] This means that reverse micelles must be present in the media and be able to impart sufficient charge to the particles at these elevated temperatures.

Many factors can contribute to the charging behavior of particles in apolar solvents, and all may be subject to temperature effects. Since the stabilization and charging of particles requires the presence of reverse micelles, the initial goal of this study was to determine the effect

of temperature on the critical micelle concentration of Span surfactants in an apolar environment, permitting determination of the thermodynamic properties of micellization. The second goal was then to find out how temperature might affect the ability of these same surfactants to charge colloidal particles.

4.3 EXPERIMENTAL

4.3.1 *Chemicals*

The six surfactants used in this study were the Span series, shown in Figure 4.1. All of the surfactants consist of the same sorbitan head group, but vary in the length and number of their hydrocarbon tails.

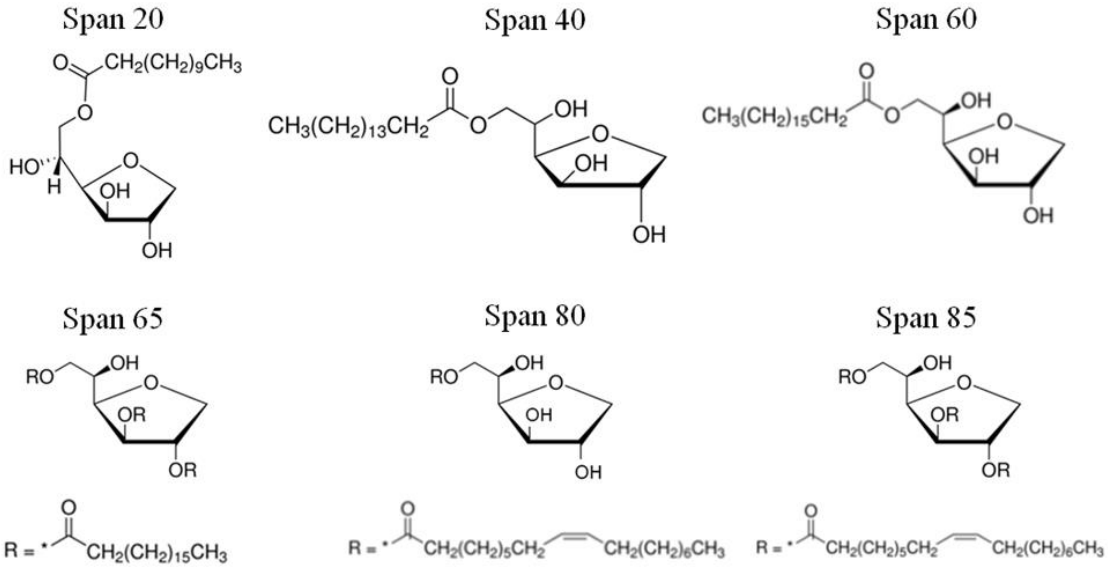

Figure 4.1. Chemical structures of the Span surfactant series.

Span 20, 40, and 60 all consist of a single, saturated tail of 11, 15, and 17 carbons respectively. Span 80, like Span 60, also has a C_{17} tail, but with a double-bond halfway down its length. Span 85 is a three-tailed analog of Span 80, with three C_{17} tails each with a double bond. Span 65 is similar to Span 60, but with three, fully-saturated C_{17} tails.

All of the surfactants except Span 60 were purchased from Sigma-Aldrich (St. Louis, MO) and used as received. Span 60 was purchased from Uniqema (New Castle, DE) and used as received. The solvent used in these studies was Isopar-L (Univar, Redmond, WA), a commercial mixture of C_{11} to C_{14} isoparaffins, which was used after treatment with molecular sieves to minimize system moisture content and Karl-Fischer titration was used to determine that the water to surfactant molar ratio never exceeded 0.8 for any system studied. For each of the six surfactants, a series of 15 Span concentrations was made ranging from 10^{-6} to 1wt% Span. The viscosity of these solutions was found to significantly depend only on temperature. While small increases in viscosity were measured for the highest surfactant concentrations, these values fell well within the error bars of the pure solvent measurements.

4.3.2 *CMC determination by conductivity and calculation of thermodynamic properties of reverse micelle formation*

Conductivities of the samples were measured using a Dispersion Technologies (Bedford Hills, NY) DT-700 Nonaqueous Conductivity Probe. Samples were allowed to equilibrate in a constant temperature bath at five temperatures before being measured.

The conductivity of each sample was measured 20 times and the average plotted as a function of surfactant concentration. Error bars were calculated using the standard deviation of the 20 measurements. Before a CMC is reached, a region of negligible charging is observed, where the conductivity is near the lower limit of detectability by the instrument used and independent of surfactant concentration. Other researchers[15,33] have observed a region before the CMC, where premicellar aggregates contribute to the conductivity of the solution. While this region likely exists in the systems used in this study, the lower limit of detection of the DT700 prevents its accurate measurement. There is evidence that ion and ion-pair formation can affect

the conductivity of non-polar systems.[34,35] However, this theory is most applicable to nonaqueous systems of intermediate dielectrics, such as alcohols, as well as very high surfactant concentrations. Due to the very low dielectric constant of Isopar, as well as the low surfactant concentrations used in this study, increases in conductivity best follow the linearly-increasing behavior predicted by intermicellar disproportionation reactions.[15,18,21] The CMC was determined by finding the intercept of two, best-fit lines through these regions as shown schematically in Figure 4.2.

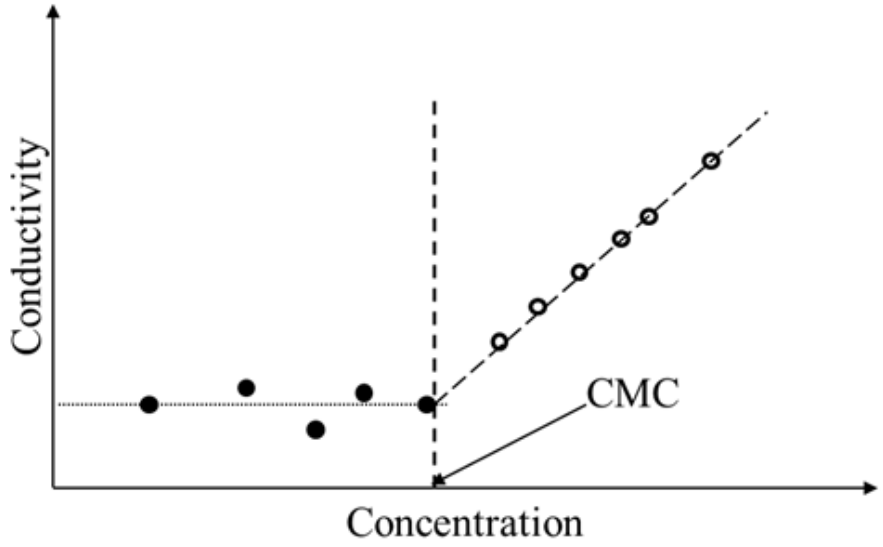

Figure 4.2. Schematic of CMC determination method.

Once the CMCs have been calculated, the free energy of micellization, ΔG_{mic}, can be calculated as

$$\Delta G_{mic} = RT\ ln(\mathrm{CMC}), \tag{4.1}$$

where R is the gas constant, and T is the temperature in kelvin.[19] The enthalpy, ΔH_{mic}, is calculated using the Gibbs-Helmholtz equation

$$\Delta H_{mic} = \frac{\partial(\Delta G_{mic}/T)}{\partial(1/T)}, \tag{4.2}$$

and the entropy of micellization is calculated as

$$\Delta S_{mic} = \frac{\Delta H_{mic} - \Delta G_{mic}}{T}. \quad (4.3)$$

4.3.3 *Electrophoretic mobility measurements*

Span samples were prepared as previously described, with concentrations ranging from 10^{-6} to 1wt%. Magnesia particles were obtained from MTI Corporation (Richmond, CA). The 30nm particles were baked at 100°C for one hour before being added to the Span samples at loadings of 0.5mg per 25mL. These dispersions were allowed to sit for 12 hours before being sonicated and measured. Electrophoretic mobilities were determined using a Brookhaven Instruments (Holtsville, NY) ZetaPALS. Samples were allowed to equilibrate at each of three temperatures before being measured five times. Error bars were calculated using the average and standard deviation of the five measurements.

4.3.4 *Small angle neutron scattering of reverse micelles*

Motivated by the need to explain trends detailed in the results section below, it appeared useful to pursue small angle neutron scattering (SANS) to provide micellar structural information. A preliminary study was performed on three of the Span surfactants- 20, 40, and 60- at the NCNR at NIST.[64] Each surfactant was dissolved in deuterated decane at a concentration of 1wt%. Samples were measured at 45°C to ensure that the surfactant was fully dissolved. Scattering data were collected with 6Å neutrons at 13m, 4m, and 1m. Only a single run was performed for each of the three surfactants. Therefore, the authors intend to use these results to determine an outer diameter of the reverse micelles, with only qualitative information about core size and aggregation numbers. The raw data was reduced and analyzed using Igor Pro macros developed by Kline.[65]

4.4 RESULTS AND DISCUSSION

4.4.1 *Critical micelle concentrations and thermodynamics of micellization*

Figure 4.3 summarizes the CMC results for all six Span surfactants at all five temperatures studied. Figure 4.3a) shows an example data set used to calculate the CMC of Span 80 at 35ºC. Error bars are of the order of 10^{-12} S/m and are smaller than the data markers. Semi-log coordinates are used before the break around 10^{-2}mM, at which conductivities were all in the range of $5\pm2\cdot10^{-12}$S/m. A clear increase in conductivity is observed after 0.05mM, indicating the formation of reverse micelles, after which the conductivity scales linearly with concentration as shown by the dashed line.

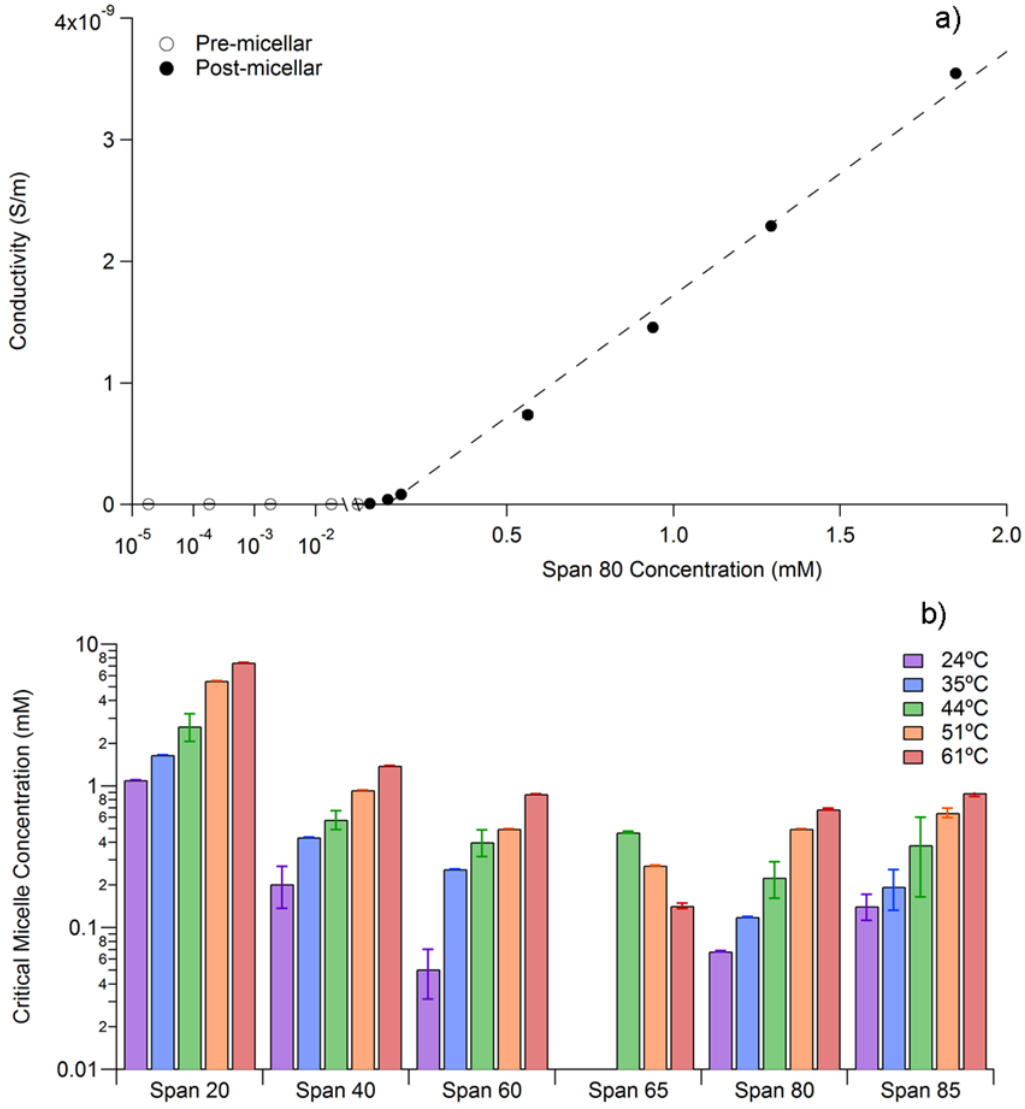

Figure 4.3. a) Conductivity vs Span 80 concentration plot used to calculate the CMC. Open circles (○) indicate pre-micellar conductivities, while closed circles (●) indicate post-micellar conductivities. b) Summary of CMCs for all six Spans in the study. The lack of bars at 24ºC and 35ºC for Span 65 indicates that no CMCs were measured at those temperatures.

As noted in Figure 4.3b), in every case except Span 65, the CMCs were lowest at the lowest temperature, 24ºC, and increased with increasing temperature. Across the 57ºC range, CMCs rose by almost an order of magnitude for the five surfactants with this behavior. The CMC of Span 20 rose from 1.10±0.01mM to 7.42±0.03mM as the temperature increased from

24ºC to 61ºC, while for Span 60 it rose from 0.05±0.02mM up to 0.88±0.01mM over the same temperature range. It can be seen that for the series of Span 20 to 60, the CMC decreases at every temperature as the surfactant tail length increases from 11, to 15, to 17 carbons.

There are no data shown for Span 65 at 24ºC and 35ºC because no micellization occurred at those temperatures. At 44ºC, a CMC of 0.47±0.01mM was measured and then decreased to 0.14±0.01mM as the temperature increased to 61ºC.

Table 4.1. Thermodynamic Properties of Micellization for Span Surfactants.

	ΔG_{mic} (44ºC) (kJ/mol)	ΔH_{mic} (kJ/mol)	ΔS_{mic} (J/mol K)
Span 20	-15.1	-39.8	-78
Span 40	-19.4	-41.9	-71
Span 60	-20.5	-39.6	-60
Span 65	-20.3	59.9	253
Span 80	-21.8	-51.9	-95
Span 85	-20.6	-41.9	-67

All the thermodynamic properties of micellization are summarized in Table 4.. It is seen that for all species except Span 65, both the enthalpy and entropy of micellization are negative, with enthalpies of the order of 40kJ/mol and entropies of the order of 70 J/molK. This is consistent with the expectation that the majority of reverse micelle formation events in apolar environments are enthalpically driven. However, Span 65 has positive values for both enthalpy and entropy, with the magnitude of the entropy term being significantly larger (approximately 250 J/mol·K) than for the other Span species. This difference in behavior must be due to a fundamental difference in how the Span 65 molecules behave in the bulk and as aggregates.

Given that Span 65 micellization is an entropically driven phenomenon, we propose that a de-crystallization event could lead to this behavior. In the bulk, the three, fully-saturated tails of Span 65 could co-crystallize with one another. Upon the formation of a reverse micelle, the

strain placed on the head groups could cause a de-crystallization of the tails, a process which would raise the entropy of the system, as pictured schematically in Figure 4.4.

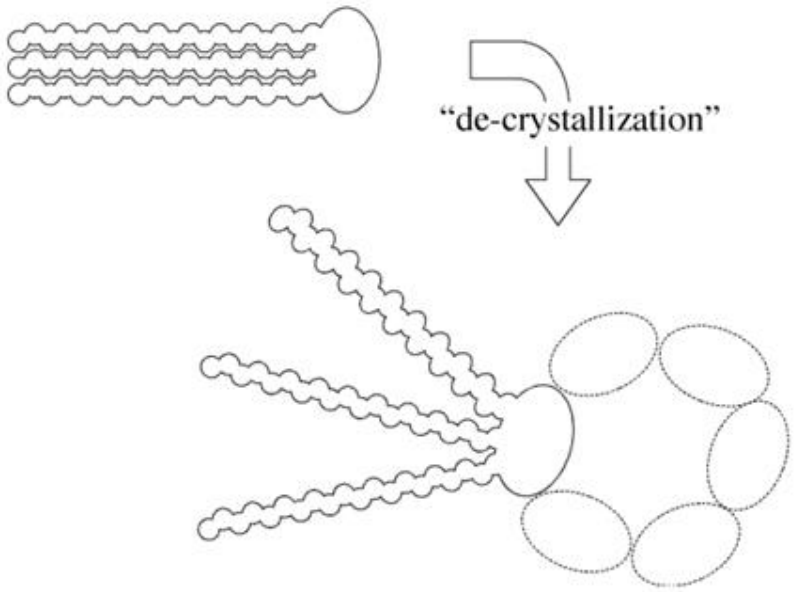

Figure 4.4. A schematic of the co-crystallization/de-crystallization of Span 65 upon reverse micelle formation.

To examine the validity of this hypothesis, differential scanning calorimetry (DSC) was performed on two samples of Span 65. One sample was solid Span 65, while the other was a 1wt% solution of Span 65 dissolved in Isopar-L. The DSC results are shown below in Figure 4.5.

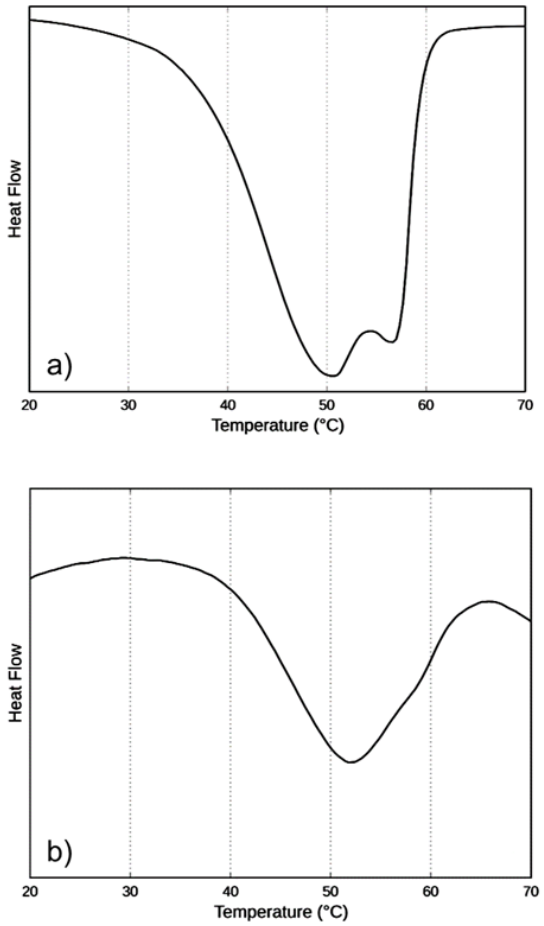

Figure 4.5. Heat flow as a function of temperature for a) a solid sample of Span 65 and b) a 1wt% solution of Span 65 in Isopar-L.

The solid sample of Span 65 shows two, superimposed, endothermic peaks, one at approximately 51°C and the other at 57°C. However, the Span 65 solution shows only one endothermic peak at 51°C. Of the two peaks in Figure 4.5a), one must correspond to the melting of the solid Span 65. In the 1wt% sample of Span 65 in Isopar-L, no melting peak should be observed, as the surfactant is dissolved. Since both samples show an endothermic peak at 51°C, this could be indicative of a de-crystallization event. These peaks begin at approximately 40°C, and no micellization occurred before 44°C, further corroborating the de-crystallization hypothesis.

4.4.2 *Particle charging behavior*

The magnesia particle mobilities as a function of surfactant concentration for five of the surfactant species are shown in Figure 4.6. Each species was measured at three temperatures, which varied depending on the solubility of the surfactant. Span 40, 80, and 85 were all measured at 22^{o}C, 35^{o}C, and 44^{o}C. Span 60 was measured at 35^{o}C, 44^{o}C, and 51^{o}C, while Span 65 was measured at 44^{o}C, 50^{o}C, and 60^{o}C. The results for Span 20 are shown in Figure 4.7a), and the summary of the maximum particle mobilities are presented in Figure 4.7b). Before a CMC is reached, no measurable mobilities are observed because no reverse micelles exist to stabilize charges. As the concentration increases past the CMC, the mobility rises, before falling off at higher temperatures due to screening caused by inter-micellar charging. All systems studied showed this behavior.

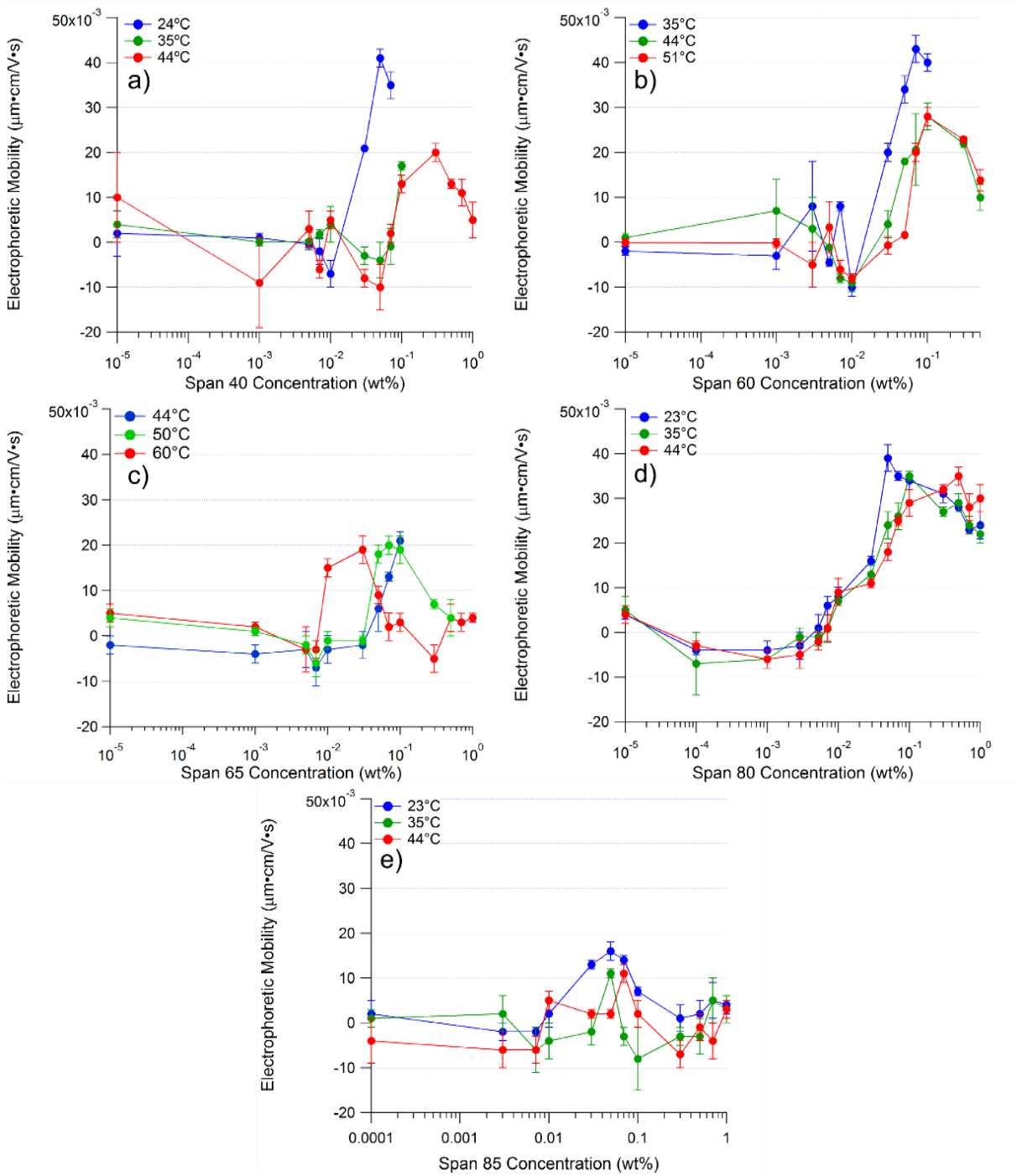

Figure 4.6. The particle charging behavior of a) Span 40, b) Span 60, c) Span 65, d) Span 80, and e) Span 85 as a function of surfactant concentration. The charging behavior was measured at three temperatures for each surfactant species.

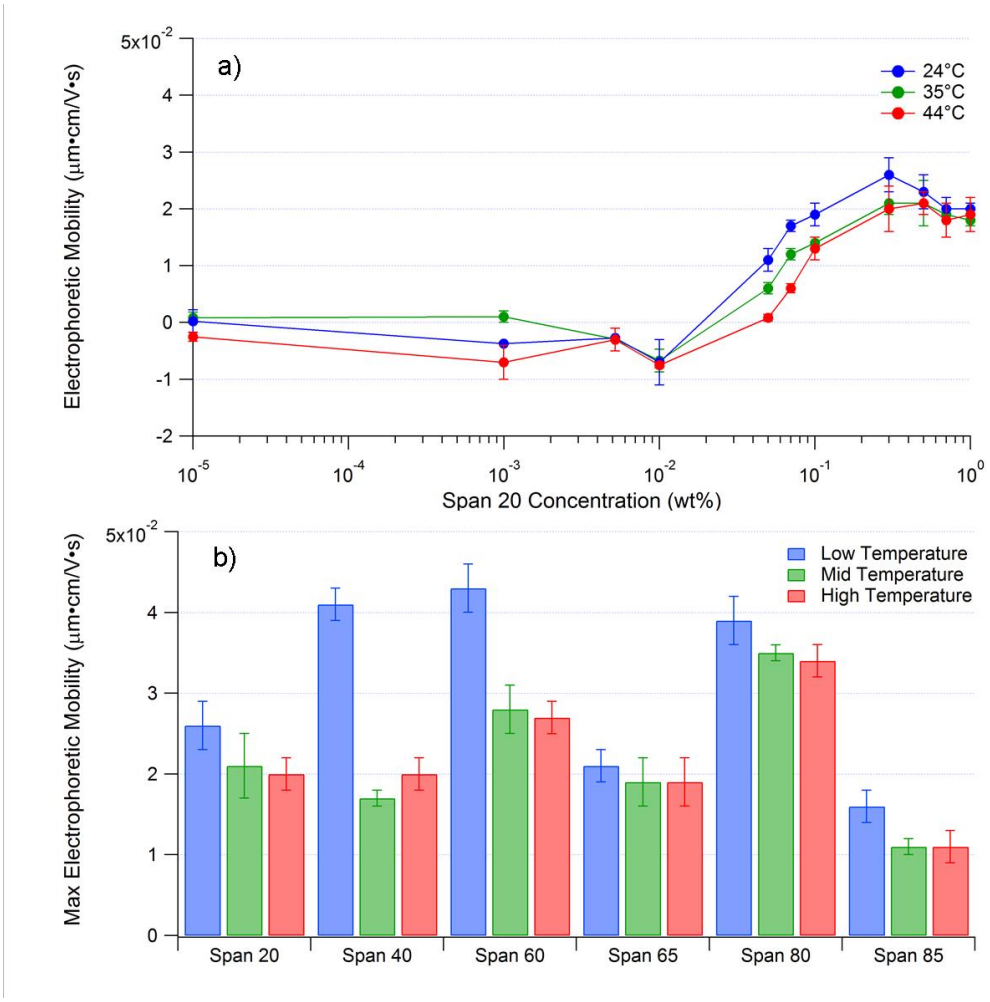

Figure 4.7. a) The particle charging behavior of Span 20 at three temperatures. No charging is observed before the CMC is reached. Particle mobility increases to a maximum value before decreasing due to micellar screening. b) The maximum particle mobilities for each surfactant at each temperature. For Span 20, 40, 80, and 85, the temperatures studied were 24, 35, and 44ºC. For Span 60, the temperatures studied were 35, 44, and 51ºC. For Span 65, the temperatures studied were 44, 51, and 61ºC.

What can be seen from Figure 4.6 and Figure 4.7a) is that as temperature increases, the maximum value of the particle mobility decreases. In order to concisely display all of the particle charging data, the maximum mobilities for each system and temperature are summarized in Figure 4.7b). It should be noted that for Span 60, the CMC at 24ºC was too close to the solubility limit to measure any significant particle charge. Therefore, the lowest temperature

used for that species was 35ºC. Since Span 65 exhibited no micellization before 44ºC, no particle charging could be measured below that temperature.

In every system studied, an increase in temperature resulted in a decrease in maximum particle mobility. Between the two higher temperatures, this decrease was generally smaller than between the two lowest temperatures. Also of note is that for Span 40, the lowest mobility was measured at 35ºC. This was due to the solubility limit being reached soon after the particles began to charge. One can also see that as the surfactant tail length increases, from Span 20, to 40, to 60, the maximum particle charging also increases.

The maximum particle mobility is a function of multiple processes: the relative acidity-basicity of the surfactant and particles, the probability of a charge-transfer event, the ability of a reverse micelle to sequester a charge, and the affinity of the reverse micelles to undergo disproportionation, which contributes to the screening experienced by the particles. To determine why an increase in temperature would decrease the maximum charge, it was determined that more information may be found in the conductivity curves. The *slopes* of the linear micellar region of these curves, in units of S/m·mM, are indicative of the charging "efficiency" of the reverse micelles. Normalizing these slopes by viscosity would ensure that any changes in slope were not due to the effect of temperature on viscosity. These normalized slopes are plotted as a function of temperature in Figure 4.8.

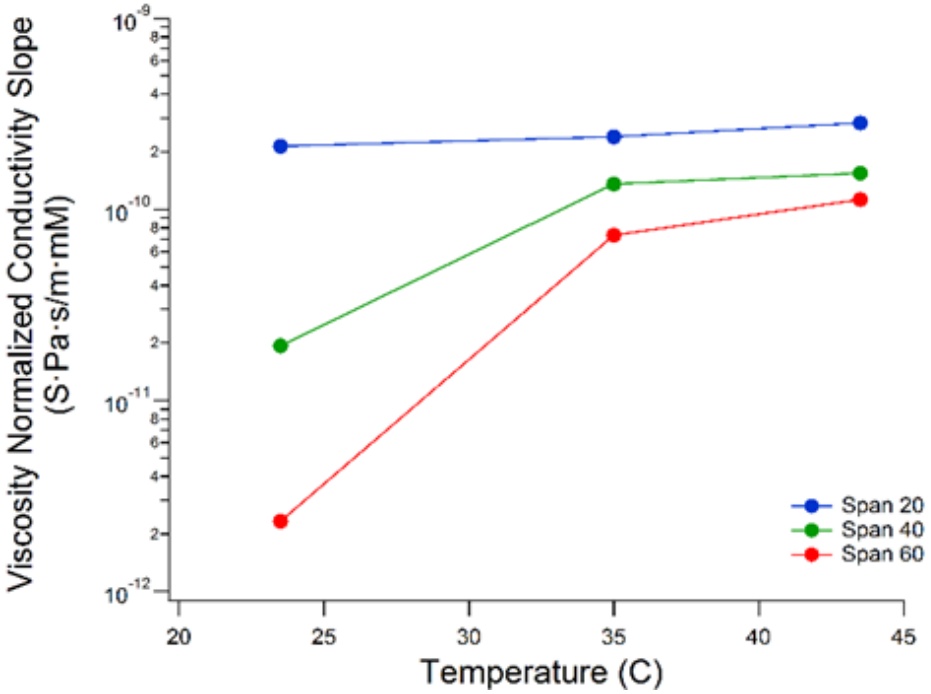

Figure 4.8. The viscosity-normalized conductivity slopes for Span 20, 40, and 60 as a function of temperature.

In all cases, the normalized slope of the conductivity curves increased as a function of temperature, with Span 60 exhibiting the largest change, almost two orders of magnitude, and Span 20 the smallest, with an increase of about 32%. It is also of note that Span 20 exhibited the highest normalized conductivity slopes at all temperatures, and Span 60 the smallest.

This would suggest that more Span 20 reverse micelles undergo disproportionation at all temperatures than Span 40 reverse micelles, and Span 40 reverse micelles more than Span 60 reverse micelles. This is corroborated by the maximum charging results. Figure 4.7b) shows that the maximum mobilities achieved by Span 20 is less than Span 40, and that Span 40 mobilities are somewhat less than those of Span 60. Again, it should be noted that the maximum charge achieved at 35°C for Span 40 was smaller because the solubility limit was reached soon after the CMC.

Figure 4.8 further suggests that as temperature increases, the probability of reverse micelles undergoing disproportionation increases. An increase in the slope means that a larger fraction of the surfactant molecules are charging in the bulk. With a larger fraction of reverse micelles charging in the bulk, particle screening would increase, and the maximum particle mobility would decrease. Again, this corroborates with the results in Figure 4.7b). Span 40 and 60 show larger increases in conductivity slope than Span 20, and show larger decreases in particle mobility than Span 20.

4.4.3 *SANS results*

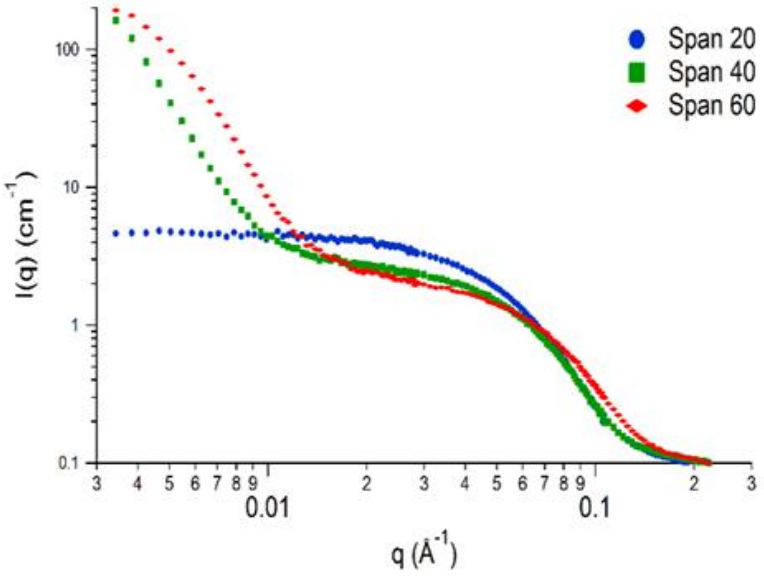

Figure 4.9. The SANS scattering intensity, *I(q)*, as a function of scattering vector, *q*, for 1wt% solutions of Span 20, 40 and 60 in *d*-decane at 45°C.

The preliminary SANS results for Span 20, 40, and 60 are shown in Figure 4.9. It can be seen that a larger amount of scattering occurs at low *q* values for Span 40 and 60, indicative of large structures. This was due to crystallization of surfactant during the transfer of solutions from the prep area to the measuring area. The Span 40 and 60 solutions were above the solubility limit at room temperature, to ensure enough reverse micelles would be present to

scatter sufficiently. It should be noted that no background scattering measurements were taken to account for the dissolved surfactant molecules. Given the relatively high concentrations and large contrast of surfactant molecules in the bulk, any scattering features of spherical reverse micelles at high q would likely be convoluted. Therefore, the data were analyzed only over the range $0.015<q<0.15 Å^{-1}$. Applying a spherical fit model to this range of the data, the radii of the Span 20, 40, and 60 reverse micelles were 4.2±0.1, 3.7±0.1, and 3.3±0.2nm respectively.

Given that all three Span species have the same sorbitan head group, and vary only in the length of the saturated alkane tail, a few qualitative statements can be made about the structures of these reverse micelles. Recall that Span 20 has the shortest tail at 11 carbons, Span 40 the next longest at 15 carbons, and Span 60 the largest at 17 carbons. Span 20 formed the largest reverse micelles at 4.2nm in radius. This implies that not only are the aggregation numbers of these reverse micelles larger than the Span 40 and 60 micelles, but that the size of the polar core is larger as well. As the length of the hydrocarbon tails increases, the size of the reverse micelles decreases, as do the aggregation numbers and polar core sizes.

Previous studies have shown that increasing the amount of water in a reverse micellar core increases the conductivity of the reverse micelles due to a larger fraction of the reverse micelles charging.[20] Comparing this theory to the results shown in Figure 4.8, one can see that Span 20, with the largest polar core, has the largest fraction of charged reverse micelles. Decreasing the size of this core decreases the fraction of micellar charging.

One can also see that the size of the polar core of a reverse micelle strongly affects the reverse micelles ability to charge particles due to screening effects. Span 20, with the largest core size and largest fraction of charged reverse micelles, exhibits the weakest ability to charge the magnesia particles. Decreasing the size of the reverse micelles, and thus core size, results in

a smaller fraction of charged reverse micelles, but a higher maximum mobility of charged particles.

4.5 CONCLUSIONS

It was found that temperature plays a significant role on the ability of Span surfactants to form reverse micelles and to charge particles in apolar environments. Increasing the temperature by 40ºC resulted in the increase in the critical micelle concentration of most surfactants by approximately an order of magnitude, and more in some cases, suggesting the primarily enthalpic nature of reverse micelle formation in these apolar solvents. However, Span 65 showed the opposite behavior. The micellization of this species was entropically driven, causing a decrease in CMC with an increase in temperature. In all cases, the ability of the reverse micelles to charge magnesia particles was reduced upon increases in temperature, due to the increased screening by charged reverse micelles in the bulk.

The surfactant structures also played a role in micellization and particle charging. Preliminary SANS data showed that the smaller the surfactant tail, the larger the reverse micelle, aggregation number, and core size. As the tail length increased, the reverse micelle size, aggregation number, and core size decreased. The larger reverse micelles had higher CMCs and a higher fraction of charged reverse micelles. This resulted in an increased ability to screen particle charge, and thus a lower maximum mobility of particles charged by these reverse micelles.

These findings are significant for researchers who require particles to be charged at elevated temperatures. The increase in CMC with temperature requires formulations which are well above the CMC at room temperature. However, care must be taken to not exceed concentrations which would result in particle screening at the desired operating temperature. To

achieve the maximum attainable mobility of the particles, the operating temperature should be chosen to be as low as possible to prevent a decrease in mobility due to the increased screening behavior of the reverse micelles. In order to further understand how the surfactant structure influences reverse micelle shape and charging capabilities, a detailed SANS studied will need to be performed. Using contrast variation techniques, the reverse micelle core size can be measured, and relationships between core size, reverse micellar structure, CMC, and particle charging can be established.

Chapter 5. THE EFFECTS OF REVERSE MICELLAR STRUCTURE ON THE PARTICLE CHARGING CAPABILITIES OF THE SPAN SURFACTANT SERIES

Michor, E.L., Ponto, B.S., and Berg, J.C. *Langmuir*, **2016**, *32*(40), pp10328-10333

5.1 ABSTRACT

This chapter investigates the effects of reverse micellar core size on the particle charging behavior of a series of acidic surfactants in apolar media. A series of Span surfactants was dissolved in deuterated decane at concentrations above the critical micelle concentration (CMC). The structures of the reverse micelles were measured using small angle neutron scattering (SANS). It was determined that as the tail length of the surfactant increased, the size of the polar, reverse micellar core decreased. Tri-tailed surfactants formed reverse micelles with the smallest polar cores, with radii of approximately 4Å. The sizes of the polar cores were correlated with the particle charging behavior of the Span surfactant series, as measured in a previous study. It was found that reverse micelles with intermediate core sizes imparted the largest electrophoretic mobilities to the particles. Reverse micelles with very small cores did not offer a large enough polar environment to favor charge stabilization, while very large polar cores favored disproportionation reactions in the bulk, resulting in increased electrostatic screening.

5.2 INTRODUCTION

Many variables must be considered when studying charging events in nonpolar environments. The environment in which the system is being studied, the components of the system, and the formation of the surfactants into reverse micelles all affect the charging events in

the system.[18,21] Previous studies in this field have focused mainly on how surfactant and particle chemistries interplay to obtain a maximum particle mobility.[12–14,26,29] Other studies have determined the effects of water content on the conductivities and maximum colloidal particle charges of apolar systems.[22,66] Impedance spectroscopy has also been used to investigate the role reverse micelles have in charge transport in apolar systems.[33,67,68] The solvent dielectric constant and structure have been shown to affect the critical micelle concentration and conductivity of Aerosol OT, even to the point that micelles, reverse or normal, will no longer form.[38] Recent studies have investigated the effects of temperature and surfactant structure on the critical micelle concentration and maximum particle mobilities.[16] While there have been investigations into the effect of solvent chemistry and structure on reverse micellar structure,[31,48,49,69–72] no studies have investigated the effect of micellar structure on the maximum electrophoretic mobility which can be imparted to particles.

Of the surfactants that form inverse micelles, a series of six sorbitan oleates, known as Spans, is of particular interest in many applications. These compounds share the same sorbitan head group, while varying in tail length, tail saturation, and number of tails, as shown in Figure 5.1. Current studies have used inverse micelles of Span 60[8] and Span 85[6,7,73] as means of protein extraction from solution, while other studies have used inverse micelles of Span 80 to synthesize mesoporous titania membranes for ultrafiltration purposes.[5] Many recent studies have looked at the ability of Span surfactants to charge particles in apolar solvents, measuring the magnitudes and signs of the particle electrophoretic mobilities.[13–15,29,63] However, most studies have looked only at how the chemistry of the surfactant head group affects the charging behavior.[12–14,26,27,63] The authors' most recent study[16] has shown that the magnitude of particle charge, of 30nm magnesia particles, increases as the tail length of the Span species increases. Preliminary small

angle neutron scattering (SANS) data[16] have suggested that this increase in charging corresponded to smaller inverse micelles. However, a more thorough SANS study, reported here, was necessary to determine the correlation between surfactant structure, the structure of the reverse micelles formed, and the charging behavior of the reverse micelles. Due to the poor refractive index and electron density differences between the Span reverse micelles and apolar solvents, light scattering and x-ray scattering techniques are limited in their usefulness, leaving only SANS as a viable means to determine these structures. The objective of this study was to use SANS to measure the sizes of Span reverse micelles and their polar cores in order to determine whether these parameters could explain the trends observed in the previous study.[16]

5.3 EXPERIMENTAL

5.3.1 *Chemicals*

The six surfactants used in this study were the Span surfactant series, shown below in Figure 5.1. Span 20, 40, and 60 all have a single, fully-saturated alkane tail, consisting of 11, 15, and 17 carbons respectively. Span 80, similar to Span 60, has a C_{17} tail, but with a double bond halfway down its length. Span 65 is a tri-tailed analog of Span 60, with three, fully-saturated C_{17} tails, while Span 85 is the tri-tailed analog to Span 80, having three C_{17} tails, each with a double bond.

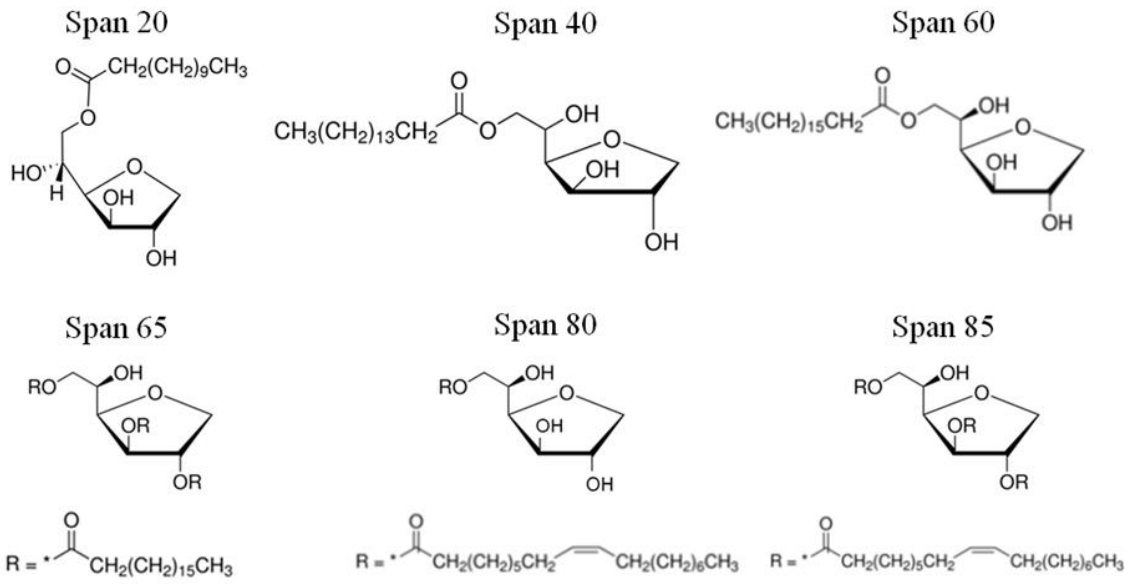

Figure 5.1. Structures of the Span surfactant series.

All of the surfactants except Span 60 were purchased from Sigma Aldrich (St. Louis, MO). Span 60 was purchased from Uniqema (New Castle, DE) and all surfactants were used as received. Surfactant purities ranged from ≥44%, for Span 20, up to ≥60%, for Span 80 and 85, with the remainder being composed of the corresponding fatty acid. No purity data could be found for Span 40 and Span 65, as the suppliers do not provide this information. The solvent used in this study was deuterated n-decane (97% purity), *d*-decane, which was purchased from Cambridge Isotope Laboratories (Andover, MA). It is worth noting that the solvent used in the previous study[16] was Isopar-L, a mixture of C_{11} to C_{15} isoparaffins. Due to the chemical distribution of this solvent, the authors were unable to obtain it in deuterated form. Deuterated decane was chosen due to its chemical similarity as a fully saturated alkane. Reverse micelles were filled with either deionized water, produced in-house, or deuterated water, purchased from Cambridge Isotope Laboratories.

Critical micelle concentrations (CMCs) of these surfactants were measured using conductometric techniques, as described in a previous paper.[16] The CMCs for Span 20, 40, and 60 were 1.133±.003mM, 0.174±.003mM, and 0.06±0.03mM respectively. A CMC of 0.042±.001mM was measured for Span 80, while Span 65 and 85 had CMCs of 0.05±.03mM and 0.26±.03mM respectively.

5.3.2 *Small Angle Neutron Scattering*

Three sets of samples were prepared for this study – one set equilibrated with H_2O vapor, one equilibrated with D_2O vapor, and one swollen with D_2O liquid. Samples were prepared at concentrations of approximately 1wt% surfactant in *d*-decane, then heated to 45ºC to ensure that the surfactant was fully dissolved. Once fully dissolved, samples were placed in humidity chambers held at 50% RH and 45ºC, and allowed to equilibrate for two hours. The swollen samples were injected with 1μL of D_2O, then stirred and sonicated to ensure that liquid was solubilized inside the reverse micellar cores.

Karl Fischer titration was used to measure the water content of the reverse micelles in units of parts per million. These values were then converted to a water-to-surfactant molar ratio for each of the six surfactants. Span 20, 40, and 60 formed reverse micelles with 0.16, 0.40, and 0.28 water-to-Span molar ratios, respectively. Span 65 and 85 were measured to have water-to-Span molar ratios of 0.20 and 0.17, respectively, while Span 80 had a water-to-Span ratio of 0.21.

Small angle neutron scattering (SANS) experiments were performed at the National Institute for Standards and Technology (NIST) Center for Neutron Research (Gaithersburg, MD). Samples were measured on the NG7 instrument with a neutron wavelength of 6Å and detector positions of 1 and 4m, covering a wave vector, q, range from 0.008 to 0.6 $Å^{-1}$.[64] The

samples were placed in demountable titanium cells with quartz windows and path lengths of 1mm. The samples were held at 45°C for the duration of the measurements. The data were reduced by accounting for the background radiation, as well as the scattering of the solvent and sample cell. By measuring the incident neutron flux, the data were normalized to absolute scale. Data reduction and normalization were performed using the Igor Pro macros developed at NIST.[65]

5.4 Results and Discussion

5.4.1 *Structures of reverse micelles*

The structures of the reverse micelles in *d*-decane were able to be measured due to the large difference in scattering length densities (SLDs) between the deuterated solvent and hydrogenated tail groups. The oxygen functionality in the head groups also offers contrast between the surfactant tails and the core of the reverse micelles. For this reason, all of the scattering profiles were fit to a core-shell model. Figure 5.2a) shows the scattering profiles for the reverse micelles which equilibrated with H_2O and Figure 5.2b) the profiles for the reverse micelles which were swollen with 1 μL of D_2O. Figure 5.3 shows the scattering profiles for the set of reverse micelles which were allowed to equilibrate with D_2O vapor at 50% RH, as well as the fit curves generated by SASview.

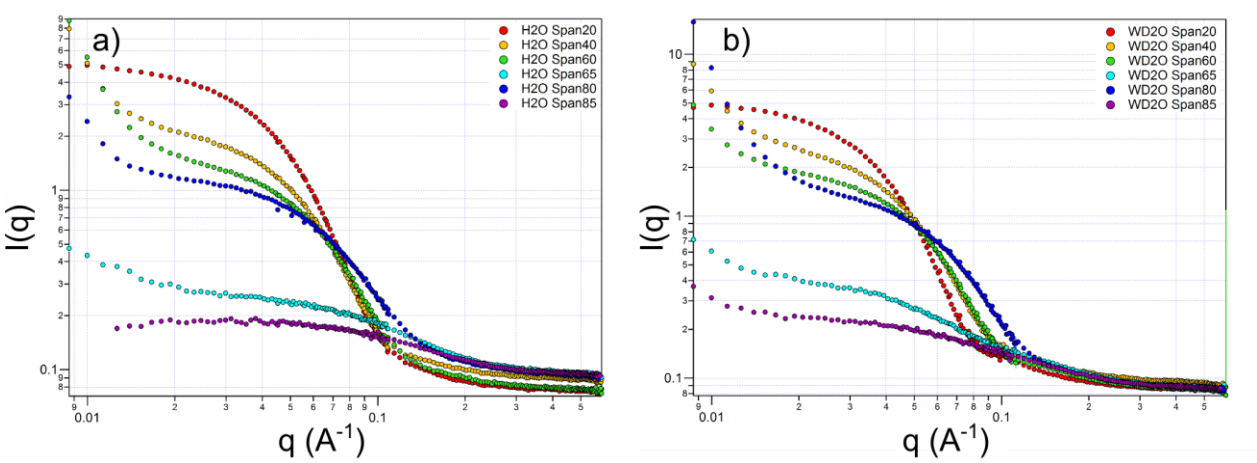

Figure 5.2. Scattering profiles (Intensity as a function of scattering vector) of the six species of Span reverse micelles equilibrated with a) H_2O and b) swollen with 1μL of D_2O. The deviations from the fit curves at low-*q* are due to the electrostatic interactions of the charged reverse micelles in the bulk.

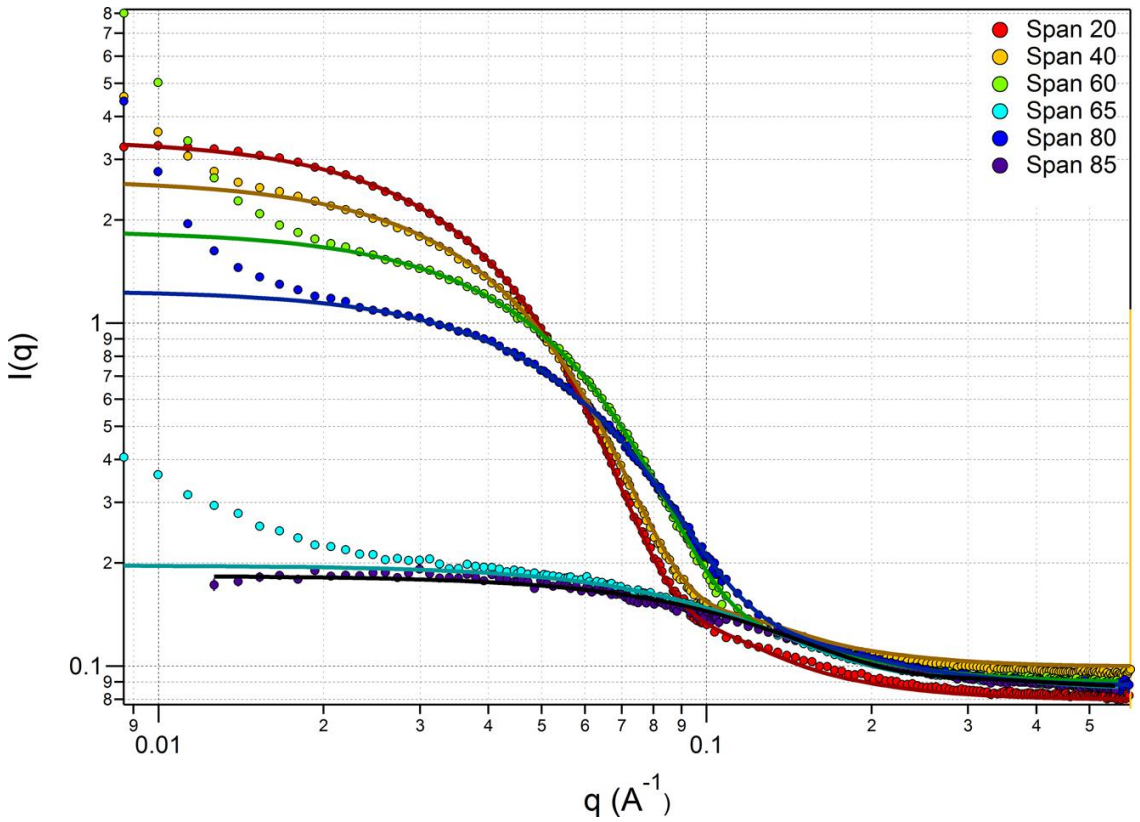

Figure 5.3. Scattering profiles (Intensity as a function of scattering vector) of the six species of Span reverse micelles equilibrated with D_2O. The solid lines through the data points represent the fits obtained using SASView. The deviations from the fit curves at low-*q* are due to the electrostatic interactions of the charged reverse micelles in the bulk.

The levelling-out of the scattering profiles at high-q values was due to the incoherent scattering of the hydrogen atoms in the surfactant tails. Many of the scattering profiles also exhibit increases in scattering intensity at low-q values. While this could be indicative of larger structures, such as undissolved surfactant or large aggregates, it is unlikely that this is the case. Dynamic light scattering experiments did not detect any structures larger than several nanometers in these samples. These increases are likely due to electrostatic interactions of charged reverse micelles in the bulk. Bulk electrostatic interactions had previously been found to lead to such increases.[61] Notably, these scattering profiles exhibit Guinier regions between approximately $0.02< q <0.08$ Å^{-1}, though the specific range varies for each individual species. What these regions suggest is that as the tail length of the surfactant increases, the size of the reverse micelle decreases. These Guinier regions also suggest that the two tri-tailed surfactants, Span 65 and 85, are significantly smaller than their single-tailed counterparts. These qualitative trends were observed for all three sets of experiments.

SasView fitting software (www.sasview.org) was used in order to obtain quantitative values for the size of the reverse micelles. The scattering profiles were fit to a spherical, core-shell form factor, and were dilute enough that no structure factor was necessary. Using this form factor, the core of the reverse micelles contain both water and the surfactant head groups, while the shell consists of the hydrogenated tails. The scattering length densities of the solvent and the micellar shell were calculated using the NIST SLD calculator, and were fixed at $6.6\text{x}10^{-6}$Å^{-2} and $-6.6\text{x}10^{-7}$Å^{-2}, respectively. The scattering scale, or volume fraction, was calculated using the molecular volumes of the individual surfactant molecules as determined using MarvinView 16.8.1, 2016, ChemAxon (www.chemaxon.com). The core radius, shell thickness, polydispersity, and core SLD were fit to the scattering data. All fits resulted in χ^2/N values less

than 10. Table 5. summarizes the calculated volume fractions and polydispersities used in the fitting, while Table 5. summarizes the results for the core radius and shell thickness for each of the six surfactants in each of the three data sets.

Table 5.1. Fitting parameters for the Span surfactant series showing volume fraction and polydispersity.

	H2O Vapor		D2O Vapor		D2O Swollen	
	Vol Fraction	Polydispersity	Vol Fraction	Polydispersity	Vol Fraction	Polydispersity
Span 20	0.00524	0.50	0.00438	0.44	0.00426	0.35
Span 40	0.00526	0.48	0.00452	0.41	0.00526	0.50
Span 60	0.00571	0.60	0.00568	0.52	0.00571	0.41
Span 80	0.00648	1.00	0.00472	0.86	0.00648	0.78
Span 65	0.00650	1.00	0.00643	1.00	0.00650	1.00
Span 85	0.00514	1.00	0.00509	1.00	0.00514	1.00

Table 5.2. Micellar size results for the Span surfactant series showing core radius, hydrocarbon shell thickness, and surfactant HLB values.

	HLB	H_2O Vapor		D_2O Vapor		D_2O Swollen	
		Radius (Å)	Thickness (Å)	Radius (Å)	Thickness (Å)	Radius (Å)	Thickness (Å)
Span 20	8.3	23.3	6.2	24.6	8.2	31.9	8.9
Span 40	6.7	19.4	7.1	22.5	8.4	21.4	8.2
Span 60	4.7	14.7	6.4	16.2	7.4	20.5	7.6
Span 80	4.3	8.3	7.4	10.2	6.9	11.5	6.9
Span 65	2.1	3.8	6.0	3.9	5.7	8.4	6.6
Span 85	1.8	3.0	6.0	3.7	5.1	4.4	6.0

Notably, there did not appear to be any systematic trend in the thickness of the hydrocarbon shell and the chain length of the surfactants. In all cases, the shell thickness was found to be between 6 and 9Å. If the tails were fully extended, shell thicknesses should be between 14 and 22Å as determined by MarvinView. It is unlikely that during the formation of reverse micelles, the surfactant tails would compress to less than half their contour length. One

possibility is that the deuterated solvent intercalated itself into the shell of the reverse micelles, significantly increasing the SLD in that region of the shell. If so, with the SLD of the shell set to a value for a fully hydrogenated tail, the fit found the region of the shell which was free of intercalated solvent. However, experiments varying the solvent contrast would need to be performed in order to fully probe this theory.

As the tail length of the surfactant molecule increased, from Span 20, to 40, to 60, the size of the polar core decreased for all three experimental sets. The addition of the double bond in the tail, from Span 60 to 80, also decreased the size of the core in every case. This suggests that shorter-tailed surfactants behave more hygroscopically than their longer-tailed counterparts. This behavior has been observed with nonionic, polyglycerol surfactants as well, where increasing tail length resulted in decreasing radii of the reverse micelles.[70] Notably, the tri-tailed surfactants form the smallest reverse micelles, with core sizes of approximately 4Å. This is likely due to the steric constraints of having three C_{17} tails. Trehalose polyisostearate surfactants have been shown to behave similarly, whereby increasing the number of tails in the surfactants resulted in smaller reverse micelles.[71] While the reverse micelles that were equilibrated with D_2O vapor were found to have core sizes slightly larger than those equilibrated with H_2O vapor, this difference is likely due to the slightly higher humidity in which those samples were held.

With the addition of 1μL of D_2O, all but one of the core radii increased. Span 40 experienced a 5% decrease in core size, but this was likely due to the D_2O not being fully solubilized inside the cores, and phase separating in the cells. Span 20 and 60 were able to swell significantly more, 26-29% increases, than Span 80, with an increase of only 12%. The tri-tailed Span 65 more than doubled in core size, while Span 85 only increased in radius by 19%. This suggests that surfactants with fully-saturated tails are able to swell more significantly than those

with unsaturated tails, possibly due to the rigidity of the unsaturated tail groups preventing the structural rearrangement necessary to accommodate a further uptake of water into the reverse micelles.

Estimates of the reverse micellar aggregation numbers were calculated using the available surface area of the polar core and the cross sectional area of the sorbitan head group, as determined by MarvinView. In order to accurately determine aggregation numbers, solvent contrast variation experiments[31] would have been necessary. Using the core radii from the D_2O vapor experiments, aggregation numbers for Span 20, 40, and 60, were 307, 258, and 134 respectively. With the addition of the double bond in the tail, Span 80 had a much lower aggregation number of 53. The two tri-tailed surfactants, Span 65 and 85, had the lowest aggregation numbers of 8 and 7 respectively. This trend can also explain the decrease in shell thickness associated with a decrease in aggregation number. With lower aggregation numbers, the packing density of surfactant tails in the shell would be lower, allowing for more intercalation of solvent molecules into the shell, and a smaller measured shell thickness.

One can correlate the hygroscopic nature of a surfactant to its Hydrophile-Lipophile Balance (HLB) value, with smaller HLB values relating to less hydrophilic species. Plotting the size of the reverse micellar core as a function of each surfactant's HLB value, as shown in Figure 5.4, a clear trend emerges. As the HLB of the surfactant increases, the size of the polar core increases as well.

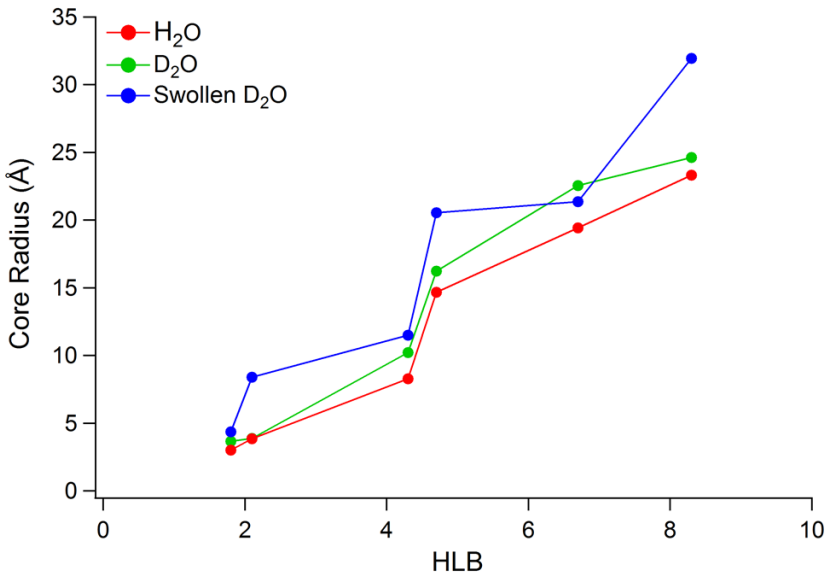

Figure 5.4. Core size of reverse micelles as a function of the surfactant HLB value.

Previous work by Gacek and Berg[29] found by normalizing the maximum particle electrophoretic mobilities of a large range of particle-surfactant pairings to the HLB of the surfactant, there exists a linear dependence on the relative difference in the acidity/basicity of the particle-surfactant pair. This finding allows researchers to estimate the maximum mobility achievable given a particle-surfactant pair. However, the HLB value is an empirical estimation of a surfactant's affinity for water. With this finding, one can see that the charging behavior of the surfactant is affected by the size of the reverse micellar cores.

5.4.2 *Correlations of micellar size and charging capabilities*

A previous study[16] investigated the capabilities of the Span series to charge magnesia particles over a range of temperatures. It was found that the maximum electrophoretic mobility which a surfactant could impart depended on the number and length of the tail groups. The tri-tailed surfactants (Span 65 and 85) imparted the lowest mobilities, while the single-tailed surfactants were able to impart much larger mobilities. Given that the Span series, except Span

65 and 85, all have the same chemical functionality in the head group, the difference in charging capabilities must arise due to differences in the reverse micelles which they form. It is possible that the lower number of hydroxyl groups in Span 65 and 85 could play a role in the weaker charging behavior of these surfactants, however the significantly smaller core radii likely are of greater importance. Given that the polar core of the reverse micelles is crucial to determining their charging behavior, the maximum particle electrophoretic mobility can be plotted as a function of the reverse micellar core radius, shown in Figure 5.5.

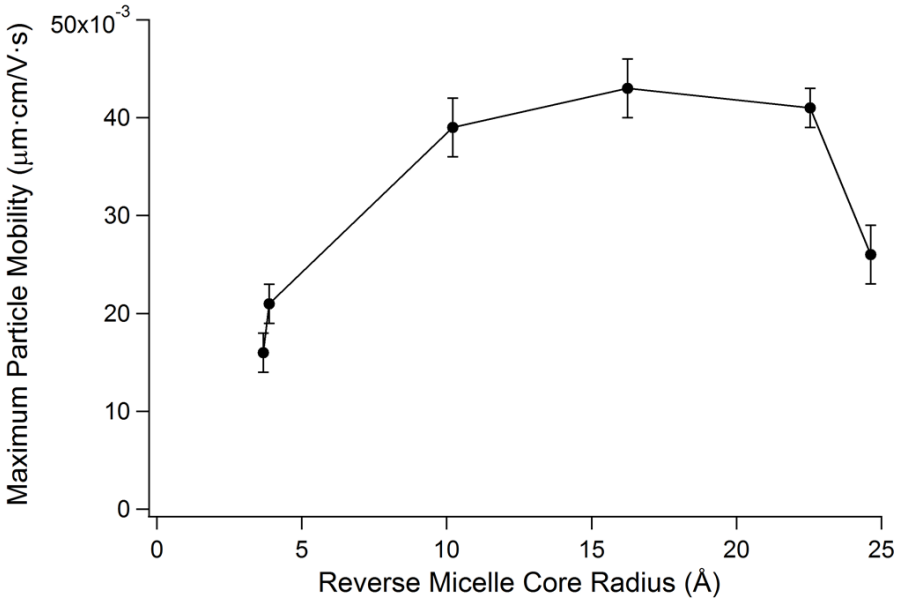

Figure 5.5. The maximum particle electrophoretic mobilities of magnesia particles in Isopar-L as a function of the core radius of the reverse micelles performing the charging.

The reverse micelles with the smallest core sizes (Span 65 and 85) imparted the lowest mobilities to the magnesia particles. As the core size increased, from Span 80 to 60, the maximum mobilities imparted also increased. However, as the core size increases further, from Span 40 to 20, the mobility goes through a maximum value, before decreasing again. This implies an optimal core size to obtain the higher particle mobility. This range appears to be relatively large, given that cores with radii between 10 and 22Å charge the magnesia particles to

similar magnitudes. If the core is too small, it becomes extremely unfavorable for a charging event to occur. On the other hand, if the core is too large, the reverse micelles favor disproportionation reactions in the bulk, resulting in a higher number of charged micelles and hence electrostatic screening of the particle charges and decreased electrophoretic mobility. These disproportionation reactions occur when two neutral reverse micelles interact to form two oppositely-charged reverse micelles. The probability of such a charging event scales as $\exp(-Z^2\lambda_B/2a)$, where Z is the valence of the charge in the core, λ_B is the Bjerrum length, and a is the radius of the core.[15] This suggests that as the core size increases, so does the probability of reverse micelles undergoing bulk charging events. Reverse micelles with intermediate core sizes offer a large enough polar environment to favorably stabilize a charge, yet not enough that disproportionation reactions result in electrostatic screening of the particles.

5.5 CONCLUSIONS

The particle charging behavior of the Span series was investigated in a previous study and compared to the reverse micellar structures investigated here. The reverse micelles with intermediate core radii imparted the highest magnitude of electrophoretic mobility to the particles. Reverse micelles with small cores sizes low probability for charging events to occur, while large core radii favor disproportionation reactions, resulting in particle charge screening.

It was found that as the tail length of the surfactant increased, the size of the micellar core decreased. The two tri-tailed surfactants exhibited the smallest core sizes due to the steric constraints of forming micelles from bulky surfactants. The two surfactants with unsaturated tails were found to exhibit the smallest increase in core size when swollen with D_2O, possibly due to the difficulty in micellar rearrangement with rigid tail groups. The size of the polar cores was directly proportional to the HLB value of the surfactant which formed the reverse micelles.

This work is relevant to research in electrophoretic displays and printers, where controlling the particle mobility is crucial to functionality of the product. This study shows that in order to achieve the maximum particle mobility, the size of the micellar core must be chosen such that charge stabilization is favorable, but disproportionation is not. This is accomplished in part by tuning the HLB, by varying the tail length, of the surfactant.

APPENDIX A - AN EXTENSION TO THE CHARGE FLUCTUATION MODEL FOR THE PREDICTION OF THE CONDUCTIVITY OF APOLAR, REVERSE MICELLAR SYSTEMS

ABSTRACT

This study investigated an extension to current theory regarding charging behavior in apolar, micellar systems. Electrical conductivity in such systems accompanying the formation of neutral reverse micelles is commonly explained by the possibility of inter-micellar collisions resulting in a pair of oppositely charged micelles. The sequestration of the resulting charges within the micelles prevents their immediate recombination. The current theory underlying the charging process has thus far been applied in only approximate form, and is only used to validate experimental trends and to abstract values for the fraction of charged micelles. The extended theory investigated here uses knowledge of the solvent and surfactant characteristics, together with water content, to attempt to predict solution conductivity in absolute terms. Experiments were performed with the solvent Isopar-L and surfactants Aerosol OT®, OLOA 11000® and Span 80®, and it was found that the extended theory predicted conductivities 30-100 times lower than experimental values, while the current theory predicted values 5-12 times lower.

INTRODUCTION

Eicke and coworkers[66] in 1989 developed a model for the conductivity of water-in-oil microemulsions. On average, each microdroplet was presumed to contain an equivalent number of positive and negative charges, but spontaneous fluctuations allowed for an imbalance which

produced a small population of charged droplets responsible for the conductivity of the system as a whole. The conductivity of such microemulsions was given by

$$\sigma = \frac{\varepsilon\varepsilon_0 kT}{2\pi\eta}\frac{\varphi}{r^3}, \tag{A.1}$$

where ε is the dielectric constant of the solvent, ε_0 is the permittivity of free space, k is the Boltzmann constant, T is absolute temperature, η is the viscosity of the solvent, φ is the volume fraction of the droplets in the system, and r is the radius of the droplets.

Kallay and Chittofrati[74] extended the formulation proposed by Eicke et al by noting that the difference between the Born radius (hydrophilic core) and Stokes radius (hydrodynamic radius) must be taken into account for small microemulsion droplets. In small droplets, i.e. micelles, the surfactant tails account for a significant portion of total micellar radius. The self energy (Born energy) of a droplet must not use the hydrodynamic radius as this would imply that the entirety of the droplet could carry charge, when, in reality, only the core can. Accounting for this difference, a better correlation between theory and experimental data was found for microemulsion "droplets" in the nanometer size regime. These droplets are presumed to be dissolved entities, i.e., swollen micelles.

In 1990, Hall[75] provided an explicit mechanism for the charging of a portion of the droplets by disproportionation, wherein two uncharged droplets interact to form two, oppositely-charged droplets, i.e.

$$2M_0 \leftrightarrow M_+ + M_-, \tag{A.2}$$

where M_o is an uncharged droplet and M_+ and M_- are positive and negative droplets, respectively. Expressions for the chemical potentials, μ, of the three species were formulated in the usual way:

$$\mu_0 = \mu_0^{\ominus} + kT\ln(C_0), \tag{A.3a}$$

$$\mu_+ = \mu_+^{\Theta} + kT\ln(C_+)\ \mu_+ = \mu_+^{\Theta} + \mathrm{kTln(C_+)}, \text{ and} \tag{A.3b}$$

$$\mu_- = \mu_-^{\Theta} + kT\ln(C_-)\ \mu_- = \mu_-^{\Theta} + \mathrm{kTln}\left(\mathrm{C_-}\right), \tag{A.3c}$$

where μ_0^{Θ}, μ_+^{Θ} and μ_-^{Θ} $\mu_o^{\Theta}, \mu_+^{\Theta}$are the standard state chemical potentials of the neutral, positive and negative drops, and C_o, C_+ and C_- are the number concentrations of the same droplets. Equilibrium of Equation A.2 requires

$$2\mu_0 = \mu_+ + \mu_-. \tag{A.4}$$

Combining Equations A.3 and A.4, gives

$$2\mu_0^{\Theta} - \mu_+^{\Theta} - \mu_-^{\Theta} = \Delta G^{\Theta} = kT\ln\left(\frac{C_+C_-}{C_0^2}\right). \tag{A.5}$$

The standard free energy of reaction A.2 may be computed as the energy associated with the charging of two neutral droplets of radius r to valencies of ±Z in an infinite medium of dielectric constant ε, as

$$\Delta G^{\Theta} = E = \frac{Z^2e^2}{4\pi\varepsilon\varepsilon_0 r}\ . \tag{A.6}$$

Combining Equations A.5 and A.6 leads to

$$kT\ln\left(\frac{C_+C_-}{C_0^2}\right) = \frac{Z^2e^2}{4\pi\varepsilon\varepsilon_0 r}. \tag{A.7}$$

Electroneutrality requires $C_+ = C_- = C_Z$, where C_Z is the concentration of droplets with charge Z. The concentration of charged species is thus

$$C_Z = C_0\exp\left(-\frac{Z^2e^2}{8\pi\varepsilon\varepsilon_0 kTr}\right). \tag{A.8}$$

With this expression for the concentration of droplets of any charge Z, the conductivity of the microemulsion becomes

$$\sigma = \frac{\sum_{Z=-\infty}^{+\infty} Z^2 C_Z e^2}{6\pi R_H \eta}, \tag{A.9}$$

where R_H is the hydrodynamic radius of each droplet, and η is the viscosity of the solvent. The summation accounts for all possible charged droplets of Z from $-\infty$ to $+\infty$. However, due to the Boltzmann distribution of charge concentrations, it becomes less and less probable for droplets to exist with large absolute values of Z. This formulation for the conductivity of apolar, microemulsion systems was more consistent with experimental data than the original model of Eicke et al.

In more recent work, by Roberts et al.[76] and Guo et al.,[15] Hall's model has been applied to apolar, micellar systems. As micelles can be thought of as less-swollen microemulsion droplets, one can apply this to Equation A.8. As r decreases, the probability of a micelle containing more than one charge falls as $\exp(Z^2)\exp(Z^2)$. In Roberts et al.[76], the assumption is made that micelles can contain only a single charge of either polarity, i.e., $Z = \pm 1$. Using this assumption, and defining $\chi = \frac{2C_Z}{C_0}$ as the fraction of charged micelles, one obtains

$$\chi = 2\exp\left(-\frac{Z^2 e^2}{8\pi\varepsilon\varepsilon_0 kTr}\right) = 2\exp\left(-\frac{\lambda_B}{2a}\right), \tag{A.10}$$

where λ_B may be recognized as the Bjerrum length, and a is the radius of the polar, micellar core. The Bjerrum length is the separation distance producing an electrostatic energy equal to kT. Using the fraction of charged micelles, the derivation for the conductivity of such a system leads to

$$\sigma = \frac{e^2(C_+ + C_-)}{6\pi\eta R_H} = \frac{e^2 \chi C_T}{6\pi\eta R_H}, \tag{A.11}$$

where $C_+ = C_- = \frac{1}{2}\chi C_T$, C_T is the total number concentration of micelles, R_H is the hydrodynamic radius of the micelles, and η is the viscosity of the system. Roberts et al. and Guo et al. then use Equations A.10 and A.11 together with the measured value of the conductivity to extract the fraction of charged micelles, χ.

It has long been thought that moisture plays an important role in charging phenomena in apolar media,[18] and the recent work of Guo et al. and Gacek et al.[22] showed that the conductivity of an apolar, micellar solution increased directly in proportion to water content. This is not surprising, as water would swell the core size, and as can be seen in Equation A.10, this would lead to an increase in conductivity. Guo et al. show conductivity as a linear function of molar water-to-surfactant ratio for both Aerosol OT® and Span 85® in hexane. The AOT curve suggests a three-fold increase in conductivity with a three-fold increase in molar water content. A simple calculation using Equation A.10 would, however, predict a *fourteen*-fold increase in conductivity with this increase in water content. This discrepancy between experimental data and theory appeared to warrant further investigation into the current model.

The present model considers the charging a neutral entity of radius *a* to a valence of unity in an infinite apolar medium. However, the presence of water in the core suggests the need for a more detailed picture. In 1969, Parsegian[77] formulated expressions for the self energies of ions in various systems, in an effort to characterize transport through apolar membranes. In one such system, an ion of radius *b* was considered to exist in a hydrophilic carrier, i.e. water, of radius *a,* which is surrounded by an infinite medium of low dielectric constant. It is reasonable to imagine that such a system could also describe the core of a charged micelle as pictured schematically in Figure A.1.

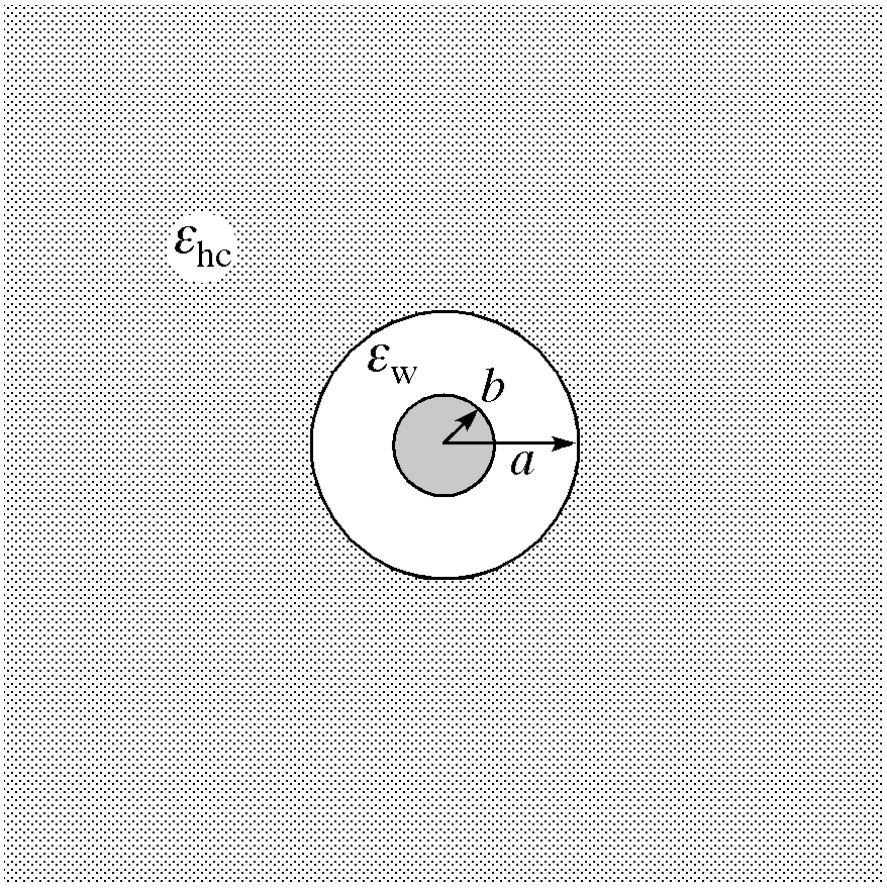

Figure A.1. Schematic of a system modeling water-swollen micelles in an apolar medium.

In Figure A.1, ε_{hc} and ε_w are the dielectric constants of the hydrocarbon medium and the water-filled core, respectively. Parsegian's expression for the self energy of such a system is

$$E = \frac{1}{4\pi\varepsilon_0}\left[\frac{e^2}{2\varepsilon_{hc}a} + \frac{e^2}{2\varepsilon_w}\left(\frac{1}{b} - \frac{1}{a}\right)\right], \tag{A.12}$$

where b is the radius of the carried ion and a is the radius of the polar carrier, which would include both the polar head groups of the micelle as well as the water within the core. This expression can be described as the work required to bring an ion of radius b and valence of unity into a polar carrier of radius a in an infinite apolar medium. Compare this with Equation 6, which does not account for the work required to bring the ion within this finite carrier (i.e. the second term in brackets). We then define the free energy of Reaction A.2 as

$$\Delta G^{\Theta} = kT\ln\left(\frac{C_+C_-}{C_0^2}\right) = \frac{1}{4\pi\varepsilon_0}\left[\frac{e^2}{\varepsilon_{hc}a} + \frac{e^2}{\varepsilon_w}\left(\frac{1}{b} - \frac{1}{a}\right)\right]. \quad \text{(A.13)}$$

Rearranging Equation A.13, and defining $C_+=C_-=C_{+/-}$, one can solve for the fraction of charged micelles as

$$\chi = 2\exp\left\{\frac{-1}{8\pi\varepsilon_0 kT}\left[\frac{e^2}{\varepsilon_{hc}a} + \frac{e^2}{\varepsilon_w}\left(\frac{1}{b} - \frac{1}{a}\right)\right]\right\}. \quad \text{(A.14)}$$

It can be seen that as the size of the ion approaches the size of the hydrophilic core, $b \rightarrow a$, the second term in the square brackets approaches zero. In this limit, Equation A.14 becomes Equation A.10. While Equation A.10 can be applicable to situations where *a* and *b* are approximately equal, one can imagine that when *a* is significantly larger than *b*, i.e. the micelles contain a significant amount of moisture, Equation A.10 would overestimate the number of charged micelles.

The present work seeks to predict quantitatively the conductivity of micellar solutions in apolar solvents containing varying amounts of water using the modified model shown in Figure A.1 and described using Equations A.11 and A.14, and to compare the computed results with experimental conductivity measurements obtained for systems consisting of a low dielectric constant solvent and three different surfactants. Computations are performed using computer models for the surfactant monomer geometric parameters, tabulated values for the micelle aggregation numbers and direct measurements of water content.

MATERIALS AND METHODS

Materials

The solvent used in these studies was Isopar-L, supplied by Exxon-Mobil Chemical Co. (Houston, TX) and used as received. It consists of a mixture C_8-C_{15} isoparaffins, with an aromatic content of less that 30 ppm, and a dielectric constant of 2.0.

The surfactants used in the study were Aerosol OT®, OLOA 11000® and Span 80®. Aerosol OT® (or AOT), sodium dioctyl sulfosuccinate, was supplied by Fischer Scientific (Pittsburgh, PA) and used as received. It is known to form spherical micelles of approximately 22 monomer units in apolar media.[31] OLOA 11000® was obtained from Chevron Oronite (San Ramon, CA). It consists of molecules with a polyisobutylene tail attached to a polyamine head group. The commercial product consists of a mixture of single and di-tail molecules with an average molecular weight of 1200 g/mol dispersed in a solution of silicone oil, with 72% active component.[32] OLOA 11000® is reported to form spherical micelles in apolar media with an aggregation number of approximately six.[78] Span 80®, or sorbitan monooleate, was obtained from Sigma Aldrich (St. Louis. MO) and used as received. Span 80® consists of a sorbitan head group attached to an oleic acid tail and has been reported to form spherical micelles in apolar media with an aggregation number of approximately 28.[79]

Methods

Solutions of each surfactant were prepared at 1 wt percent (17 mM, 6.4 mM and 18 mM in Aerosol OT®, OLOA 11000® and Span 80®, respectively) in Isopar-L, at least an order of magnitude above the values of the critical micelle concentration (CMC) in each case, as shown in Table A.2. Molecular sieves were added, and the solutions stored in a desiccators for 24 h. Each solution was divided into five aliquots of 100 mL each for treatment with varying amounts of de-ionized water. After thorough mixing and sonication, the samples were allowed to

equilibrate for approximately 12 h. The conductivity of each sample was then measured at a temperature of 21°C using a DT-700 nonaqueous conductivity probe from Dispersion Technologies, Inc. (Bedford Hills, NY). At least 20 repeat measurements were made for each data point.

The predicted conductivity for each system using Equation A.11 requires the number density of the micelles, C_T, the solution viscosity, η, the hydrodynamic radius of the micelles, R_H, and the fraction χ of the micelles carrying charge. The number density of the micelles was computed in each case by dividing the nominal monomer number density, i.e., the monomer molarity multiplied by Avogadro's number, by the micelle aggregation number, with results shown in Table A.2. This assumes that effectively all the surfactant inventory was in the form of micelles. The solutions were sufficiently dilute in all cases that their viscosities were assumed to be the same as that of the solvent, Isopar-L, which was measured at 21°C to be 1.55 cP. The hydrodynamic radius of the micelles was computed making use of Marvin molecular modeling software (Marvin 5.10.2, 2012, ChemAxon). Values for both the polar head group size and surfactant tail length were calculated and are shown in Table A.2, and the monomers were assembled into spherical micelles of the appropriate aggregation number, assuming no changes in the monomer geometry upon micelle formation. All micelles were assumed to be spherical, and surfactant molecules were assumed to be evenly distributed over the sphere. The micelle size also depended on the size of the polar core in each case, which in turn depended on the amount of water it housed. The total water content in each sample, as measured by Karl Fischer titration, was assumed to be distributed evenly among all the micelles, whose aggregation number was assumed to remain unchanged with water content, and the water core radius computed using the bulk density of water. The total polar core radius was computed for each surfactant and water

content by adding the radius of the water core and the length of the polar head group. Finally, the hydrodynamic radius for each surfactant was calculated by adding the polar core radius to the length of the surfactant molecule tail.

The fraction, χ, of the micelles carrying charge is computed in accord with Equation A.14 in terms of the total polar core radius, *a,* determined as above, and the radius *b* of the charge carrier(s) in the micelle. The latter are assumed to be single hydronium and hydroxyl ions, whose radii are 1.9Å and 1.7Å, respectively, so that the average value of 1.8Å is used for *b.*

Table A.2. Monomer and micellar properties for the three investigated surfactants in the solvent Isopar-L at 21°C.

	AOT	OLOA 11000	Span 80
Molecular weight (g/mol)	444	1200	429
Head group length (Å)	6	8.8	8
Tail group length (Å)	7	28.1	19.5
Critical micelle concentration (mM)	0.0045[1]	1.1[2]	0.058[2]
Aggregation number	22[3]	6[4]	28[5]

1 [27] ; 2 [28] ; 3 [31]; 4 [78]; 5 [79]

RESULTS AND DISCUSSION

The measured conductivities for each surfactant system as a function of the water-to-surfactant molar ratio are shown in Figure A.2. Computed conductivities based of the approximate theory of Equations A.10 and A.11 and the extended model using Equation A.14 are shown for comparison. It is evident that in all cases neither theory accurately predicts the experimentally measured conductivities, however the approximate theory is closer to experimental values than the extended theory.

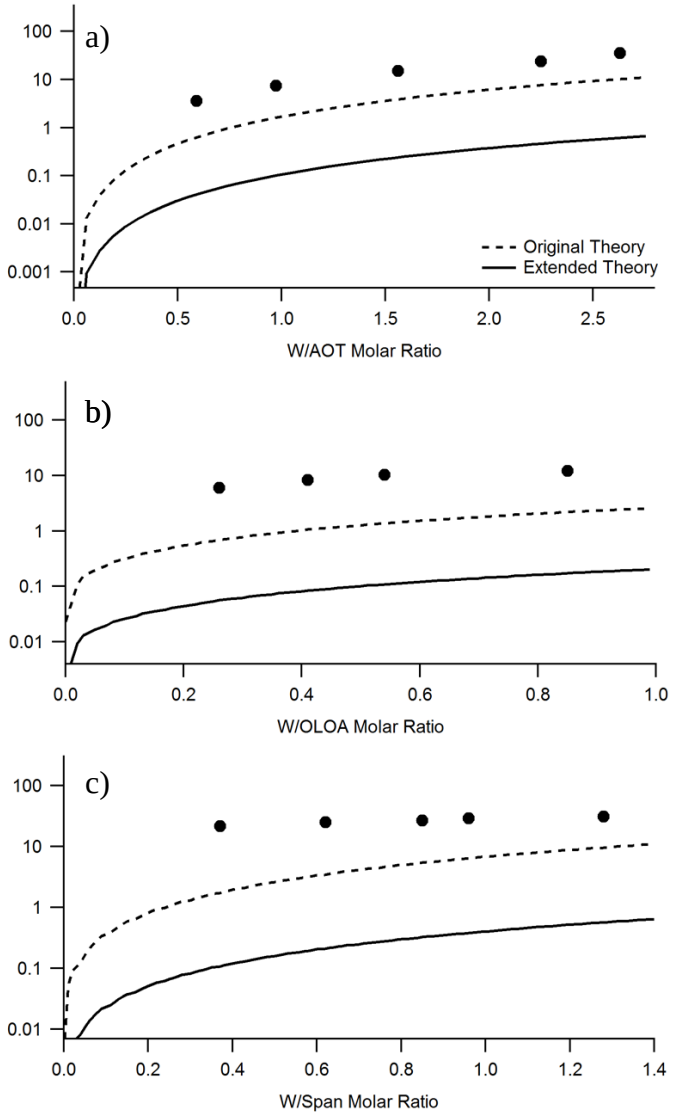

Figure A.2. The measured conductivity (●) of 1 wt% solutions of a) AOT, b) OLOA 11,000 and c) Span 80® in Isopar-L at varying water-surfactant molar ratios. Error bars, based on a minimum of 20 measurements, are within the markers. Continuous lines are the computed results based on the approximate model (– – –) and the extended model (——), respectively.

Examining Equation A.14, one can see that as the size of the polar core approaches the size of the ion it is carrying, the second term in the exponential drops out, and Equation A.14 simplifies to Equation A.10. Thus at lower water-to-surfactant ratios, i.e. where the total polar core size is closer to the size of the carried ion, the conductivity as predicted by the approximate model is closer to that predicted by the extended model. However, as the head group length is

included in the hydrophilic core, the complete absence of water would not result in the reduction of Equation A.14 to Equation A.10. The core radius would still differ from the ion size by the length of the head group. This means that even at water-to-surfactant ratios of zero, the two theories would not predict equal conductivities.

Conductivities as predicted by the extended model, Equation A.14, are 30-100 times lower than experimentally measured values while conductivities predicted by the original theory (Equation A.10) are closer to experimental values but still lower by a factor of 5-12. It is clear that the extended theory does not provide a better representation of the experimental systems. Thus the issue of how reverse micelles are actually charging in apolar systems remains open. It may be the case that the use of the Born equation for the calculation of self-energies of such small systems is invalid, resulting in much higher energies than are realistic.[80] These higher energies would suggest that reverse micellar charging is less favorable than in reality, and predict lower conductivities.

Given that neither model appears to provide good predictions of the measured conductivities for the systems investigated, different extensions may be contemplated. It must be noted that at very low water contents, an equal distribution of water throughout the micelles would result in there being only 1 or 2 water molecules in each core. Such a limit would require a far more rigorous model. As noted, the model presented here uses a continuum approach in order to maintain analytical expressions for the conductivity of such systems. Factors such as differences in dielectric properties between the surfactant shell around the core and the solvent; possible ion-dipole interactions of the carried ion with the head groups could also be taken into account. Future work may also use additional experimental techniques, such as small angle neutron scattering (SANS), to measure directly the various size parameters of these micelles.

CONCLUSIONS

An extension is proposed to the charge fluctuation model of Eicke,[66] Hall[75] and others,[15,74,76] to predict the conductivity of micellar surfactant solutions in apolar media. While the original model treats the entire polar core of the micelle as the charge-bearing entity, the new model accounts for the difference between the solubilized ion size and the total polar core size. It is implemented using modeling software to calculate the sizes of the surfactant molecules, independent measurements of the system water content, together with known or measured micelle aggregation numbers. While the original theory produces conductivities generally an order of lower than the measured values of the conductivity for water-laden solutions of surfactants Aerosol OT®, OLOA 11000® and Span 80® in the solvent Isopar-L, the extended theory predicts values up to two orders of magnitude lower than experimentally measured conductivities. This study warrants further investigation as to how reverse micelles carry charge in apolar systems.

APPENDIX B – THE ELECTROVISCOUS EFFECT IN APOLAR MEDIA

The research presented in the following study was unpublished work, performed in 2013. The goals of this study were to investigate whether electroviscous effects existed in apolar dispersions, and to determine whether current theories could accurately predict their behaviors.

INTRODUCTION

When dispersed in a medium, colloidal particles can become charged by a variety of mechanisms. This charge is balanced by a diffuse double-layer of counter-ions around the particle. The concentration of counter-ions is largest near the particle surface, and then falls away to bulk concentration, n_∞, as the distance from the particle surface approaches infinity. The surface of the particle has a specific surface potential, designated ψ_o, and the bulk potential is designated as ψ=0. Using these boundary conditions, the Poisson-Boltzmann equation can be solved to obtain the potential profile surrounding a charged colloidal particle. Out of this solution comes the Debye parameter,

$$\kappa = \sqrt{\frac{2e^2 z^2 n_\infty}{\varepsilon \varepsilon_o kT}}\,, \qquad \text{(B.1)}^{19}$$

where e is the elementary charge, z is the counter-ion valence, ε is the dielectric constant of the medium, k is the Boltzmann constant, and T is the absolute temperature. The Debye parameter quantifies a solvent's electrostatic screening capability, and is only a function of solvent properties, not particle properties. The Debye length, κ^{-1}, has units of length and gives the distance away from the particle's surface that the dimensionless potential, ψ/ψ_o, falls to $1/e$, and is the distance away from a particle's surface that another particle can "feel" the electrostatic

repulsion. In aqueous media, the Debye length is on the order of a few nanometers, while in apolar environments, this value can be can be as large as several microns.

To quantify a particle's magnitude of charge, its zeta potential can be used. The true surface potential of a particle cannot be measured due to the diffuse double-layer of counter-ions. The potential of a particle is measured at its hydrodynamic slip plane, which is then designated its zeta potential.

The presence of particles in a fluid increases its viscosity, and for the case of low volume fraction, ϕ, dispersions ($\phi < 0.02$), can be given by[81]

$$\mu = \mu_o(1 + 2.5\phi) \tag{B.2}$$

where μ is the viscosity and μ_o is the viscosity of the pure medium.

Given the limited practical use of Equation B.1, models have been proposed to describe the viscous behavior of dense dispersions (large ϕ). In a current paper by Brouwers,[82] the relative viscosity, μ/μ_o, of a non-charging dispersion of spherical particles is given by

$$\mu / \mu_o = \left(\frac{1-\phi}{1-\frac{\phi}{\phi_m}} \right)^{[\mu]\frac{\phi_m}{1-\phi_m}}, \tag{B.3}$$

where ϕ_m is the maximum particle volume fraction, taken as 0.64, and $[\mu]$ is the intrinsic viscosity, taken as 2.5.

Electroviscous effects

The viscosities of charged dispersions are often higher than those of uncharged dispersions. This effect is important for practical systems, given that dispersion stability often requires the particles to be charged. This phenomenon was first studied by Smoluchowski[83] in

1916 for the case of thin double-layers and low zeta potentials. His work was furthered by Booth[84] in 1950 and again by Russel[85] in 1978 for more general cases. The effect of particle charge on dispersion viscosity can be broken up into three effects. The primary effect accounts for the resistance of the counter-ion double-layer to deformation in shear fields. Booth[84] derived the following expression for this effect,

$$[\mu]_B = 2.5\left\{1 + \frac{4\pi(\varepsilon\varepsilon_o\zeta)^2}{k\mu_o a^2}\left[(\kappa a)^2(1+\kappa a)^2 Z(\kappa a)\right]\right\}, \tag{B.4}$$

where $[\mu]_B$ is the intrinsic viscosity, k is the specific conductivity of the medium, a is the radius of the particle, and $Z(\kappa a)$ is a function of κa which depends on the magnitude of κa. The intrinsic viscosity is given by[81]

$$[\mu]_B = \frac{\mu - \mu_o}{\mu_o \phi}, \tag{B.5}$$

and quantifies a solute's (in this case, particle's) contribution to the system viscosity. In apolar media, κa is small and $Z(\kappa a)$ is given by[84]

$$Z(\kappa a) = (200\pi\kappa a)^{-1} + \frac{11\kappa a}{3200\pi}. \tag{B.6}$$

The primary effect is often of lesser importance than the secondary electroviscous effect, which accounts for the effective increase in effective hydrodynamic size of particles due to the presence of the diffuse double-layer. In the case of low shear rates, Russel[85] derived the expression for the reduced viscosity as follows,

$$\mu_{red} = [\mu]_B\left(1 + \frac{2}{5}\phi\right) + \frac{3}{40}\ln\left(\frac{\alpha}{\ln\alpha}\right)\left[\ln\frac{\alpha}{\ln(\alpha/\ln\alpha)}\right]^4 \frac{\phi}{(\kappa a)^5}, \tag{B.7}$$

where the reduced viscosity is given by[81]

$$\mu_{red} = \frac{\mu/\mu_o - 1}{\phi}, \tag{B.8}$$

and α is a dimensionless parameter given by

$$\alpha = \frac{4\pi\varepsilon\varepsilon_o\zeta^2 a^2 \kappa}{kT}\exp(2\kappa a). \tag{B.9}$$

This parameter is a ratio of the electrostatic energy to the thermal energy in a system. Thus, for highly charged particles with small double-layers (large κa), α is much greater than unity. The tertiary electroviscous effect accounts for the expansion and contraction of adlayers on particle surfaces, which requires a polymer or other large structure must be adsorbed on the surface of the particles. This effect can be ignored in this study, since no large structures or polymers are present.

The goals of this study were twofold: to determine whether electroviscous effects are present in apolar dispersions of charged particles and to investigate the validity of Equations B.4-B.9 to predict the viscosities of these dispersions.

MATERIALS AND METHODS

Materials

The solvent used in these experiments was Isopar-L, a commercial mixture of C_8 to C_{15} isoparaffins supplied by Exxon Mobil Chemical (Houston, TX), which was used as supplied. This solvent has a dielectric constant of 2.0 and a viscosity of 1.5cP. The particles were 250nm silica (SiO2) spheres from Fiber Optics Center Inc. (New Bedford, MA). The particles were monodisperse and were used as supplied. The surfactant used as a charging agent in this study was Aerosol OT (AOT), also known as sodium dioctyl sulfosuccinate, and was supplied by

Fischer Scientific (Pittsburgh, PA). This surfactant forms spherical micelles of approximately 22 monomer units in apolar media,[31] and has critical micelle concentration in Isopar-L 10^{-3} wt%.[27]

Viscosity and zeta potential measurements

The zeta potentials were measured using a ZetaPALS zeta potential analyzer from Brookhaven Instruments Corp. (Holtsville, NY). The measurements were carried out with a sinusoidal voltage at a frequency of 2Hz using a field strength of 40V. Given the apolar medium used in this study, κa was much less than 0.1, and the zeta potentials were calculated from the electrophoretic mobilities using the Hückel limit (Equation (3.1)

. The viscosity was measured using an Anton Paar MCR 300 rheometer and the CC-27 cup and bob tool. The bob has a radius of 13.32mm and a length of 40mm. The cup has a radius of 14.46mm. The viscosities were measured using a linear shear ramp program with shear rates of 12-18s^{-1}. These values were used to prevent the formation of Taylor vortices which would occur after shear rates of 18s^{-1}. Over this range, the viscosity was independent, within error, of shear rate. The reported viscosities are the average of 35 data points in a shear ramp program.

Sample Preparation

Solutions of AOT in Isopar-L were prepared at three concentrations – 0.47, 1.0, and 1.5 wt% - all of which are multiple orders of magnitude above the CMC. Silica particles were added at volume fractions ranging from 10^{-4} to 0.02, sonicated, and allowed to charge over 48 hours. The samples were then redispersed using a shear mixer, and measured in the ZetaPALS and the MCR 300.

RESULTS AND DISCUSSION

In order to determine if electroviscous effects are present in these apolar systems, the viscosities of the samples must be compared to Equations B.2 and B.3, as shown in Figure B.1.

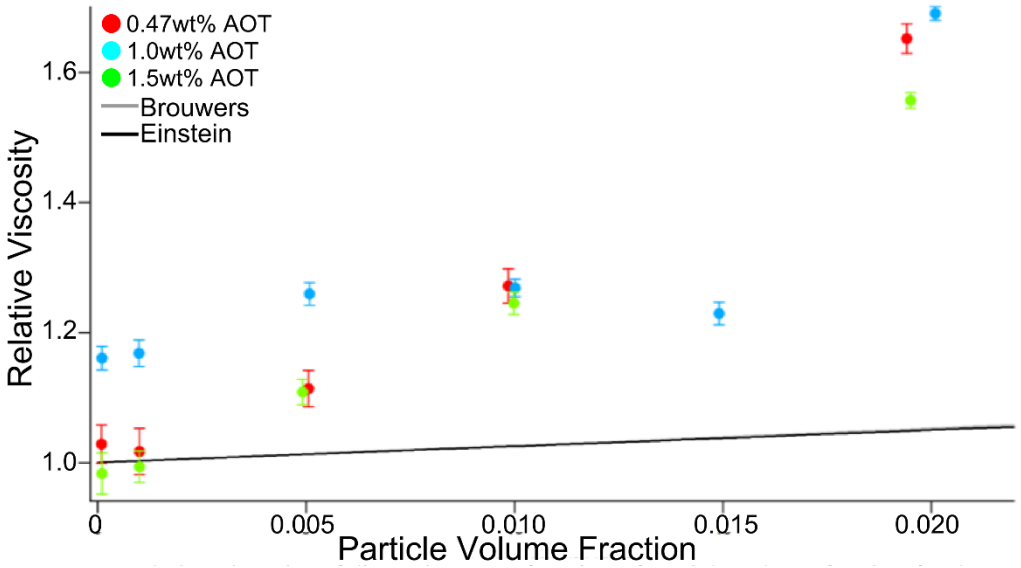

Figure B.1. Relative viscosity of dispersions as a function of particle volume fraction for three AOT concentrations. Both the Brouwers and Einstein equations are shown for reference. Over the given range of volume fractions, the two equations predict the same viscosities.

The two lowest volume fraction samples for the 0.47wt% and 1.5 wt% had relative viscosities that are predicted by Equations B.2 and B.3. The majority of the dispersions, however, had relative viscosities 10-60 percent higher than Equations B.2 and B.3 would predict for non-charging dispersions, suggesting significant electroviscous effects being present in those systems. The zeta potentials of these dispersions are shown in Figure B.2.

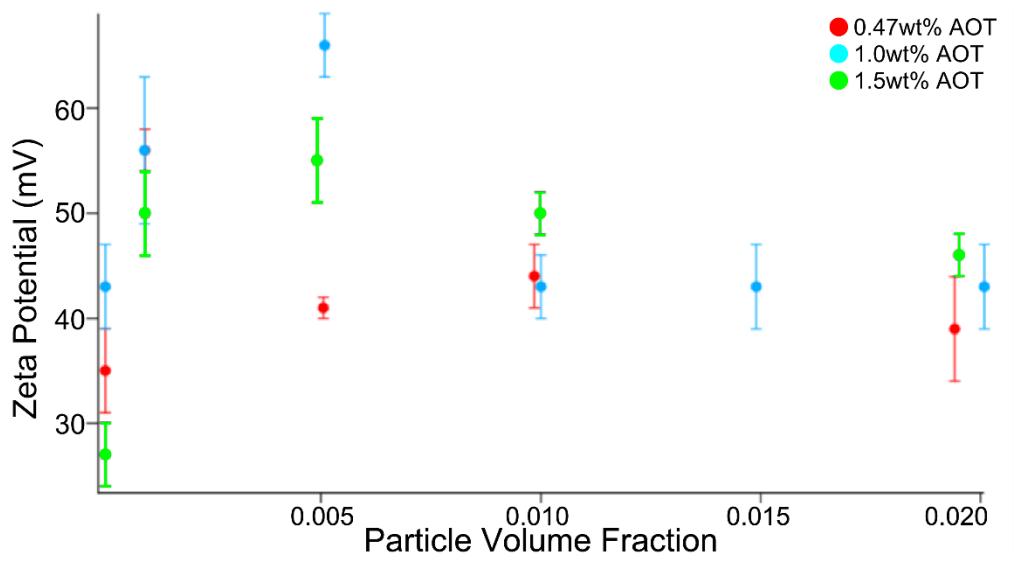

Figure B.2. Zeta potential as a function of particle volume fraction for three AOT concentrations.

These dispersions experience a maximum in zeta potential at particle volume fractions of $5x10^{-3}$ before approaching a lower, steady-state value of approximately 45 mV at higher loadings. As the surfactant concentration increases from 0.47wt% to 1wt%, more reverse micelles are present to stabilize charges on particle surfaces, thus allowing for higher zeta potentials to be imparted to them. However, as the surfactant concentration increases further, to 1.5wt%, the electrostatic screening of charged reverse micelles in the bulk lowers the measured zeta potentials of the particles. As Figure B.1 shows, the two lowest particle loadings for the 0.47wt% and 1.5wt% AOT solutions do not have any measurable electroviscous effects partly due to the lower zeta potentials of these samples than the zeta potentials of the 1.0wt% AOT samples at the same particle loading. This, combined with the very low particle loadings can both contribute to the lack of measured electroviscous effects. The rest of the samples exhibit viscosities significantly higher than those predicted for non-charging systems, validating the presence of electroviscous effects in these apolar systems.

The second goal of this study was to determine the ability of Equations B.4 - B.9 to accurately describe the electroviscous behavior of apolar dispersions. The two experimental

variables that were controlled in this study were AOT concentration and particle loading (i.e. volume fraction). Specifying both of these parameters yields a single zeta potential and viscosity, making it convenient to plot the relative viscosity as a function of zeta potential.

As there are no models available to predict the zeta potential of an apolar dispersion, Equations B.4 - B.9 were used to construct curves of relative viscosity as a function of zeta potential. Each curve represents a single particle volume fraction at a given AOT concentration. Figure B.3-B.5 plot these curves as well as the data points acquired from each given system (specified AOT concentration and particle loading). The colors represent a single particle loading. For example, the light blue curves and data points represent a particle loading of 2 volume percent.

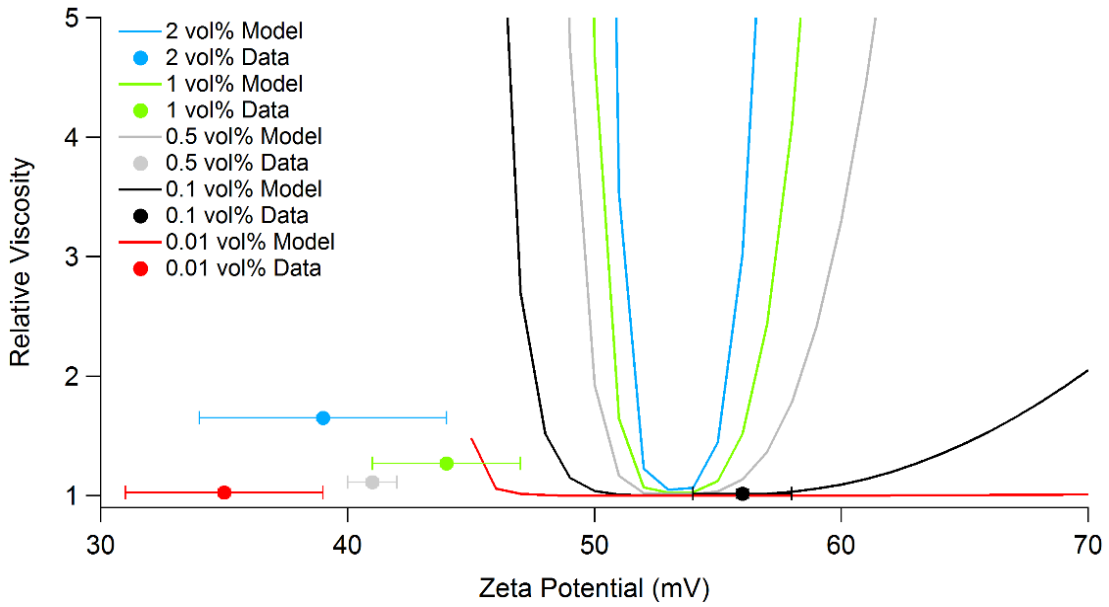

Figure B.3. Relative viscosity as a function of zeta potential in 0.47wt% AOT solutions. Colored markers represent measured data points, while the colored curves represent the relative viscosity as predicted by Equations B.4 - B.9. Each color represents a specific particle loading.

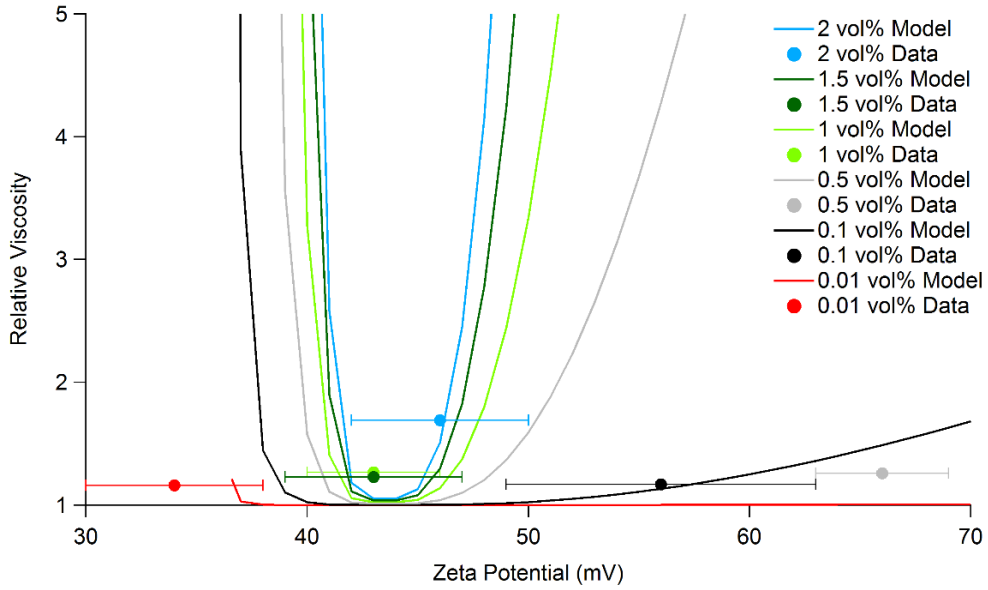

Figure B.4. Relative viscosity as a function of zeta potential in 1wt% AOT solutions. Colored markers represent measured data points, while the colored curves represent the relative viscosity as predicted by Equations B.4 - B.9. Each color represents a specific particle loading.

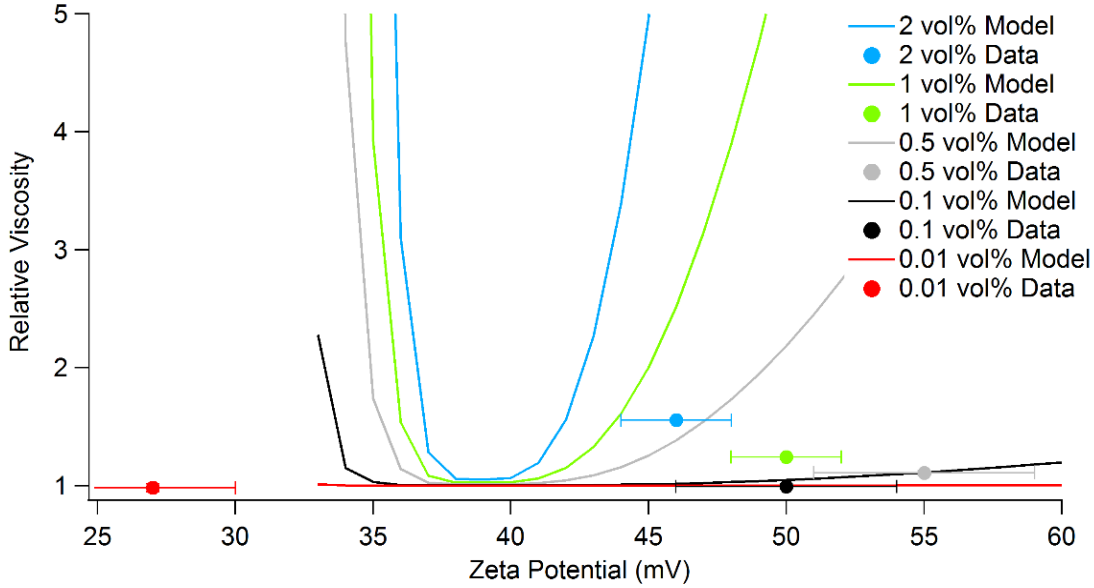

Figure B.5. Relative viscosity as a function of zeta potential in 1.5wt% AOT solutions. Colored markers represent measured data points, while the colored curves represent the relative viscosity as predicted by Equations B.4 - B.9. Each color represents a specific particle loading.

If Equations B.4 - B.9 accurately predicted the electroviscous effects in these systems, the marker of a given color would fall on the curve of that same color. While Figure B.4 shows that

the data points fall on their respective curves within error, the data from the 0.47wt% and 1.5wt% systems do not fall on the modeled curves. Figure B.3 shows all but the data point for 0.1vol% shifted to lower zeta potentials than the model predicts. In Figure B.5 all but the 0.01vol% datum are shifted to higher zeta potentials than the model predicts.

A possible reason for this is the flocculation or aggregation of particles. In most systems, the low zeta potentials, below 40mV, of the particles would not provide enough electrostatic repulsion to prevent flocculation. As the particles flock together, the effective size of each "particle" increases. With an increase in particle size, the predicted viscosity curves shift to lower zeta potentials, as shown in Figure B.6.

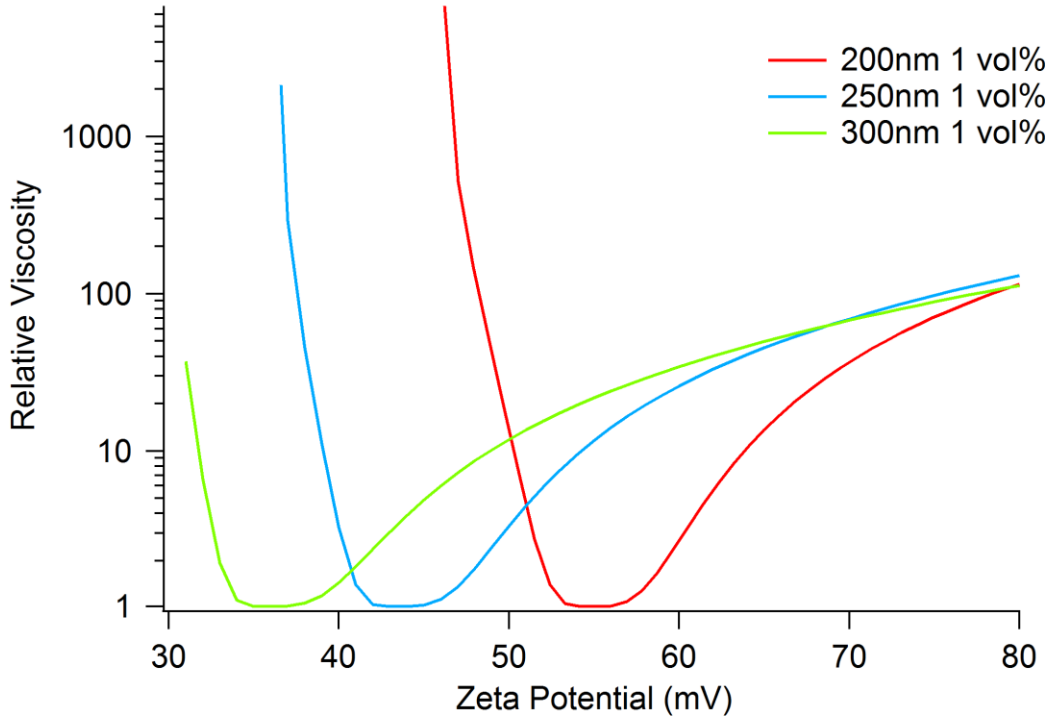

Figure B.6. Relative viscosity as a function of particle zeta potential for at a loading of 1vol% for three particle sizes.

The increase from 200nm particles to 300nm particles results in the model curves shifting the minimum down by about 20mV. This curve was generated using Equations B.4 - B.9 and

assuming a 1wt% AOT solution at 1vol% particles. If the particles in the 0.47wt% AOT systems flocculated, thus increasing their effective size, the predicted viscosity curves would be centered around a lower zeta potential, as the measured data is. It should be noted that the 0.1vol% point would no longer fall on the proper curve if this were the case.

In Figure B.5, one can see that four of the five experimental points acquired higher zeta potentials than the model curves predict, which cannot be explained by flocculation. Flocculation increases the size of the "particles," thus shifting the model curves to lower zeta potentials as shown in Figure B.6. Higher zeta potentials would suggest smaller particles, but silica does not dissolve in Isopar-L and particles smaller than the starting 250nm would not be present in these systems. An increase in the zeta potential of the model curve minimum could be attributed to lower AOT concentrations, as shown in Figure B.3-Figure B.5. At 0.47wt% AOT, the curves are centered on 53mV while at 1.5wt% AOT, the curves are centered on 39mV. However, AOT easily dissolves into Isopar-L and is soluble at concentrations up to 10wt%, making it unlikely that this shift to higher zeta potentials was due to a lower-than-expected AOT concentration. Given that, for the majority of the data collected, the data do not fall on the predicted curves, it is safe to assume that the models presented by Russel and Booth do not accurately describe electroviscous behavior in apolar media.

Varying the zeta potential, while holding all other variables constant, results in curves that exhibit a minimum in relative viscosity at a given value of zeta potential. Decreasing surfactant concentration or particle radii both increase the zeta potential value at which this minimum occurs, while increasing the particle loading results in narrower curves, without shifting the location of the minimum. As the zeta potential drops below this minimum value, the relative viscosity increases to infinity, suggesting that as the particles' charge decreases past a

certain value, the dispersion's viscosity would approach infinity, which in nonphysical and is an artifact of the equations used to model this system. For zeta potentials below this asymptotic value, the models return non-real values of viscosity.

In Equation B.7, one can note that as α, a ratio of electrostatic energy to thermal energy, approaches unity, the reduced viscosity approaches infinity. A value of unity occurs when the electrostatic energy is equal to the thermal energy, kT. This can occur when either the zeta potential or κa is a small value. In apolar systems, the Debye length, κ^{-1}, can be up to three orders of magnitude larger than that of an aqueous system, resulting in κa values that are orders of magnitude smaller than in aqueous media, and possibly α values of unity. Values of α less than one can also occur when the electrostatics are very weak, such as when the zeta potentials are low. In Equation B.7, this would involve the natural logs of negative numbers, which would return an undefined value for μ_{red}. Multiple data points presented in this study have values of α less than 1. The sample at 0.01vol% particles and 1.5wt% AOT had a zeta potential of 27mV. Plugging these values into Equation B.9 returns an α value of 0.68, and a non-real value of μ_{red}. The highest zeta potential samples for each AOT concentration (from Figure B.2) had values of 66, 56, and 45mV for the 1.5, 1.0, and 0.47wt% solutions respectively, resulting in the largest values of α in this study. These α values were 2.93, 3.26, and 1.01 for the 1.5, 1.0, and 0.47wt% solutions respectively.

In Russel's paper, all of the samples studied had α values between 103 and 105. This was because B.7 was derived assuming electrostatics strong enough to overcome interparticle forces (van der Waals), which is often the case in aqueous systems. In apolar media, however, electrostatics are often not strong enough to neglect particle-particle interactions resulting in flocculation or aggregation events, as described earlier. Since Equations B.7 and B.9 were

derived assuming that these forces can be neglected, it is reasonable to suggest that a new expression for electroviscous effects must be developed for apolar dispersions, which accounts for the van der Waals forces experienced by the particles.

CONCLUSIONS

It has been determined that electroviscous effects are present in apolar systems, and can result in viscosities 10-60% higher than what would be expected for a non-charging colloidal dispersion. The expressions developed by Booth and Russel, however, do not accurately describe the electroviscous behavior of these apolar systems. The electrostatic forces in an apolar medium are weaker than those present in aqueous environments, making it such that interparticle forces are non-negligible and must be included in the derivation of a new expression for viscosity of such systems.

APPENDIX C – FUTURE WORK

This final section will discuss two projects which continue the work presented in this dissertation. The first proposed project would investigate the charging behavior of mineral oxide particles in a series of solvents with intermediate dielectric constants using Aerosol OT. The second project would use small angle neutron scattering to determine the effect of solvent dielectric constant and structure on the structure and aggregation number of Aerosol OT reverse micelles.

PROJECT 1 – Surfactant-mediated particle charging in leaky dielectrics

Several groups have studied the effects of solvent on the charging behavior of mineral oxide particles. It was found that acid-base mechanisms dominate the charging of particles dispersed in nonaqueous media.[86] The donicity of the solvent has been found to strongly influence both the magnitude and polarity of the charge which is imparted to mineral oxides. Particles become negatively charged when the solvent acts as a stronger donor than the particle, and positively charged when the solvent is a stronger acceptor than the particle.[87] There exists a donicity value for which the polarity of the particles switch from positive to negative. This donicity of zero charge was defined as the aqueous point of zero charge of the particle type.[88] The addition of surfactant molecules to these systems adds the possibility of other charging mechanisms. Both the surfactant and solvent molecules can undergo acid-base charging mechanisms with the surface functional groups on the particle. Specific adsorption of ionized surfactant molecules can also confer charge to the particle surfaces.[89] While there has been significant research published on the charging of colloidal particles with surfactants in apolar

media, there have not been many studies investigating this behavior in solvents of intermediate dielectric constant.[89]

Linear alcohols are unique among leaky dielectrics, as they all have similar donicities, but decrease in dielectric constant as the length of the alkane chain increases. A previous study[90] by Romo investigated the effect of alcohol chain length and water content on the charging of Al_2O_3 and $Al(OH)_3$ particles. It was found that all C_3 to C_5 alcohols charged alumina negatively and aluminum hydroxide positively, all to magnitudes of ±26mV. The addition of water to the systems flipped the sign of the alumina particles, and increased the magnitude of the charge on the aluminum hydroxide particles. This shows the importance of solvent donicity and controlling water content in these systems. The small range of alcohols used in this study did not offer a sufficient range of solvent dielectric constants to probe its effect on particle charge.

The following study has multiple goals. First, to investigate the effect, if any, of alcohol chain length on the charging of a series of mineral oxide particles with a range of points of zero charge (PZCs). The second goal is to investigate the micellization of Aerosol OT (AOT) in the same series of alcohols. The final goal is to study the interplay between AOT and alcohols on the charging of the mineral oxide particles in the series of solvents.

MATERIALS AND METHODS

A series of eight, linear alcohols will be used as solvents in this study: from methanol to n-octanol. These solvents have a range of dielectric constants from 32, for methanol, to 3.4, for n-octanol. Aerosol OT (AOT), supplied from Sigma Aldrich will be purified according to the techniques presented in Mesa et al.[91] This preparation will remove impurities which could potentially affect its micellization behavior as noted in Peri.[92] Three mineral oxide particles will be dispersed in these solvents: silica, alumina, and magnesia.

Solutions of AOT in each solvent will be made at 15 concentrations of surfactants, and measured using conductometric techniques to determine the critical micelle concentration (CMC) of AOT in each solvent. Small angle x-ray scattering (SAXS) will be performed on these same samples to determine structural characteristics of the reverse micelles. Due to the small size of reverse micelles and low contrast with the solvents, it may not be possible to collect adequate data to determine their size. In this case, the scattered intensity of the x-rays will be measured at a fixed angle to corroborate the presence of reverse micelles in the systems.

Dispersions of each of these three particles will be made in each of the eight solvents, and measured using phase analysis light scattering (PALS) and conductometric techniques. The magnitude of the particle's mobility should be a function of its PZC, as the charge is generated according to acid-base mechanisms. The same particle types will then be dispersed in AOT solutions in each of the eight solvents. The maximum particle mobility will be measured for each AOT-particle pairing in each of the eight solvents. System conductivities will also be measured for each sample to determine if additional charge is generated due to the presence of AOT reverse micelles.

HYPOTHESES

A previous study[38] suggests that micellization of AOT becomes more favorable as the dielectric constant of the solvent alcohol decreases. It is likely that this trend would continue for higher alcohols, with AOT having the highest CMC in methanol, and lowest in n-octanol. If structural data can be collected using SAXS, the AOT micelles would possibly increase in size and aggregation number as the chain length of the alcohol increased. Peri[92] observed the aggregation number of AOT reverse micelles increasing as the size of the solvent molecules increased from methanol and carbon tetrachloride up to iso-octane and n-hexadecane.

Dispersions of particles in the alcohols should charge according to acid-base mechanisms. Silica should charge negatively to a higher magnitude than alumina. Magnesia should have the lowest magnitude of charge, potentially with a positive polarity. As the dielectric constant of the solvent decreases, with increasing alcohol length, the probability of charging events decreases. Therefore, the particles should have the highest magnitude of charge in methanol, and the lowest, if any, in n-octanol.

It is difficult to determine how the AOT micelles would interact with the particles in leaky dielectrics, especially those with a higher dielectric constant. In n-octanol, with ε=3.4, AOT would likely micellize as it does in apolar solvents. The reverse micelles, however, could allow the octanol to impart charge to the particle surface as the lower alcohols do, due to the presence of a polar environment for charge stabilization. In more polar alcohols, charge could also be imparted by the absorption of charged surfactant ions.[89] This would confer a negative charge to the particle surface.

PROJECT 2 – The structure of AOT reverse micelles in leaky dielectrics

The previous project will potentially show trends in maximum particle mobility AOT can impart as a function of the length of the alcohol. While it is currently unknown whether the more polar environment of lower alcohols will facilitate or hinder AOT in charging particle surfaces, it is likely that these lower alcohols will dominate the charging of particle surfaces. As the length of the alcohol increases, and dielectric constant decreases, AOT should become the dominant species in charging the particles. This behavior should also correlate to the structures of the AOT reverse micelles in the alcohols.

Peri[7] found that AOT forms small aggregates in solvents with small molar volumes, such as carbon tetrachloride, but which increase in size as the size of the solvent increased. The author postulates that the smaller solvents can more easily fit between the hydrocarbon tails, thus "pinching-off" the micelles at a smaller size. The solvents used in this study all had dielectric constants below 5, but chemistries varying from CCl_4 to branched and linear alkanes. This change in micellar size could possibly be attributed to these differing chemistries and not just solvent size.

The goal of this project is twofold. The first is to investigate the size and aggregation numbers of AOT in four linear alcohols of increasing size using small angle neutron scattering (SANS). The second goal is to correlate the charging behavior of these reverse micelles, as studied in Project 1, with the micellar size and structure.

MATERIALS AND METHODS

Four linear alcohols will be used as solvents in this study: methanol, n-propanol, n-hexanol, and n-octanol. Each alcohol will be purchased in both its hydrogenated and deuterated forms. Aerosol OT, sodium di-octylsulfosuccinate, will be used as the surfactant to form reverse micelles. The AOT will be purified in order to remove any impurities which may interfere with micelle formation.

Solutions of AOT will be made at 1wt%, which has been shown to provide sufficient scattering statistics using SANS.[93] Five solvent compositions will be made, ranging from fully hydrogenated to fully deuterated solvent. AOT will then be measured in each solvent mixture. Using the technique illustrated in Kotlarchyk et al.,[31] the aggregation number and size of the reverse micelles can be calculated from scattering parameters abstracted from the Guinier plots in each solvent mixture. This process will be repeated for each of the four alcohols.

HYPOTHESES

If the theory presented in Peri is correct, AOT should form the smallest aggregates in methanol, which would then increase in size and aggregation number as the size of the alcohol increases. This behavior should also be expected due to the enthalpic nature of reverse micellar formation. The dipole-dipole attractions of the head groups, necessary for the formation of reverse micelles, are weaker in the more polar solvents. These weaker interactions may only allow for small aggregates of AOT molecules to form. As the solvent becomes less polar, these attractions become stronger, thus allowing for more AOT molecules to come together to form a reverse micelle.

APPENDIX D – REFERENCES

(1) Klinkenberg, A.; van der Minne, J. L. *Electrostatics in the Petroleum Industry*; Elsevier: New York, 1958.

(2) Nelson, S.; Pink, R. Solutions of Metal Soaps in Organic Solvents .3. the Aggregation of Metal Soaps in Toluene, Isobutyl Alcohol, and Pyridine. *J. Chem. Soc.* **1952**, No. MAY, 1744–1750.

(3) Nelson, S.; Pink, R. Solutions of Metal Soaps in Organic Solvents .14. Direct-Current Conductivity in Solutions of Some Metal Oleates in Toluene. *J. Chem. Soc.* **1954**, No. DEC, 4412–4417.

(4) Eastoe, J.; Warne, B. Nanoparticle and Polymer Synthesis in Microemulsions. *Curr. Opin. Colloid Interface Sci.* **1996**, *1* (6), 800–805.

(5) Ju, X.; Huang, P.; Xu, N.; Shi, J. Studies on the Preparation of Mesoporous Titania Membrane by the Reversed Micelle Method. *J. Membr. Sci.* **2002**, *202* (1–2), 63–71.

(6) Dong, X.-Y.; Meng, Y.; Feng, X.-D.; Sun, Y. A Metal-Chelate Affinity Reverse Micellar System for Protein Extraction. *Biotechnol. Prog.* **2010**, *26* (1), 150–158.

(7) Liu, Y.; Dong, X.-Y.; Sun, Y. Protein Separation by Affinity Extraction with Reversed Micelles of Span. *Sep. Purif. Technol.* **2007**, *53* (3), 289–295.

(8) Naoe, K.; Ura, O.; Hattori, M.; Kawagoe, M.; Imai, M. Protein Extraction Using Non-Ionic Reverse Micelles of Span 60. *Biochem. Eng. J.* **1998**, *2* (2), 113–119.

(9) Cummings, S.; Xing, D.; Enick, R.; Rogers, S.; Heenan, R.; Grillo, I.; Eastoe, J. Design Principles for Supercritical CO2 Viscosifiers. *Soft Matter* **2012**, *8* (26), 7044–7055.

(10) Peach, J.; Eastoe, J. Supercritical Carbon Dioxide: A Solvent like No Other. *Beilstein J. Org. Chem.* **2014**, *10*, 1878–1895.

(11) Chaitanya, V. S. V.; Senapati, S. Self-Assembled Reverse Micelles in Supercritical CO2 Entrap Protein in Native State. *J. Am. Chem. Soc.* **2008**, *130* (6), 1866–1870.

(12) Gacek, M. M.; Berg, J. C. Investigation of Surfactant Mediated Acid–Base Charging of Mineral Oxide Particles Dispersed in Apolar Systems. *Langmuir* **2012**, *28* (51), 17841–17845.

(13) Espinosa, C. E.; Guo, Q.; Singh, V.; Behrens, S. H. Particle Charging and Charge Screening in Nonpolar Dispersions with Nonionic Surfactants. *Langmuir* **2010**, *26* (22), 16941–16948.

(14) Guo, Q.; Lee, J.; Singh, V.; Behrens, S. H. Surfactant Mediated Charging of Polymer Particles in a Nonpolar Liquid. *J. Colloid Interface Sci.* **2013**, *392*, 83–89.

(15) Guo, Q.; Singh, V.; Behrens, S. H. Electric Charging in Nonpolar Liquids Because of Nonionizable Surfactants. *Langmuir* **2009**, *26* (5), 3203–3207.

(16) Michor, E. L.; Berg, J. C. The Temperature Effects on Micelle Formation and Particle Charging with Span Surfactants in Apolar Media. *Langmuir* **2015**, *31* (35), 9602–9607.

(17) HP ElectroInk FAQ Document. Hewlett-Packard Development Co. 2012.

(18) Morrison, I. D. Electrical Charges in Nonaqueous Media. *Colloids Surf. Physicochem. Eng. Asp.* **1993**, *71* (1), 1–37.

(19) Berg, J. C. *An Introduction to Interfaces and Colloids: The Bridge to Nanoscience*, 1st ed.; World Scientific Publishing Co. Pte. Ltd., 2010.

(20) Michor, E. L.; Berg, J. C. Extension to the Charge Fluctuation Model for the Prediction of the Conductivity of Apolar, Reverse Micellar Systems. *Langmuir* **2012**, *28* (45), 15751–15755.

(21) Smith, G. N.; Eastoe, J. Controlling Colloid Charge in Nonpolar Liquids with Surfactants. *Phys. Chem. Chem. Phys.* **2012**, *15* (2), 424–439.
(22) Gacek, M.; Bergsman, D.; Michor, E.; Berg, J. C. Effects of Trace Water on Charging of Silica Particles Dispersed in a Nonpolar Medium. *Langmuir* **2012**, *28* (31), 11633–11638.
(23) Gacek, M. M.; Berg, J. C. The Role of Acid-Base Effects on Particle Charging in Apolar Media. *Adv. Colloid Interface Sci.* **2015**, *220*, 108–123.
(24) Pugh, R. J.; Matsunaga, T.; Fowkes, F. M. The Dispersibility and Stability of Carbon Black in Media of Low Dielectric Constant. 1. Electrostatic and Steric Contributions to Colloidal Stability. *Colloids Surf.* **1983**, *7* (3), 183–207.
(25) Kosmulski, M. Chemical Properties of Material Surfaces. In *Surfactant Science Series*; Marcel Dekker: New York, 2001; Vol. 102, p 754.
(26) Gacek, M. M.; Berg, J. C. Effect of Synergists on Organic Pigment Particle Charging in Apolar Media. *ELECTROPHORESIS* **2014**, *35* (12–13), 1766–1772.
(27) Gacek, M.; Brooks, G.; Berg, J. C. Characterization of Mineral Oxide Charging in Apolar Media. *Langmuir* **2012**, *28* (5), 3032–3036.
(28) Poovarodom, S.; Berg, J. C. Effect of Particle and Surfactant Acid–base Properties on Charging of Colloids in Apolar Media. *J. Colloid Interface Sci.* **2010**, *346* (2), 370–377.
(29) Gacek, M. M.; Berg, J. C. Effect of Surfactant Hydrophile-Lipophile Balance (HLB) Value on Mineral Oxide Charging in Apolar Media. *J. Colloids Interface Sci.* **2015**, *449*, 192–197.
(30) Dey, J.; Kumar, S.; Srivastava, A.; Verma, G.; Hassan, P. A.; Aswal, V. K.; Kohlbrecher, J.; Ismail, K. Effect of Ethylene Glycol on the Special Counterion Binding and Microstructures of Sodium Dioctylsulfosuccinate Micelles. *J. Colloid Interface Sci.* **2014**, *414*, 103–109.
(31) Kotlarchyk, M.; Huang, J. S.; Chen, S. H. Structure of AOT Reversed Micelles Determined by Small-Angle Neutron Scattering. *J. Phys. Chem.* **1985**, *89* (20), 4382–4386.
(32) Parent, M. E.; Yang, J.; Jeon, Y.; Toney, M. F.; Zhou, Z.-L.; Henze, D. Influence of Surfactant Structure on Reverse Micelle Size and Charge for Nonpolar Electrophoretic Inks. *Langmuir* **2011**, *27* (19), 11845–11851.
(33) Schmidt, J.; Prignitz, R.; Peschka, D.; Münch, A.; Wagner, B.; Bänsch, E.; Peukert, W. Conductivity in Nonpolar Media: Experimental and Numerical Studies on Sodium AOT–hexadecane, Lecithin–hexadecane and aluminum(III)-3,5-Diisopropyl Salicylate–hexadecane Systems. *J. Colloid Interface Sci.* **2012**, *386* (1), 240–251.
(34) Dukhin, A. S.; Parlia, S. Ion-Pair Conductivity Theory Fitting Measured Data for Various Alcohol-Toluene Mixtures across Entire Concentration Range. *J. Electrochem. Soc.* **2015**, *162* (4), H256–H263.
(35) Dukhin, A. S. Critical Concentration of Ion-Pairs Formation in Nonpolar Media. *Electrophoresis* **2014**, *35* (12–13), 1773–1781.
(36) Aurand, C. Moisture Determination by Karl Fischer Titration: Background of the Chemistry and Recent Developments. Supelco/Sigma-Aldrich 2010.
(37) Bodycomb, J. Introduction to Dynamic Light Scattering for Particle Size Determination. Horiba Scientific 2014.
(38) Michor, E. L.; Berg, J. C. Micellization Behavior of Aerosol OT in Alcohol/Water Systems. *Langmuir* **2014**, *30* (42), 12520–12524.

(39) Feigin, L.; Svergun, D. *Structure Analysis by Small-Angle X-Ray and Neutron Scattering*; Plenum Press: New York.
(40) Hammouda, B. *Probing Nanoscale Structures- The SANS Toolbox*; National Institute for Standards and Technology Center for Neutron Research, 2015.
(41) Hollamby, M. J.; Tabor, R.; Mutch, K. J.; Trickett, K.; Eastoe, J.; Heenan, R. K.; Grillo, I. Effect of Solvent Quality on Aggregate Structures of Common Surfactants. *Langmuir* **2008**, *24* (21), 12235–12240.
(42) Sheu, E. Y.; Chen, S. H.; Huang, J. S. Structure and Growth of bis(2-Ethylhexyl) Sulfosuccinate Micelles in Aqueous Solutions. *J. Phys. Chem.* **1987**, *91* (12), 3306–3310.
(43) Goncharenko, A. V.; Lozovski, V. Z.; Venger, E. F. Lichtenecker's Equation: Applicability and Limitations. *Opt. Commun.* **2000**, *174* (1–4), 19–32.
(44) Mikhail, S. Z.; Kimel, W. R. Densities and Viscosities of Methanol-Water Mixtures. *J. Chem. Eng. Data* **1961**, *6* (4), 533–537.
(45) Mikhail, S. Z.; Kimel, W. R. Densities and Viscosities of 1-Propanol-Water Mixtures. *J. Chem. Eng. Data* **1963**, *8* (3), 323–328.
(46) Pang, F.-M.; Seng, C.-E.; Teng, T.-T.; Ibrahim, M. H. Densities and Viscosities of Aqueous Solutions of 1-Propanol and 2-Propanol at Temperatures from 293.15 K to 333.15 K. *J. Mol. Liq.* **2007**, *136* (1–2), 71–78.
(47) Yusa, M.; Mathur, G. P.; Stager, R. A. Viscosity and Compression of Ethanol-Water Mixtures for Pressures up to 40,000 Psig. *J. Chem. Eng. Data* **1977**, *22* (1), 32–35.
(48) Eastoe, J.; Fragneto, G.; Robinson, B. H.; Towey, T. F.; Heenan, R. K.; Leng, F. J. Variation of Surfactant Counterion and Its Effect on the Structure and Properties of Aerosol-OT-Based Water-in-Oil Microemulsions. *J. Chem. Soc. Faraday Trans.* **1992**, *88* (3), 461–471.
(49) de la Iglesia, P.; Jaeger, V. W.; Xi, Y.; Pfaendtner, J.; Pozzo, L. D. Structure Characterization and Properties of Metal–Surfactant Complexes Dispersed in Organic Solvents. *Langmuir* **2015**, *31* (33), 9006–9016.
(50) Trickett, K.; Xing, D.; Eastoe, J.; Enick, R.; Mohamed, A.; Hollamby, M. J.; Cummings, S.; Rogers, S. E.; Heenan, R. K. Hydrocarbon Metallosurfactants for CO2. *Langmuir* **2010**, *26* (7), 4732–4737.
(51) Umer, A.; Naveed, S.; Ramzan, N.; Rafique, M. S. Selection of a Suitable Method for the Synthesis of Copper Nanoparticles. *Nano* **2012**, *7* (5), 1230005.
(52) Murugadoss, G. Synthesis, Optical, Structural and Thermal Characterization of Mn2+ Doped ZnS Nanoparticles Using Reverse Micelle Method. *J. Lumin.* **2011**, *131* (10), 2216–2223.
(53) Cabaleiro-Lago, C.; Garcia-Rio, L.; Hervella, P. The Effect of Changing the Microstructure of a Microemulsion on Chemical Reactivity. *Langmuir* **2007**, *23* (19), 9586–9595.
(54) Kondo, M.; Heisler, I. A.; Meech, S. R. Ultrafast Reaction Dynamics in Nanoscale Water Droplets Confined by Ionic Surfactants. *Faraday Discuss.* **2010**, *145*, 185–203.
(55) Kitahara, A.; Satoh, T.; Kawasaki, S.; Kon-No, K. Specific Adsorption of Surfactants Containing Mn or Co on Polymer Particles Revealed by Zeta-Potential in Cyclohexane. *J. Colloid Interface Sci.* **1982**, *86* (1), 105–110.
(56) Smith, G. N.; Brown, P.; James, C.; Kemp, R.; Khan, A. M.; Plivelic, T. S.; Rogers, S. E.; Eastoe, J. The Effects of Counterion Exchange on Charge Stabilization for Anionic Surfactants in Nonpolar Solvents. *J. Colloid Interface Sci.* **2016**, *465*, 316–322.

(57) Dean, J. A. *Lange's Handbook of Chemistry*, 15th ed.; McGraw-Hill.
(58) Kemp, R.; Sanchez, R.; Mutch, K. J.; Bartlett, P. Nanoparticle Charge Control in Nonpolar Liquids: Insights from Small-Angle Neutron Scattering and Microelectrophoresis. *Langmuir* **2010**, *26* (10), 6967–6976.
(59) Sainis, S. K.; Merril, J. W.; Dufresne, E. R. Electrostatic Interactions of Colloidal Particles at Vanishing Ionic Strength. *Langmuir* **2008**, *24* (23), 13334–13337.
(60) Schmidt, J.; Prignitz, R.; Peschka, D.; Münch, A.; Wagner, B.; Bänsch, E.; Peukert, W. Conductivity in Nonpolar Media: Experimental and Numerical Studies on Sodium AOT–hexadecane, Lecithin–hexadecane and aluminum(III)-3,5-Diisopropyl Salicylate–hexadecane Systems. *J. Colloid Interface Sci.* **2012**, *386* (1), 240–251.
(61) Ermi, B. D.; Amis, E. J. Influence of Backbone Solvation on Small Angle Neutron Scattering from Polyelectrolyte Solutions. *Macromolecules* **1997**, *30* (22), 6937–6942.
(62) Liu, Y.; Dong, X. Y.; Sun, Y. Characterization of Reversed Micelles of Cibacron Blue F-3GA Modified Span 85 for Protein Solubilization. *J. Colloid Interface Sci.* **2005**, *290* (1), 259–266.
(63) Dukhin, A. S.; Goetz, P. J. How Non-Ionic "electrically Neutral" Surfactants Enhance Electrical Conductivity and Ion Stability in Non-Polar Liquids. *J. Electroanal. Chem.* **2006**, *588* (1), 44–50.
(64) Glinka, C. J.; Barker, J. G.; Hammouda, B.; Krueger, S.; Moyer, J. J.; Orts, W. J. The 30 M Small-Angle Neutron Scattering Instruments at the National Institute of Standards and Technology. *J. Appl. Crystallogr.* **1998**, *31* (3), 430–445.
(65) Kline, S. R. Reduction and Analysis of SANS and USANS Data Using IGOR Pro. *J. Appl. Crystallogr.* **2006**, *39* (6), 895–900.
(66) Eicke, H. F.; Borkovec, M.; Das-Gupta, B. Conductivity of Water-in-Oil Microemulsions: A Quantitative Charge Fluctuation Model. *J. Phys. Chem.* **1989**, *93* (1), 314–317.
(67) Yezer, B. A.; Khair, A. S.; Sides, P. J.; Prieve, D. C. Determination of Charge Carrier Concentration in Doped Nonpolar Liquids by Impedance Spectroscopy in the Presence of Charge Adsorption. *J. Colloid Interface Sci.* **2016**, *469*, 325–337.
(68) Yezer, B. A.; Khair, A. S.; Sides, P. J.; Prieve, D. C. Use of Electrochemical Impedance Spectroscopy to Determine Double-Layer Capacitance in Doped Nonpolar Liquids. *J. Colloid Interface Sci.* **2015**, *449*, 2–12.
(69) Shrestha, L. K.; Yamamoto, M.; Arima, S.; Aramaki, K. Charge-Free Reverse Wormlike Micelles in Nonaqueous Media. *Langmuir* **2011**, *27* (6), 2340–2348.
(70) Shrestha, L. K.; Shrestha, R. G.; Aramaki, K. Intrinsic Parameters for the Structure Control of Nonionic Reverse Micelles in Styrene: SAXS and Rheometry Studies. *Langmuir* **2011**, *27* (10), 5862–5873.
(71) Shrestha, L. K.; Sato, T.; Dulle, M.; Glatter, O.; Aramaki, K. Effect of Lipophilic Tail Architecture and Solvent Engineering on the Structure of Trehalose-Based Nonionic Surfactant Reverse Micelles. *J. Phys. Chem. B* **2010**, *114* (37), 12008–12017.
(72) Shrestha, L. K.; Dulle, M.; Glatter, O.; Aramaki, K. Structure of Polyglycerol Oleic Acid Ester Nonionic Surfactant Reverse Micelles in Decane: Growth Control by Headgroup Size. *Langmuir* **2010**, *26* (10), 7015–7024.
(73) Dong, X.-Y.; Wu, X.-Y.; Sun, Y. Refolding of Denatured Lysozyme Assisted by Artificial Chaperones in Reverse Micelles. *Biochem. Eng. J.* **2006**, *31* (1), 92–95.
(74) Kallay, N.; Chittofrati, A. Conductivity of Microemulsions: Refinement of Charge Fluctuation Model. *J. Phys. Chem.* **1990**, *94* (11), 4755–4756.

(75) Hall, D. G. Conductivity of Microemulsions: An Improved Charge Fluctuation Model. *J. Phys. Chem.* **1990**, *94* (1), 429–430.
(76) Roberts, G. S.; Sanchez, R.; Kemp, R.; Wood, T.; Bartlett, P. Electrostatic Charging of Nonpolar Colloids by Reverse Micelles. *Langmuir* **2008**, *24* (13), 6530–6541.
(77) Parsegian, A. Energy of an Ion Crossing a Low Dielectric Membrane − Solutions to 4 Relevant Electrostatic Problems. *Nature* **1969**, *332* (5183), 844–846.
(78) Shen, Y.; Duhamel, J. Micellization and Adsorption of a Series of Succinimide Dispersants. *Langmuir* **2008**, *24* (19), 10665–10673.
(79) Almela, A.; Elizalde, M.; Benito, R. The Aggregation of Span-80 in Toluene. *J. Solut. Chem.* **1993**, *22* (3), 231–241.
(80) Bockris, J.; Reddy, A. *Modern Electrochemistry*; Plenum Press: New York, 1998.
(81) Morrison, F. A. *Understanding Rheology*; Oxford University Press, 2001.
(82) Brouwers, H. J. H. Viscosity of a Concentrated Suspension of Rigid Monosized Particles. *Phys. Rev. E* **2010**, *81* (5), 51402.
(83) von Smoluchowski, M. Drei Vorträge Über Diffusion, Brownsche Bewegung Und Koagulation von Kolloidteilchen. *Phys. Z* **1916**, *17*, 557.
(84) Booth, F. The Electroviscous Effect for Suspensions of Solid Spherical Particles. *Proc. R. Soc. Lond. Math. Phys. Eng. Sci.* **1950**, *203* (1075), 533–551.
(85) Russel, W. Bulk Stresses Due to Deformation of Electrical Double-Layer Around a Charged Sphere. *J. Fluid Mech.* **1978**, *85* (APR), 673–683.
(86) Verwey, E. J. W. Properties of Suspensions, Especially in Non-Aqueous Media. *Recl. Trav. Chim. Pays-Bas* **1941**, *60* (8), 618–624.
(87) Labib, M. E.; Williams, R. The Use of Zeta-Potential Measurements in Organic Solvents to Determine the Donor—acceptor Properties of Solid Surfaces. *J. Colloid Interface Sci.* **1984**, *97* (2), 356–366.
(88) Labib, M. E.; Williams, R. An Experimental Comparison between the Aqueous pH Scale and the Electron Donicity Scale. *Colloid Polym. Sci.* **1986**, *264* (6), 533–541.
(89) Lyklema, J. Principles of the Stability of Lyophobic Colloidal Dispersions in Non-Aqueous Media. *Adv. Colloid Interface Sci.* **1968**, *2* (2), 67–114.
(90) Romo, L. A. Effect of C3, C4 and C5 Alcohols and Water on the Stability of Dispersions with Alumina and Aluminum Hydroxide. *Discuss. Faraday Soc.* **1966**, *42* (0), 232–237.
(91) La Mesa, C.; Coppola, L.; Ranieri, G. A.; Terenzi, M.; Chidichimo, G. Phase Diagram and Phase Properties of the System Water-Hexane-Aerosol OT. *Langmuir* **1992**, *8* (11), 2616–2622.
(92) Peri, J. B. The State of Solution of Aerosol OT in Nonaqueous Solvents. *J. Colloid Interface Sci.* **1969**, *29* (1), 6–15.
(93) Michor, E. L.; Ponto, B. S.; Berg, J. C. Effects of Reverse Micellar Structure on the Particle Charging Capabilities of the Span Surfactant Series. *Langmuir* **2016**, *32* (40), 10328–10333.

Edward L. Michor

SUMMARY

Dedicated Chemical Engineer and interdisciplinary scientist with strong analytical, writing and communication skills. Skilled designer of experiments with a proven record of innovation and high impact publications. Passionate project team leader and teacher of science and engineering. Life-long learner with a strong understanding of instrumentation. Advocate of energy efficiency and sustainable process design.

HIGHLIGHTS

- Design of experiments
- Project management
- Teaching and instruction
- Complex problem solving
- Theoretical and experimental
- Instrumentation
- Nanoscience
- Surface science
- Colloidal dispersions
- Rheology
- Small angle scattering
- Chromatographic techniques

EDUCATION

2011-2016	University of Washington – Seattle, WA **Ph.D – Chemical Engineering** Currently in 6th year - Graduating December 2016 – GPA: 3.82
2011-2014	University of Washington – Seattle, WA **Master's of Science – Chemical Engineering** Received in 2014 – GPA: 3.82
2007- 2011	University of Minnesota - Minneapolis, MN **Bachelor's of Chemical Science – Chemical Engineering** Graduated in 2011 – GPA: 3.51

PROJECTS

2011- 2016 **Graduate Research Assistant – University of Washington**
Adviser: Prof. John Berg

- Studied the effects of temperature and surfactant structure on micellization thermodynamics and particle charging capabilities in apolar media
- Studied the effects of solvent on micellization in intermediate-dielectric media

2011- 2016 **Graduate Teaching Assistant – University of Washington**
Course: Surface and Colloid Science Laboratory

- Design new experiments to teach colloidal theory to students
- Instruct students on experimental theory and practices

June – Sept 2013 **Ink R&D Intern – Xerox Corporation**
Wilsonville, OR

- Set up SMS Inverse Gas Chromatograph and develop SOPs for its use
- Characterized surface energy profiles of a series of nanoparticles

2007-2011 **Undergrad Research Assistant – University of Minnesota**
Advisers: Prof. Aditya Bhan and Prof. Lanny Schmidt

- Investigated ethanol dehydration reactions over acidic zeolite catalysts
- Design and construction of gas flow reactor systems
- Studied the reforming of butanol to butenes in stratified, autothermal reactors

TECHNICAL SKILLS

Software: IgorPro, Mathematica, COMSOL Multiphysics, SASView, Inkscape, Zotero, Image J, Microsoft Office

Techniques: Small Angle X-ray Scattering (SAXS) and Small Angle Neutron Scattering (SANS), Static Light Scattering (SLS) and Dynamic Light Scattering (DLS), Phase Analysis Light Scattering (PALS), Atomic Force Microscopy (AFM), Thermogravimetric Analysis (TGA), Dynamic Scanning Calorimetry (DSC), Rheometry, High Performance Liquid Chromatography (HPLC), Inverse Gas Chromatography (IGC), Conductometric Techniques, BET Surface Area Analysis, Karl Fischer Titration, Goniometry, sedimentation by x-ray analysis, emulsion analysis, bubble tensiometry, surface tension analysis, three-point bend test, tensile and toughness testing, optical microscopy

AWARDS AND VOLUNTEERING

- Gold National Scholarship (University of Minnesota)
- Completed Institute of Technology Honors Program (University of Minnesota)
- Achievement Rewards for College Scientists (ARCS) Fellowship (University of Washington)
- ACES Chemical Engineering Graduate Student group - Social Chair
- University of Washington Engineering Discovery Days
- Bryant Elementary School Science Fair Mentor
- Honors Peer Mentor – University of Minnesota

PUBLICATIONS and PRESENTATIONS

E. Michor and J. Berg. "The effects of reverse micellar structure on the particle charging capabilities of the Span surfactant series." *Langmuir*, **2016**, *32*(40), 10328-10333
E. Michor and J. Berg. "The particle charging behavior of ion-exchange surfactants in apolar media." *Colloids and Surfaces A,* **2017,** *512*, 1-6**.**
E. Michor and J. Berg. "The temperature effects on micelle formation and particle charging with Span surfactants in apolar media." *Langmuir*, **2015**, *31*(35), 9602-9607.
E. Michor and J. Berg. "The Micellization Behavior of Aerosol OT in Alcohol/Water Systems." *Langmuir*, **2014**, *30*(42), 12520-12524.

M. Gacek, D. Bergsman, **E. Michor**, and J. Berg. "Effects of Trace Water on Charging of Silica Particles Dispersed in a Nonpolar Medium." *Langmuir*, **2012**, *28*(31), 11633-11638.
H. Sun, S. Blass, **E. Michor**, and L. Schmidt. "Autothermal Reforming of Butanol to Butenes in a Staged Millisecond Reactor: Effect of Catalysts and Isomers." *Applied Catalysis A: General*, **2012**, *455-456*, 35-41.
M.J. Skinner, **E. Michor**, et al. "Ethanol Dehydration to Ethylene in a Stratified Autothermal Millisecond Reactor." *Chemsuschem*, **2011**, *4*(8), pp 1151-1156.

"The effects of temperature on particle charging with Span® surfactants," The 89th ACS Colloids and Surface Science Symposium, Carnegie Mellon University, Pittsburgh, PA. (June 2015)
"The effects of reverse micellar structure on particle charging in apolar solvents," Graduate Student Symposium, University of Washington, Seattle, WA. (September 2016)